PARTIAL INERTING AND MINIMUM IGNITION ENERGY (MIE) PREDICTION OF COMBUSTIBLE DUSTS

A Dissertation

by

PURVALI VINAY CHAUDHARI

Submitted to the Office of Graduate and Professional Studies of
Texas A&M University
in partial fulfillment of the requirements for the degree of

DOCTOR OF PHILOSOPHY

Chair of Committee,	Chad Mashuga
Committee Members,	Zhengdong Cheng
	James Holste
	Eric Petersen
Head of Department,	M. Nazmul Karim

August 2019

Major Subject: Chemical Engineering

ABSTRACT

Minimum Ignition Energy (MIE) is a critical dust hazard parameter guiding elimination of ignition sources in solids handling facilities. Partial inerting is an important but underutilized mitigation technique in which MIE of a dust cloud is increased through inerting, reducing the risk of an accidental dust explosion or more accurately, a dust deflagration. This dissertation has reported advances in MIE testing and prediction to prevent and mitigate dust explosions.

In this work, a novel purge add-on device to the standard MIE test apparatus was designed which facilitated purging the Hartmann tube before MIE testing. Through experimentation and CFD modeling, this dissertation has attempted to refine the existing MIE testing standard for partial inerting applications by introducing purge time as an essential parameter. The effective experimental purge time required for partial inerting testing in the MIE apparatus was determined to be > 40 s and validated through the ANSYS Fluent CFD purging model. In addition, this work has demonstrated that purging the MIE apparatus Hartmann tube before experimentation significantly affected the measured values in partially inerted atmospheres (O_2 < 21 vol. %). It is recommended through this research that purging should be an essential step while MIE testing and reporting. Using this improved methodology, an accurate MIE with changing oxygen concentrations for the combustible dusts Niacin, Anthraquinone, Lycopodium clavatum and Calcium Stearate was obtained and a mathematical equation for MIE-O_2 was proposed.

Furthermore, Quantitative-Structure Property (QSPR) models for MIE prediction using machine learning algorithms such as Random Forests (RF) and Decision Trees (DT) were developed. A binary classification model was developed for predicting the MIE category of the

combustible dusts. The results indicated good MIE predictability through the RF algorithm indicated by the Receiver Operating Characteristic – Area Under Curve (ROC-AUC) of 0.95. Additionally, RF algorithm was used to identify the molecular descriptors which most significantly affected the MIE prediction accuracy.

Thus, through experimentation and modeling, this study aims to provide a scientific foundation for a partial inerting MIE test method to supplement existing testing standards (such as ASTM E2019-03) and provides a solid framework for MIE prediction of combustible dusts.

DEDICATION

To my parents & sister, Vinay, Sunita & Tanushree Chaudhari

To my husband and love, Shrayank Gupta

ACKNOWLEDGEMENTS

I would like to express my sincere gratitude towards my advisor and committee chair, Dr. Chad Mashuga for guiding me in my journey as a graduate student and for providing me with opportunities to be successful through and after my Ph.D. His support in my research, towards my career and personal development has kept me motivated through these years. I would like to thank Late Dr. M. Sam Mannan for his guidance and for providing opportunities for my career and personality development through the Mary Kay O'Connor Process Safety Center.

I sincerely appreciate the time and guidance that I have received from my committee members Dr. James Holste, Dr. Eric Petersen and Dr. Zhengdong Cheng. Their inputs and suggestions in my research have helped me gain an in-depth understanding of my field. I would like to sincerely thank Dr. Qinsheng Wang for being on my committee for my final defense exam and for taking out time to have discussion with me about my work. I would like to sincerely express my gratitude to our collaborator Dr. Lisa Perez (Laboratory of Molecular Simulations, Chemistry Department), for her guidance and for helping me explore and develop interest in a relatively new field. I am thankful for her time, discussions with her and for her valuable inputs in my research. I would like to sincerely thank our industrial collaborator Dr. Stanley Kolis from Eli Lilly & Company for his insights and advice in my research. He has helped me develop a new outlook towards this field and I am forever grateful for the wonderful learning opportunities provided by our collaborative project with Lilly.

I would also like to thank the resources provided by the Texas A&M High Performance Research Computing facility (https://hprc.tamu.edu) and the Laboratory of Molecular Simulations. I would like to thank Mr. Bharatvaaj Ravi from my research group for conducting CFD simulations

to support my experimental findings. This entire process of collaboration has helped me learn CFD and triggered my interest in the field of modeling. I would also like to thank Mr. Nilesh Ade from my research group for his help and discussions in machine learning and for his valuable collaborative contributions to my research. I would like to extend my special thanks to the Mary Kay O'Connor Process Safety Center (MKOPSC), Mashuga research group, the MKOPSC staff and my research colleagues. Special thanks also goes to Ms. Sheera Helms for her administrative support during this process. I would like to specially thank Capt. Jim Pettigrew from OESI for all his help and encouragement in this process.

I am forever indebted to my friend Pratik Krishnan for always being there for me and for being a strong pillar of strength in my professional and personal journey throughout the 5 years of my PhD. I would also like to express my gratitude towards my friends Harsha Reddy, Ankita Bhat and Smit Shah, Aryan Thaker and Sourabh Bodas for always being there for me. My friends support and friendship has truly kept me going all these years! I am grateful to my former roommates, Akshata Kulkarni and Chanda Bhat for their support and love during some of the most difficult and testing times in these 5 years. I would like to thank my friends Abhijeet Shinde, Sourav Bandyopadhyay, Ishan Bajaj, Bhagyeshri Belokar and Jyoti Sharma for bringing enthusiasm and fun into graduate life. I would like to specially thank my friend Dr. Nirupama Gopalaswami for being a great mentor and support to me. I would also like to sincerely thank my friend Dr. Srikanth PVK for all his guidance and help in the process.

I am forever indebted to my grandparents Shravan & Kunda Patil for the sacrifices they have made for me and for always encouraging me to achieve high in life. To my Late grandparents, Suman & Muralidhar Chaudhari, I am forever thankful for their love and for instilling a culture of receptiveness to new ideas in me. I am forever thankful to my mother and father-in-law, Padma

and Shrikrishna Gupta for their love, support and understanding during this process.

I am forever indebted to my parents and sister for their love, sacrifices and encouragement throughout my life and for instilling the spirit of toughness, independence and achievement in me. Finally, I am extremely fortunate to have my best friend as my husband who has constantly encouraged and inspired me and has always believed in my dreams! I am forever indebted to him for the numerous professional and personal sacrifices that he had to make just so that I could get the best opportunities!

CONTRIBUTORS AND FUNDING SOURCES

This work was supervised by Dr. Chad Mashuga and a dissertation committee consisting of Dr. Jim Holste, Dr. Zhengdong Cheng, Dr. Qingsheng Wang of the Department of Chemical Engineering and Dr. Eric Petersen of the Department of Mechanical Engineering. The experiments performed towards this research were designed, and conceptualized by Purvali Chaudhari. Some experiments in this work were performed independently by Purvali Chaudhari while others with help from Hallie Graham, David Trettin, Benjamin Hall, Ethan Licon, Delaney Maberry, Kelly Weikel and Turzo Bose. The CFD simulations in this work were performed by Bharatvaaj Ravi from Chemical Engineering Department. The molecular modeling in this work was conducted by Purvali Chaudhari with help and guidance from Dr. Lisa Perez. In Section 4.3.1, results depicted were used from the Random Forest/Decision Tree Python codes developed by Nilesh Ade, Chemical Engineering. Inputs in Section 4, have been provided in part by industrial collaborator Dr. Stanley Kolis from Eli Lilly & Company. The publication resulting from Section 3 (published in 2019) has inputs in part provided by Pranav Bagaria from Chemical Engineering Department. All other work conducted for the dissertation was completed by the student independently.

This work has been supported by Research Assistantship provided by Texas A&M University. This work has been sponsored in part by the Lilly Research Award Program awarded by the Eli Lilly & Company. Its contents are solely the responsibility of the authors and do not necessarily represent the official views of the Texas A&M University or Eli Lilly & Company.

NOMENCLATURE

ASTM	American Society for Testing and Materials
ANN	Artificial Neural Networks
AUC	Area Under Curve
B3LYP	Becke, 3-paramater, Lee, Yang, Parr
CaRo15	Calibration RoundRobin 2015
CFD	Computational Fluid Dynamics
DT	Decision Tree
GFA	Genetic Function Approximation
KNN	k-Nearest Neighbors
L	Inductance in circuit
LMIE	Lowest Minimum Ignition Energy
LOC	Limiting Oxygen Concentration
MIE	Minimum Ignition Energy
MIKE3	Minimum Ignition Energy Kühner III
PSD	Particle Size Distribution
QSPR	Quantitative Structure-Property Relationship
RF	Random Forest
ROC	Receiver Operating Characteristic
SVM	Support Vector Machine
UHP	Ultra High Purity

TABLE OF CONTENTS

Page

LIST OF FIGURES

Page

LIST OF TABLES

Page

1 INTRODUCTION*

1.1. Dust explosions

Dust explosions have been a major safety concern in powder manufacturing and handling facilities resulting in catastrophic loss of life and property [1-5]. Combustible dust is present in industries as a raw material, byproduct or final product. Dust explosions result in tremendous overpressures, high temperatures and generate toxic gases due to combustion reaction [1-5].

In the United States, from 1980-2005, 281 combustible dust explosions have resulted in 119 fatalities and 718 injuries resulting in extensively damaging facilities [5-8]. Thus, in the period from 1980 – 2005, the 3 workers per month are affected in the U.S by dust explosions, which is a significant consequence. Dust explosions are a problem not only in United States but also in facilities around the world. Some of the major dust explosions incidents in recent years are observed in Table 1. Despite recurring incidents, there is still a lack of general awareness of dust hazards [6].

*Parts of this section have been reprinted with permission from: P. Chaudhari, B. Ravi, P. Bagaria, C. Mashuga, "Improved partial inerting MIE test method for combustible dusts and its CFD validation", Process Safety and Environmental Protection 2019, vol. 122, pp. 192-199, 2019, Copyright 2019 by Chaudhari et al.[33] and P. Chaudhari, and C. Mashuga, "Partial inerting of dust clouds using a modified standard minimum ignition energy device", Journal of Loss Prevention in the Process Industries, vol. 48, pp. 145-150, 2017, Copyright 2019 by Chaudhari and Mashuga [38].

Table 1 Major dust explosion incidents worldwide and their consequences [5]

Incident	Location and Year	Material	Consequence
AL Solutions	U.S., 2010	Titanium-Zirconium Powder	3 fatalities
Foxconn Plant Explosion	China., 2011	Aluminum Dust	4 fatalities, 18 injuries
U.S. Ink Fire	U.S., 2012	Gilsonite, Carbon Black and Petroleum Distillate Powder Mixture	7 injuries
Kunshan Explosion	China, 2014	Metal Powder	146 fatalities
Formosa Fun Coast	Taiwan, 2015	Colored Cornstarch	15 fatalities, 500 injuries

The five key elements required for a dust explosion are the fuel (combustible dust), confinement of combustible dusts, the oxygen content in the confined atmosphere, dust dispersion and presence of an ignition source [9]. These elements can be represented in the form of a dust pentagon (see Figure 1).

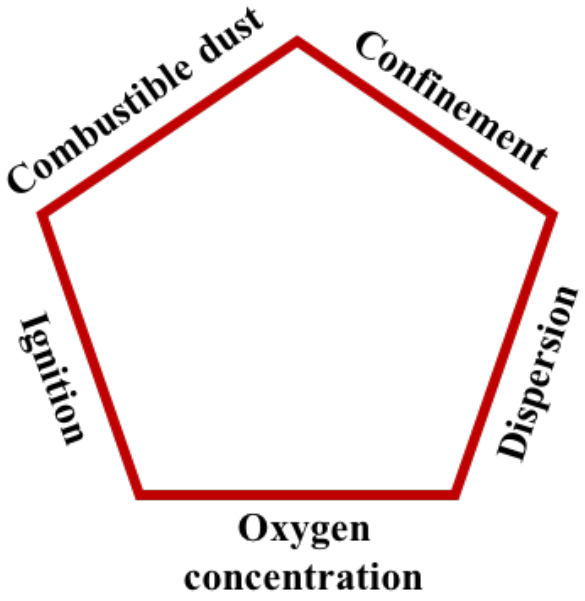

Figure 1 : Dust explosion pentagon

Further, each side of this pentagon can be associated with some critical parameters affecting dust explosion. The fuel (combustible dust) can be associated with parameters such as the dust shape, morphology, polydispersity, composition and its dispersibility. The confinement aspect of the pentagon can be associated with Minimum Explosible Concentration (MEC) while the dispersion side can be associated with dust turbulence during its dispersion. The oxygen content can be associated with the parameter Limiting Oxygen Content (LOC) which is the minimum oxygen concentration required for the dust to ignite. Finally, the ignition aspect of the pentagon is associated with parameters such as the Minimum Ignition Energy (MIE) which is the smallest amount of energy required to ignite the combustible dust and the Auto-Ignition Temperature (AIT) which is the lowest temperature at which the dust spontaneously ignites. The severity or the consequence of a dust explosion can be measured through the over pressure

generated during the explosion. The explosion severity is measured by the parameters P_{max} and K_{st}. The P_{max} indicates the maximum explosion overpressure generated during the dust explosion while the K_{st} determines the rate of pressure rise during a dust explosion. The main focus of this research has been the MIE, a critical dust explosion parameter which has been discussed in detail below.

1.2. Minimum Ignition Energy (MIE)

One of the critical parameters to be considered during dust explosion risk assessment is MIE. MIE is the smallest amount of energy required to ignite a dust cloud at a given temperature and pressure, and it quantifies the ignition probability of the dust [3, 10]. As MIE of a dust is an important dust explosion parameter, this aspect has been the focus of this research.

Figure 2 shows the contribution of different types of ignition sources present in process industries. Flame and direct heat account for the most common ignition sources in industry. Impact sparks, friction sparks, static electricity and electrical sparks account for ~ 46 % of the ignition sources present in the process industries [4]. Spark ignition can be associated with the measured MIE and therefore elimination of spark generating sources is an important dust explosion prevention method.

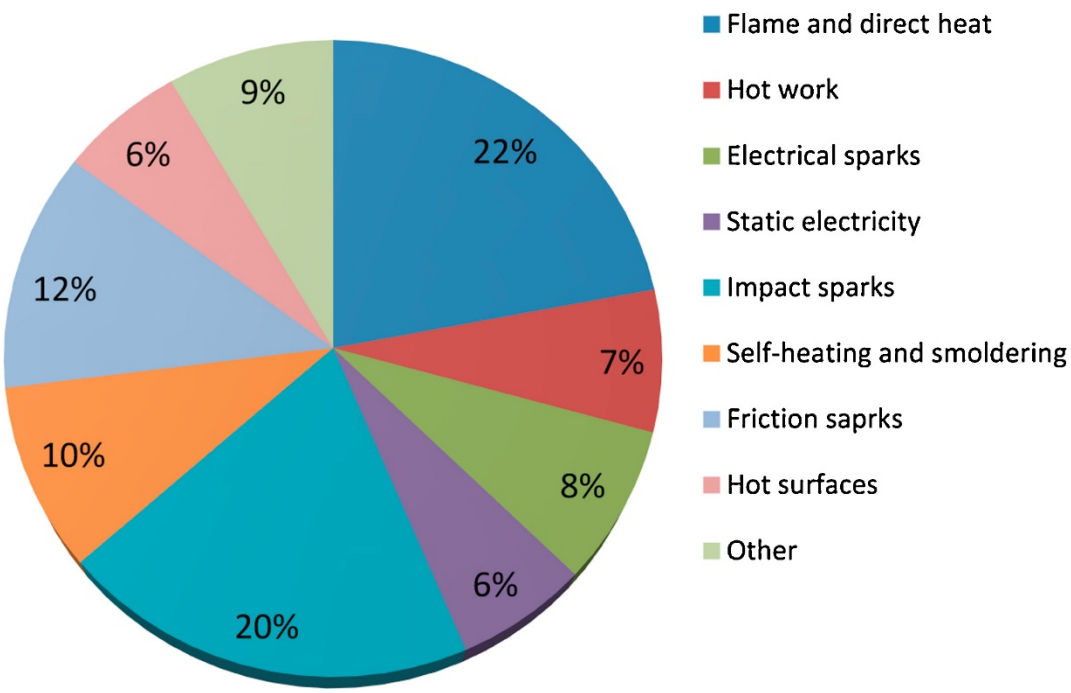

Figure 2 : Ignition sources present in process industries [4]

In the case of sparks as ignition sources, dust explosion preventive measures such as elimination of various ignition sources, grounding conductive parts of equipment and grounding personnel are implemented in combustible dust handling facilities. Dust MIE measurements have been traditionally conducted in the Hartmann explosion tube where ignition is provided by capacitive sparks [3]. A number of factors affect MIE measurements such as the dust particle size, shape, its polydispersity, oxygen content, ignition delay time between the dust dispersion and spark discharge and the presence of an inductance in the circuit. The effect of these factors on MIE has been extensively studied in literature. However, there still exist certain gaps in understanding the effect of certain factors on MIE measurement. Dust MIE measurement and testing has been discussed in the sections below.

1.3. Dust explosion research overview

1.3.1. Dust explosion prevention and mitigation

As dust explosion is a prevalent problem, dust explosion prevention and mitigation becomes important. Table 2 summarizes the commonly used dust explosion prevention and mitigation methods in industries. These methods can be categorized into passive and active explosion prevention [11].

Table 2 Dust explosion prevention and mitigation methods (redrawn from [12, 13])

Explosion Prevention		**Explosion Mitigation**
Preventing ignition sources	**Prevention of explosive dust clouds**	
a) Hot surfaces b) Open flames c) Burning metal particles d) Electrostatic discharges e) Electric sparks and arcs	a) Process design to prevent dust cloud generation and particle size breakage (inherently safer design) b) Inerting dust cloud by inert dust c) Inerting dust cloud by inert gas d) Keeping dust concentration outside explosible range	a) Explosion pressure resistant equipment b) Explosion isolation c) Explosion venting d) Automatic explosion suppression e) Partial inerting of dust cloud using inert gas f) Good housekeeping

Passive engineered safety

Passive engineered safety devices perform their function simply by their presence and do not require any actuation after the initiating event of the dust explosion. Some examples of passive devices for dust explosion mitigation are explosion relief venting, physical barriers isolating plant sections in order to prevent secondary dust explosions [11].

Active engineered safety

Active engineered safety devices require activation for explosion mitigation. Maintenance and testing are of further importance when operating these devices. Some examples of active devices for dust explosion include automatic dust explosion suppression system, mechanical isolation valves, inerting using an inert gas or partial inerting.

Additionally, some other procedural dust explosion prevention techniques include addition of inert solids to the dust to render it noncombustible, good housekeeping and removal of ignition sources in the facility. However, these methods are not always practical and their applicability depends on the nature of the facility [11].

1.3.2. Partial inerting

There are numerous dust explosion mitigation methods practiced in industries. To minimize the risk of a dust explosion, a common industrial practice is to inert combustible dust processes with a non-reactive gas [3, 14]. Inerting is a common practice in the chemical industry for reactors, grinding, mixing processes, vessels, silos, mills, filling facilities, and dryers [2, 14]. For combustible dust processes, often designers and operators fully inert the process or use no inerting at all (all-or-nothing approach). This decision is influenced by the value of the MIE and the equipment's ability to be effectively inerted. The decision to completely inert the process (100% nitrogen atmosphere) can be hazardous and comes with the risk of asphyxiation and proper

precautions must be taken during its implementation. It is a myth, assumed by many that complete oxygen removal is essential to prevent dust explosions [15-16].

Partial inerting can be used as an intermediate inerting technique, where, rather than complete oxygen removal, the oxygen levels are reduced by substitution with an inert gas (e.g. nitrogen, carbon dioxide, argon) such that the MIE of the dust is significantly raised, thereby substantially reducing the probability of ignition [17]. Some of the many advantages of partial inerting are: cost effectiveness, improved safety with regard to the asphyxiation hazard posed by complete inerting, improved product quality for products requiring oxygen, and reduced explosion vent area [17-18].

Following this, a few studies have explored the concept of partial inerting [19-21]. Hoppe and Jaeger have used the term partial inerting and discussed its implementation on an industrial scale [14]. Eckhoff has emphasized on partial inerting as an important dust explosion mitigation consideration [17]. Studies conducted by Glarner [22] and Glor and Schwenzfeuer [19] have experimentally confirmed that a slight reduction in oxygen can markedly change the Minimum Ignition Energy (MIE) of combustible dust clouds. Devlikanov *et al*. observed that the rate of pressure rise of a dust cloud explosion (K_{st}) varied linearly with the oxygen content [23]. The slight reduction in the oxygen content in many studies has been observed to significantly decrease ignition sensitivity and combustion rate of dust cloud. Thus, partial inerting is a relatively newer concept for dust explosion mitigation and has a wide application potential in industry. While there is literature on partial inerting, comprehensive understanding of the effect of partial inerting on the dust explosion parameters is required.

1.3.3. Partial inerting MIE testing

In order to understand the influence of oxygen content on MIE of dusts, it is important to understand the dust explosion mechanism. Heat from ignition source melts and vaporizes the dust particle. The vaporized dust particles undergo the combustion reaction with the oxygen present in the atmosphere. When oxygen content in atmosphere or surrounding is reduced, more energy is required for vaporization and reaction of the dust particles [24]. The MIE required to ignite combustible dust increases with reduction in oxygen content, making it more difficult for the dust to undergo combustion reaction.

The earliest record of effect of inert gas (nitrogen) on MIE was reported by Glarner [22]. Glor and Schwenzfeuer experimentally investigated the effect of changing the oxygen content on the MIE for a number of common combustible substances [19]. Additionally, they proposed a model to describe the MIE behavior of any dust as a function of the oxygen concentration.
Precise measurement of the MIE is critical in determining the likelihood of a dust explosion. Several partial inerting studies have experimentally investigated the effect of oxygen content on MIE for various dusts [19, 22, 25-26]. The nature of the MIE-oxygen relationship is dependent on the type of dust. While some dusts have an almost linear MIE-oxygen relationship, others seem to vary nonlinearly.

MIE measurement of combustible dusts is conducted by following standard test procedure ASTM E2019-03 [27]. A number of commercially available devices for MIE testing through different manufacturers follow this test method for MIE testing. The MIKE3 device is one of the standard devices used by experts worldwide for decades to conduct MIE testing of dust clouds [19, 25-26, 28-32]. If partial inerting tests are conducted in MIKE3 device employing standard test method, the composition of the gas used for dispersion differs from the atmospheric air present in

the tube. This difference in composition, result in MIE measurements at a different oxygen composition than desired. However, if we deviate from the standard test method, the MIE tube is purged with the gas composition which is similar to that used for dispersion. This change in test procedure, though minor, can significantly affect the measurement of MIE values depending on the atmosphere in which MIE measurements are conducted (see Figure 3). To date, investigations in the area of partial inerting have mainly focused on the impact of nitrogen on MIE values rather than the experimental method used.

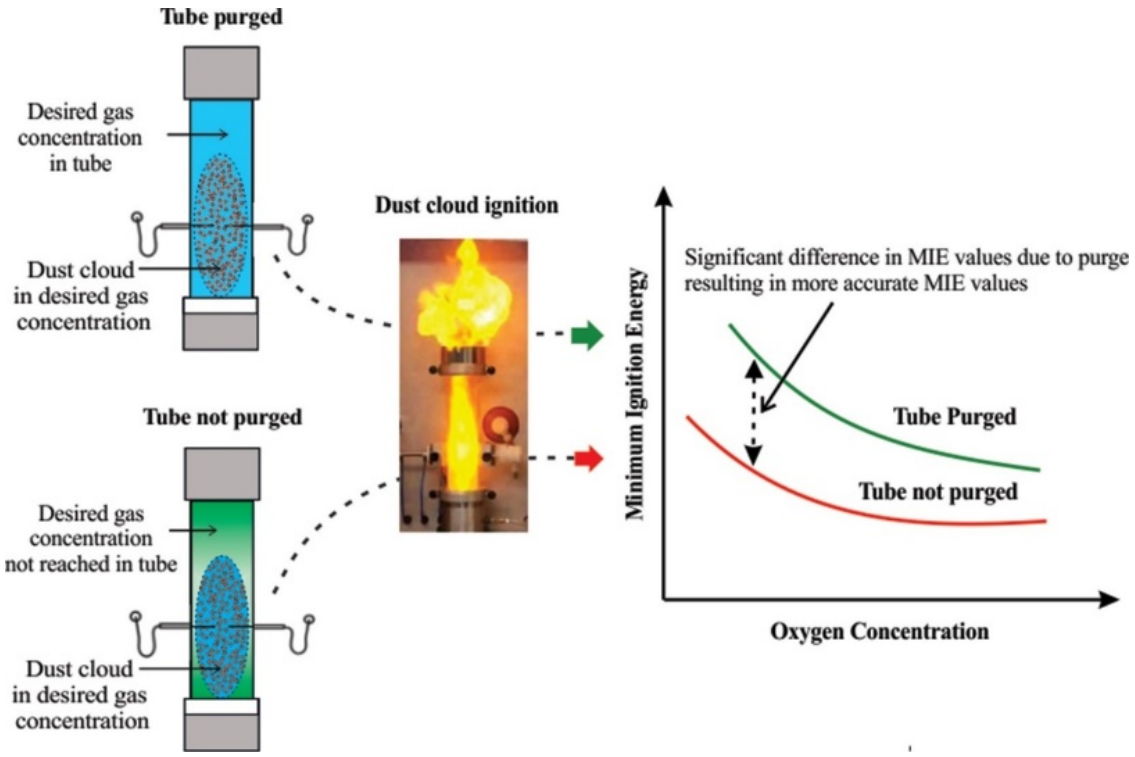

Figure 3 : Importance of tube purging in MIE testing [33]

Several partial inerting studies have been conducted where tube pre-purging has not been mentioned while testing. Some researchers have only briefly mentioned maintaining oxygen-nitrogen compositions in the Hartman tube consistent with the gas used for dust dispersion [25-26]. Ackroyd *et al*. filled the tube near the electrodes before testing [25], while Choi *et al*. reported the implementation of a purge through a small opening in the lid assembly at the top of the device [26]. However, the experimental details and specifications of the employed purging techniques and their effectiveness have not been discussed in previous works and needs to be investigated.

This improved MIE test method of purging the tube before testing can further be extended to hybrid dust-combustible gas system. While, MIE is a parameter associated with combustible dust in oxygen- nitrogen atmospheres, for hybrid explosions, the hybrid MIE can be described as the lowest energy required to ignite a combustible dust-flammable gas cloud [34]. In literature, several hybrid dust explosion explosion studies with various different combinations of combustible dust and flammable gas [35-37]. While these studies investigated hybrid MIE testing, none of these have conducted testing by pre-purging the Hartmann tube before the dust dispersion and ignition, which is an important step in obtaining accurate MIE results [38]. It can be estimated that pre-purging the tube for hybrid systems can result in relatively more conservative MIE values. Therefore, it is important to investigate the influence of the effect of purging the tube before MIE experimentation in order to obtain precise MIE data for combustible dust systems in inerted atmospheres and hybrid dust systems which are often encountered in solids handling and processing industries.

1.4. MIE prediction

Experimental testing of ignition characteristics of combustible dusts can be an expensive and time consuming process. In process industries, when designing a process for any particular

material, it is essential to know the MIE - the minimum amount of energy which can result in ignition of that material. Prediction of MIE of combustible powders can hasten this process where testing of such dusts can be circumvented and decisions can be made solely based on the prediction results. Accurate prediction of MIE will be very useful in simulating real situations in industries and help in avoiding ignition sources above a certain energy range in the facility. Therefore, there is a need for development of models which can accurately predict the ignition behavior of combustible dusts.

One of the earliest mathematical equations relating the MIE of dusts to various dust parameters has been reported by Jost (1950) [39]. This equation is based on several assumptions some of them being, spherical shape of dust particles and flame temperature > 1000^{o}C. Based on this equation, Kalkert and Schecker conducted a comparison between experimental and theoretical MIE variation with particle diameter for some dusts which indicated good agreement [40]. Thus they have emphasized in their work the dependency of MIE with the cube of particle diameter for any dust. This observation has been used in literature but is known to hold true only for certain dusts. Gubin and Dik have modeled the spark ignition of combustible dusts. The MIE of dusts due to spark ignition was found to be a function of thermal effects of reaction, mass concentration of dust, particle diameter, specific heat of gas and dust [41]. Bidabadi *et al*. have developed a thermal model to estimate the flame propagation speed in various oxidizer concentrations [42]. They have investigated flame speed as a function of particle diameter and minimum ignition energy as a function of dust concentrations for various particle diameters.

MIE being a probabilistic parameter, a number of statistical studies have been conducted [3, 43-44]. Wähner *et al*. have used liner regression for MIE determination of hydrogen, ethane and propane [44]. Bernard *et al*. in their work, have used Langlie test method for MIE

determination for different dust and gas systems [43].

It was observed that while some of these models have been developed from fundamental considerations, most models have used substantial amount of experimental data for their development. Moreover, the existing fundamental mathematical models have made numerous assumptions to come to a single equation that can predict the MIE of any dust as a function of its parameters. Thus, a number of fundamental and empirical MIE prediction models for dusts have been proposed in literature [17, 19-22].

1.4.1. Quantitative Structure-Property Relationship (QSPR) for MIE prediction

An extensively utilized mathematical tool for correlating material properties to its molecular structures is Quantitative-Structure Property Relationship (QSPR) [51-53]. Several studies have explored Quantitative Structure-Property Relationship (QSPR) models relating molecular structures to the physical properties of compounds such as boiling point [54-55], flash point temperature [56] and auto-ignition temperature [57-58]. Further, QSPR has also been employed to investigate the reactive properties such as onset temperature and energy of reaction [59].

MIE prediction models for combustible dusts giving consideration to the molecular structure of compounds need to be investigated in detail. For dusts, an alternative approach using QSPR by Reyes *et al*. predicted explosion severity parameters (K_{st} and P_{max}), but did not investigate MIE [45]. While, Wang *et al*. have developed a QSPR model which considers molecular structure for MIE prediction of gaseous and liquid hydrocarbon fuels, this model does not predict MIE for combustible dusts [46,50]. The combustion mechanism and the modeling efforts required for dusts are much more complex than gases and liquids. For gases and liquids, individual molecule models can often sufficiently explain bulk properties. However, for dusts, the

interaction energies between individual molecules must also be considered [47-49], which is absent from previous studies. In 2016, Baati has developed local and global MIE prediction models of dusts, liquids and gases [60]. Their most robust prediction equation for dusts in this study consisted of 27 parameters, making it infeasible due to the large number of input parameters required in the model. In addition, in their study they have mentioned that there could be no conclusive outcome whether molecular structures influence material MIE and have not explained the logical correlation of the descriptors to MIE.

While MIE point values are important, most often the range of MIE is reported in literature (For example, MIE of a certain compound is reported to be in a range from 300 mJ – 1000 mJ). The MIE measurement devices available generally allow MIE testing only for certain energy ranges. In solids handling facilities, dust MIE range instead of point MIE value are taken into account while planning dust explosion prevention and protection measures. Therefore, it would be useful to develop a classification model instead of a regression model for MIE prediction of combustible dusts which can inform about the MIE range the dust will lie in based on the dust's molecular structure information. Such classification model for dusts is currently not explored in literature. Thus, MIE prediction for combustible dusts with consideration of their molecular structure and properties needs to be thoroughly investigated further.

1.4.2. Machine learning methods for material property prediction

Machine learning has been implemented to identify trends and correlations in data for predictions in finance, pharmaceutical and chemical industry [61-63]. Machine learning algorithms such as Random Forests (RF), Decision Trees (DT), Artificial Neural Networks (ANN), Support Vector Machines (SVM) and k-Nearest Neighbors (KNN) have been used to develop QSPR models [64-74]. In this research, QSPR has been combined with machine learning to

develop MIE prediction models. While there are many machine learning algorithms available, this section discusses only those few that were implemented in this research. Decision tree is a supervised machine learning algorithm which allow a top-down visual representation and easy interpretability of the dataset [75-76]. It enables classification of dataset into a flow chart like representation (see Figure 4). A decision tree starts at the tree root and splits the data into initial node of the decision tree enables decision making to move to the next node until eventually a final pure leaf is reached. At each step the attributes and the values that the decision tree selects are made by reduction of entropy which is the measure of uncertainty in a random variable. The samples at each node belong to the same class. A collection of several decision trees is included in the Random Forest algorithm which makes the RF algorithm more robust for model development. Decision Trees and Random Forests can be used for both regression and classification problems.

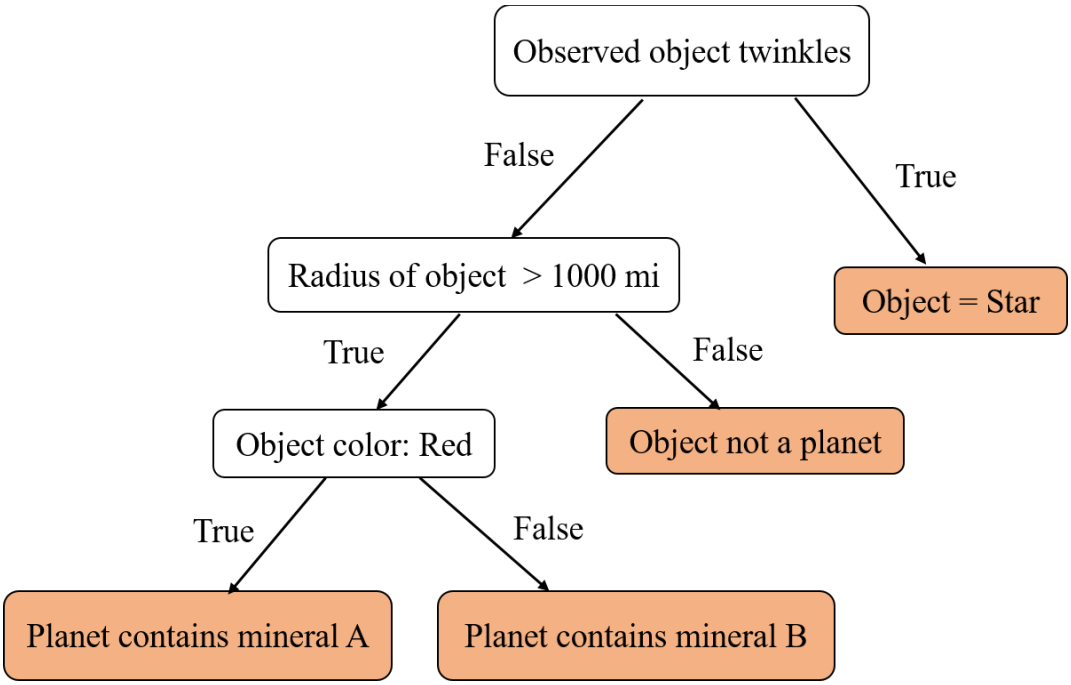

Figure 4 : Example of decision tree representation of data observed through a telescope

Another machine learning algorithm implemented in this research is the Artificial Neural Networks (ANN) which consists of a different layers and nodes (see Figure 5) [76]. Each node has one or more inputs and a single output. Each input has a weight associated with it and all the weights are summed and sent to an activation function that determines the output. Thus, the contributions from each starting node is considered in the final output.

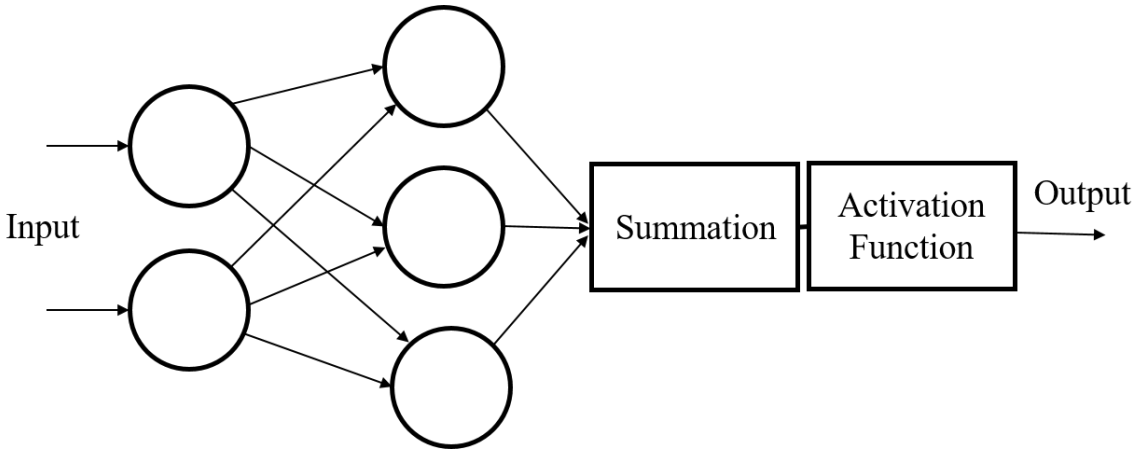

Figure 5 : The input-output representation in Artificial Neural Networks (ANN)

Combustible dust MIE prediction using QSPR through RF, DT and ANN models has not been successfully implemented in literature before. Therefore, exploration of RF and DT algorithms for QSPR model development can help in identifying the most important parameters that influence MIE and assist in graphically represent this information to make it more interpretable.

1.5. Problem statement and objectives

Based on the above literature review, it is evident that there are several gaps that need to be addressed in dust explosion testing and prediction. Precise combustible dust MIE measurement and prediction will assist in comprehensive understanding of the risks involved with dust explosions and eventually aid in prevention of such incidents. Therefore, the primary objective of this research will be to tackle the problem of more accurate MIE measurement by designing an add-on device to the existing testing device and advancing the exiting test procedure used for MIE testing. Thereafter, the MIE prediction models employing molecular modeling will be developed.

The following are the main objectives of this research:

1) Develop equipment and technique for accurate partial inerting MIE testing

As observed from literature, although MIE testing has been conducted by researchers in Hartmann tube for a long time, the partial inerting MIE testing standard is not yet defined and lacks accuracy in testing. An add-on purge device to the existing MIKE3 device has been designed to enable more precise partial inerting testing. The standard experimental test procedure for partial inerting MIE testing has been improved to include purging the MIE tube before dust dispersion and ignition. Purge time, a parameter which has not been defined in MIE testing previously has been investigated in this research.

2) Effect of partial inerting test method on MIE measurement

MIE-O_2 relationships obtained experimentally through ASTM E2019-03 test method and improved test method have been compared. The importance of employing top purge in MIKE3 device tube before MIE testing which results in precise determination of MIE values has been demonstrated. A similar methodology was extended to exhibit the importance of improved test method on hybrid dust MIE measurements.

3) Molecular structure based model development for MIE prediction

As per above literature review, limited fundamental and empirical equations for MIE prediction exist in literature which have been observed to deviate significantly from experimental MIE values. Applying machine learning algorithms for QSPR modeling of MIE of combustible dusts needs to be explored further. Thus, a molecular structure based model using machine learning techniques have been developed for MIE prediction through this objective.

This research focuses on accurate MIE measurement in partially inerted atmospheres. A purge add-on device has been designed and an improved MIE test method has been proposed in this

work. Thereafter, this work goes on to demonstrate the effect of improved test method on the measured MIE. The partial inerting curves of several combustible dusts were generated and an equation for predicting MIE with changing oxygen concentration has been developed. In addition to experimental MIE testing and measurement, this research has also focused on MIE prediction through molecular structure information. Thus, this research has employed both experimental and modeling approaches to address some of the concerns involved with MIE testing and MIE prediction of combustible dusts.

2 IMPROVED PARTIAL INERTING TEST METHOD FOR COMBUSTIBLE DUSTS AND ITS CFD VALIDATION*

2.1 Introduction

For certain combustible dusts, MIE testing can be very expensive due to limited availability of dusts or not feasible due to limited and discrete range of MIE testing devices. In such cases, consistently collected and accurate data sets for determining the MIE-oxygen relationship are necessary for predicting the dust MIE at any desired oxygen concentration without the need for actual testing. This section has used a modified MIKE3 device to develop and refine the fundamental understanding of the test method for partial inerting MIE testing. The goal of this study was to examine the purge time required to produce partial inerting MIE measurements at known oxygen concentrations. In addition, an ANSYS Fluent CFD model was developed to help guide the experimental efforts and provide a validation of the modifications and method used. The CFD simulation of the purge flow is an important step as it allows for an estimated purge time required at any oxygen concentration, ensuring that the desired oxygen content is achieved in the Hartmann tube with minimal consumption of specialty gases.

---

*Parts of this section have been reprinted with permission from: P. Chaudhari, B. Ravi, P. Bagaria, C. Mashuga, "Improved partial inerting MIE test method for combustible dusts and its CFD validation", Process Safety and Environmental Protection 2019, vol. 122, pp. 192-199, 2019, Copyright 2019 by Chaudhari et al.[33] and P. Chaudhari, and C. Mashuga, "Partial inerting of dust clouds using a modified standard minimum ignition energy device", Journal of Loss Prevention in the Process Industries, vol. 48, pp. 145-150, 2017, Copyright 2019 by Chaudhari and Mashuga [38].

Additionally, the experimentally verified CFD model in this study would assist in extending this experimental test method (including purge time) to other combustible dust gas systems such as hybrid systems (flammable gas-air-combustible dust mixtures).

2.2 Materials

The importance of the variability in oxygen content used for MIE measurements is observed in Figure 6. The vertical red dotted lines show the narrow oxygen variability of Ultra High Purity (UHP) air, and the vertical green dashed lines show the potential variability in zero grade air. For dust C, the change in the MIE with oxygen concentration around 21% oxygen is insignificant. Therefore, the selection of gas used in testing will not dramatically affect the measured MIE values. However, the MIE for dust A and dust B can vary significantly with small changes in oxygen concentration and have a steep slope in the range of composition of zero grade air in Figure 6. Therefore, a high gas composition variability is deemed undesirable for testing, since the MIE values may change significantly for certain substances whose MIE is highly sensitive to oxygen content. The gas compositions used in this study were accurate to within 1% of the oxygen composition, ensuring the gas compositional variability was negligible for this study. Additionally, the gas strictly adhered to the standards of < 0.1 ppm carbon dioxide and < 0.36 ppm moisture. The gas compositions used in this study were oxygen: 12.03 %, 13.00%, 14.00%, 15.00%, 16.11%, 17.98%, and 21.05 %, with nitrogen making up the balance.

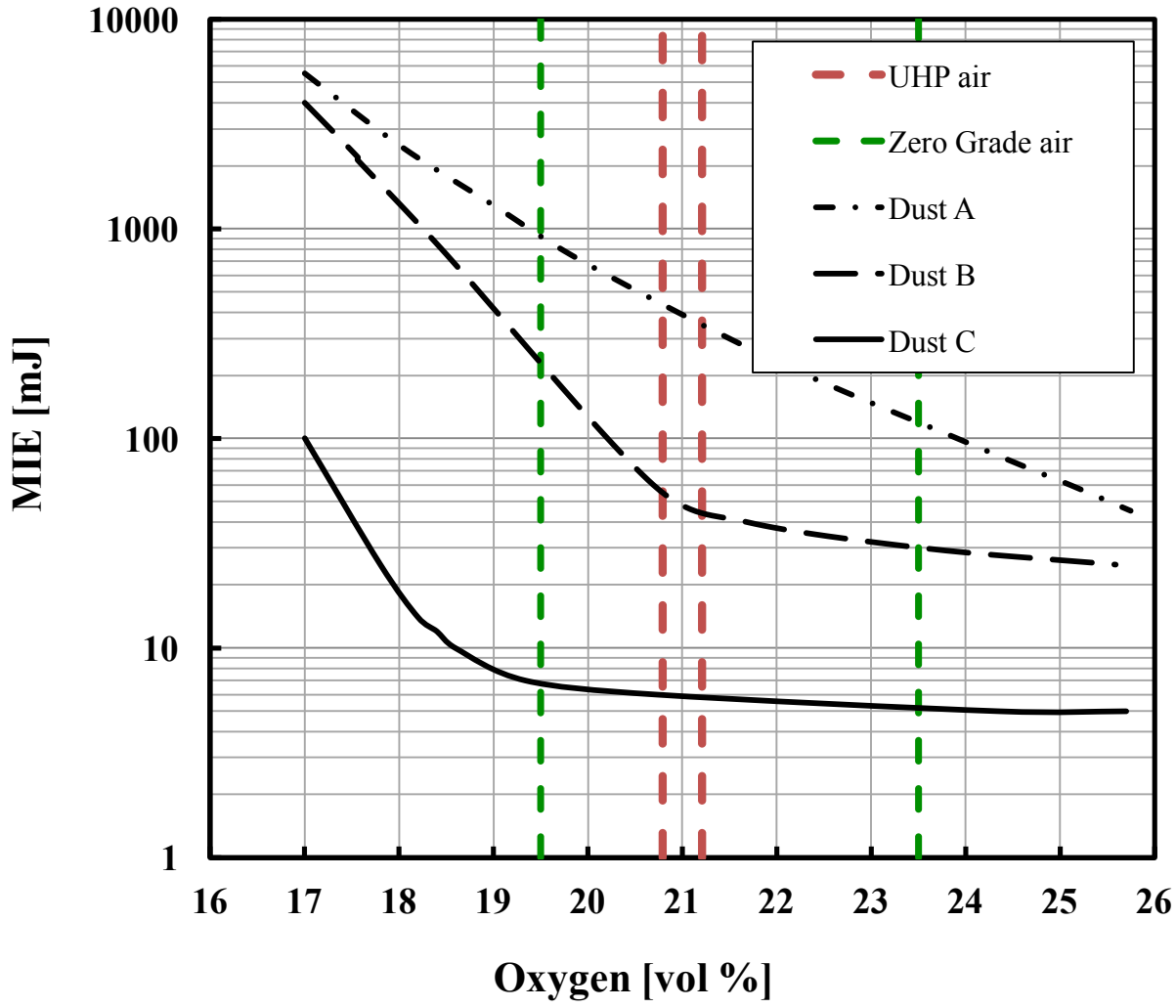

Figure 6 : Influence of variability in oxygen concentration of dispersion gas on dust MIE [33]

2.3 Methodology

2.3.1 MIKE3 device modification

The MIKE3 MIE device observed in Figure 7 is one of the devices used worldwide for testing the ignition sensitivity of combustible dust clouds. In the MIE device, at the bottom of the glass Hartmann tube there is a dust dispersion nozzle around which the dust is placed for testing.

A dust dispersion in the tube is formed by the release of air from a 7 barg reservoir which flows through the nozzle. After dispersion, an adjustable delay occurs, followed by the delivery of an ignition energy by a capacitive spark between the two tungsten electrodes. The device allows MIE measurement at energy levels of 1, 3, 10, 30, 100, 300, and 1000 mJ. The ignition time delay can be adjusted manually in the device at 90, 120, 150 and 180 ms. The inductance in the spark gap circuit can be adjusted to either 0 mH or 1 mH. Despite having these variables, the current MIKE3 MIE device has not been designed with a provision to purge the tube prior to dust dispersion for partial inerting MIE testing.

Figure 7 : Minimum Ignition Energy Device (MIKE3) [33]

To overcome this limitation, an innovative modification of the device was made which utilizes a single gas source of desired composition to purge the tube and then drive the dispersion. Figure 8 shows a schematic of the MIE device and highlighted modifications. Gas from a cylinder is split with one segment providing purging of the 1.2 L Hartman tube from the top through a purge device and the other segment connects in the standard way to the MIE device for dispersion. A needle valve on the flowmeter is used to regulate the purge gas flow to the Hartman tube. Figure

8 shows the placement of the purge device in the MIKE3 device. It is placed between the lid components of the original MIKE3 device.

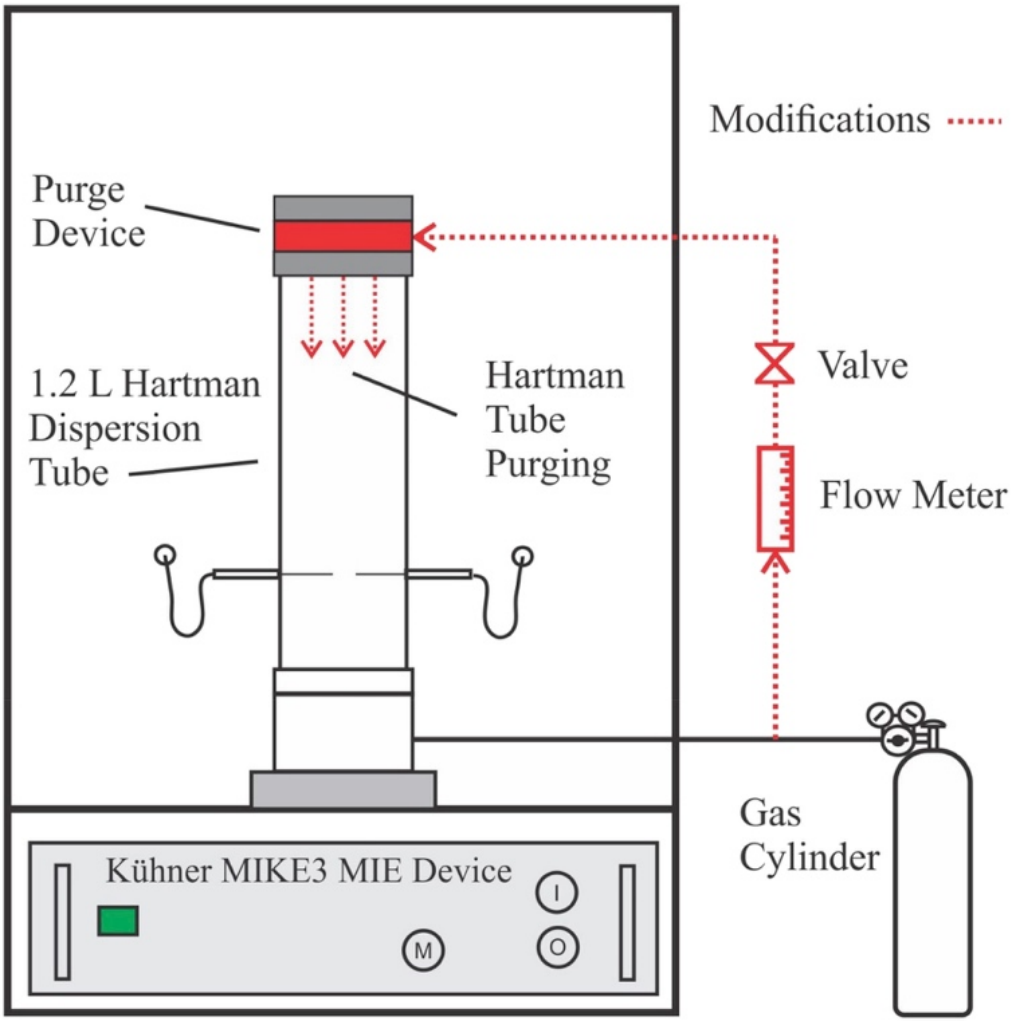

Figure 8 : Purge device and modification to a Minimum Ignition Energy apparatus [38]

The purge device seen in Figure 9 essentially consists of two plates, sandwiched between the two lid parts. The lower plate has a gas inlet which opens into a flow channel running along its

circumference with small openings. These openings/ holes facilitate gas flow into the Hartmann tube.

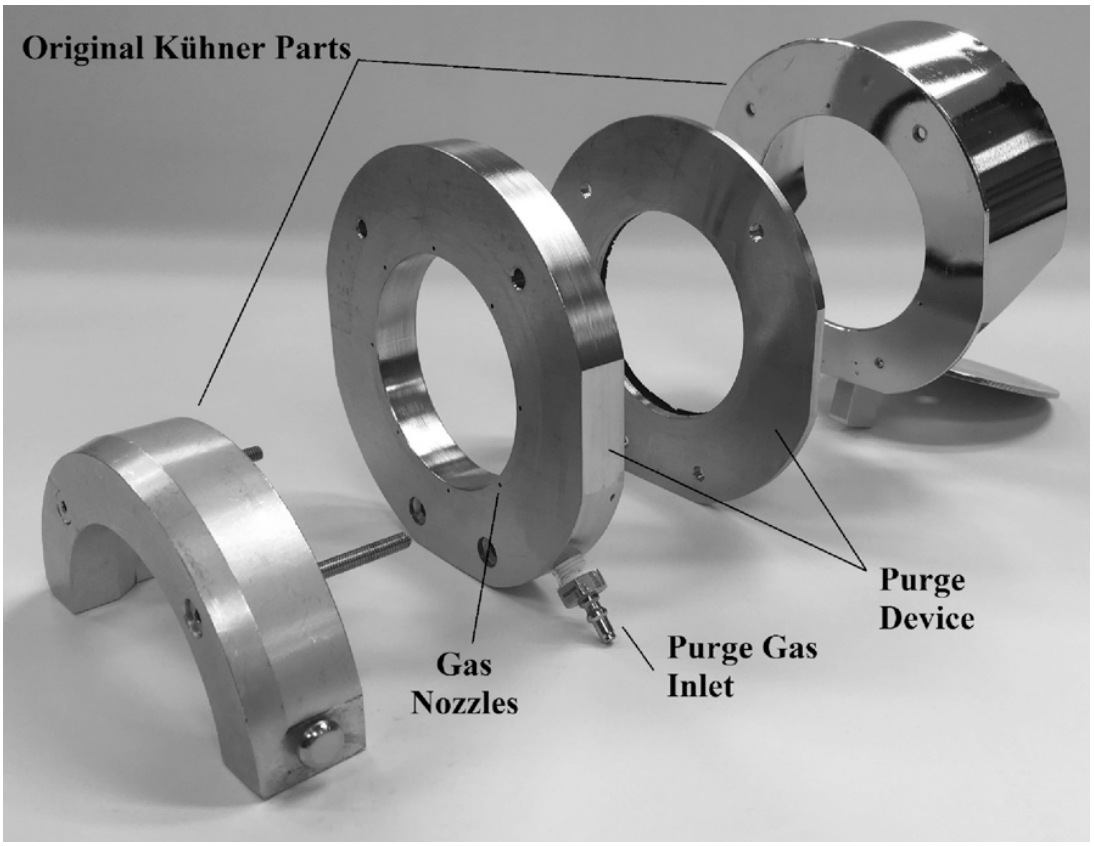

Figure 9 : MIE purge device insertion between original Kühner parts [38]

The purge device is fabricated from corrosion resistant 316 stainless steel. A seal surface was added to the MIKE3 lid to prevent any atmospheric oxygen from entering the tube. The importance of the seal is discussed further in the results section. A provisional patent for the purge device described in this work has been filed [77].

A criterion for proper design is reduced amount of leakage out of the add-on device, uniform flow of gas mixture into the Hartmann tube and uniform mixing of oxygen in the tube

during the purge flow. Uniform distribution of oxygen in the tube is an important design aspect determining the number of openings required for purging. Further, convergence of the experimental oxygen concentration with the simulated oxygen concentration would also reinforce validity of the purge device design.

In general, partial inerting testing in the MIKE3 MIE device can follow standards such as ASTM E2019-03 (ASTM E2019-03, 2013)[27] or the European Standard (EN ISO/IEC 80079-20-2) [78]. In this work, partial inerting testing by purging the MIE tube with test gas prior to experimentation for niacin, lycopodium, calcium stearate and anthraquinone was conducted to determine the MIE-O_2 correlation for dusts.

The purge flow rate of 10 L/min was maintained for 1 minute in order to ensure the 1.2 L Hartmann tube is completely purged prior to dust dispersion and ignition. Purge time has been discussed in detail in section 2.3.2. Even though the preignition atmosphere in the tube was controlled, the lab temperature and humidity were monitored during every test and were maintained at 70 +/- 5 ^{o}F, and 50 +/- 5 % relative humidity.

2.3.2 Oxygen concentration and purge time measurements

Before experimentation, the Hartmann tube initially contains ambient atmospheric air with variable oxygen and humidity levels which are known to influence the MIE measurement. Because of this the tube is purged from the top at 10 L/min to obtain the desired oxygen-nitrogen mixture. It is important to determine the time required for the desired gas purge mixture to displace the initial ambient atmosphere in the tube, as this determines the purge time that is required for every MIE test. In the range of oxygen levels used in this study (12.03 - 21.05 %), the maximum purge time will occur when the purge gas containing 12.03 % oxygen displaces the initial ambient air, since this is the largest difference in the oxygen concentrations.

In order to determine the purge time, a polycarbonate tube was fabricated with the same dimensions as the Hartmann tube, including openings for the oxygen sensor. While the purge gas filled the tube from the top at 10 L/min, an ammeter was used to measure the current output from the oxygen sensor at the lowest opening (point 1) in the tube (see the oxygen sensor measurement setup in Figure 10). This current corresponded to the oxygen content present at that time at point 1. Therefore, the time required to reach the desired oxygen content of 12.03% at point 1 was determined, which is the maximum purge time required for testing. Similarly, the oxygen sensor setup was used to determine oxygen concentration as a function of time at varying heights (points 1, 2, 3) in the tube during the 12.03 % oxygen purge.

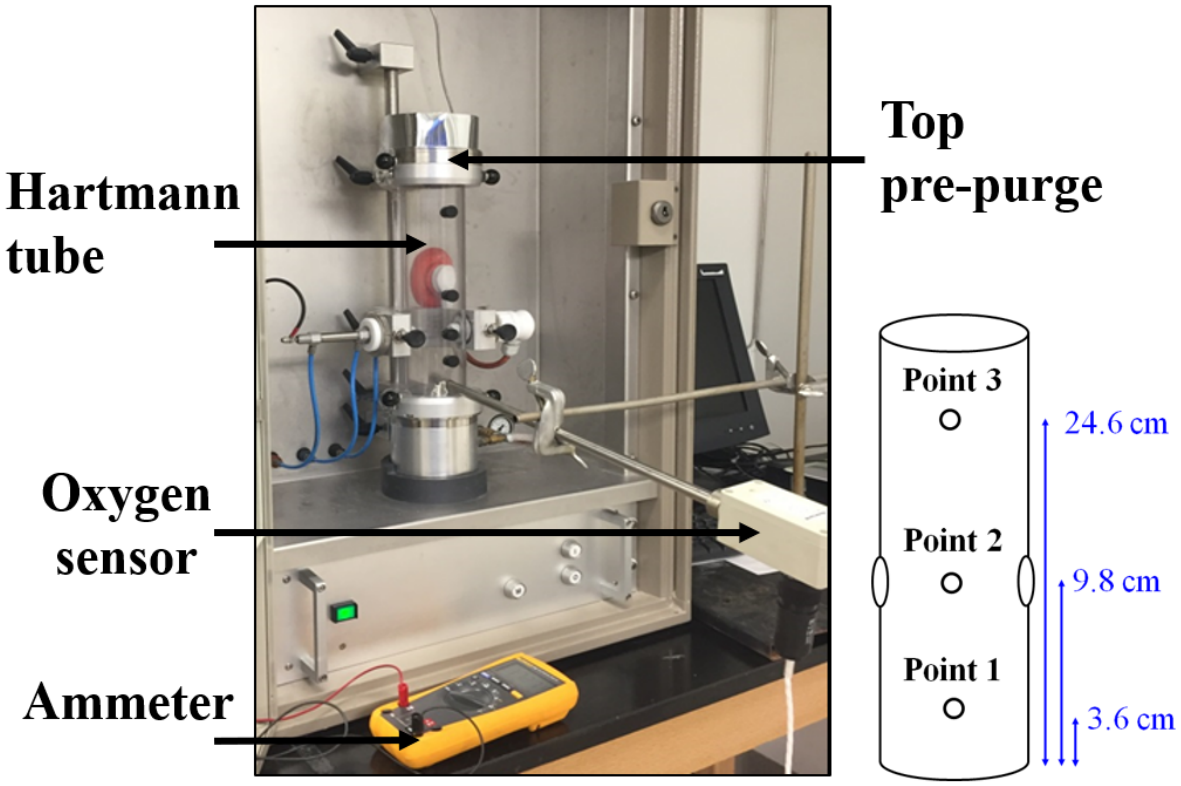

Figure 10 : Oxygen sensor measurement setup [33]

2.4 ANSYS Fluent CFD simulations of purging

The purge gas (12.03% O2, 87.97% N2) flow into the 1.2 L Hartman tube was modeled using ANSYS Fluent version 18.2, utilizing the Fluent solver for simulating the fluid flow and species mixing [79].

2.4.1 Model geometry

The tube was built in the Design Modeler representing the actual geometry. The 8 openings at the top of the tube serve as inlets for the purge gas and a circular slit aligning with the circumference of the upper wall served as an outlet that represented the flap valve hardware to maintain atmospheric pressure inside the tube during purging (see Figure 11).

2.4.2 Grid and mesh independence

The meshing was carried out to maximize the polyhedral cells inside the tube domain which are suitable for modeling computational fluid dynamics for the compressible flow with improved volume occupancy, solver convergence and accuracy over other types of cells. A three-dimensional structured and unstructured portion of grid was generated (see Figure 11). The purge gas entry points and the electrode positions were unstructured grid. Different meshes were evaluated for mesh sensitivity analysis by monitoring the oxygen concentration at different mesh sizes. The mesh (as shown in Figure 11) had four zones divided into three portions for monitoring purposes viz. upper, middle and lower portions.

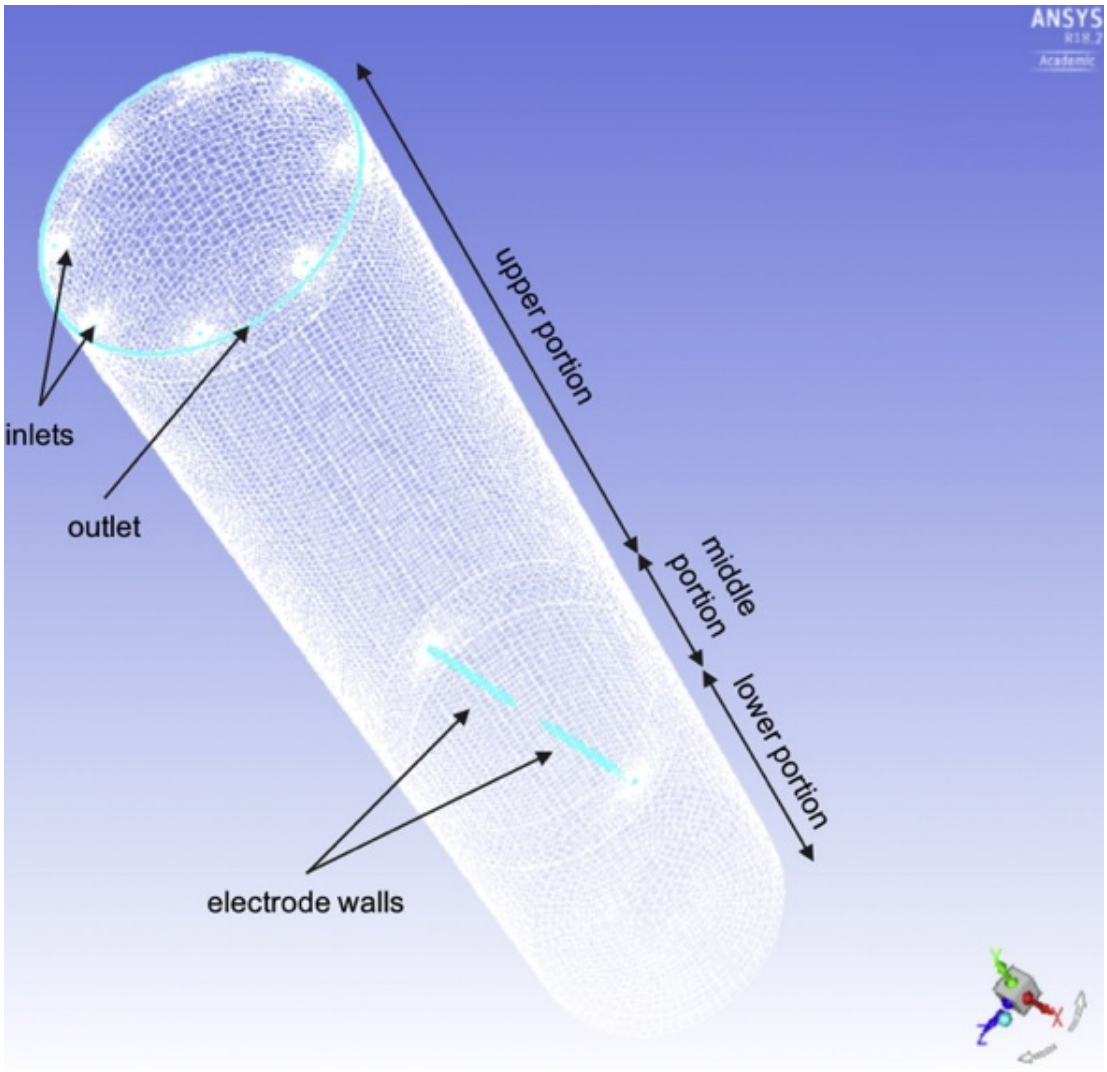

Figure 11 : Computational grid with electrodes developed in ANSYS Fluent [33]

Monitor points were set to obtain a volume average of the oxygen mole fraction in each of these portions. A coarse mesh with ~1.0 million nodes, a fine mesh with ~1.5 million nodes and a finer mesh with ~2.2 million nodes were generated and solved to monitor the oxygen mole fraction as part of the mesh independence study.

The mesh shown in Figure 11 was finalized through rigorous trial and error by checking mesh independence, convergence and stability of the solution. The fine mesh was found to be a

valid point to stop refining since the error percentage in volume average of oxygen concentration inside the tube was less than 0.2% with respect to all the time steps when compared with a finer mesh and thus reaching mesh independence to obtain the actual solution. This mesh comprised of 1,523,492 (~1.5 million) mesh nodes where the equations were solved.

2.4.3 Boundary conditions

A species transport model was used to simulate the mixing of the oxygen-nitrogen purge gas mixture flowing through the inlets into the ambient atmosphere inside the tube. The inlet boundary condition was a mass flow inlet type (0.2 g/s at each hole), and the outlet boundary condition was a pressure outlet type (to maintain atmospheric pressure inside the tube).

2.4.4 Solution methodology

The fluid flow equations were discretized for the Hartmann tube using the finite-volume method. The spatial discretization of mass, momentum, species transport and energy equations were third order with Monotonic Upwind Scheme for Conservation Laws (Third-order MUSCL) providing the maximum accuracy possible. A real gas Redlich-Kwong equation of state was used for the gas mixture since it best represents the oxygen-nitrogen system. A second order implicit scheme was used for transient formulation with a time step of 0.1 s.

The simulated purge time found by the CFD model to obtain 12.03% oxygen was compared to the experimentally determined time using an oxygen sensor (discussed in section 2.5).

2.4.5 Flow model

The purge gas underwent a sudden expansion as it passed through the 8 inlet holes at the top of the Hartman tube. At the inlets, the compressible gas initially had a higher velocity, and then loses kinetic energy during the sudden expansion process immediately after entrance into the tube. The maximum Reynolds number ($Re = 1591$) reached by the flowing air mixture was at the

inlets. The flow was considered to be laminar if Reynolds number, $Re < 2000$. The expansion leads to a lower Reynolds number which justifies the use of the laminar viscous model for the fluid flow throughout the computational domain.

2.5 Results

2.5.1 Experimental purge time required for different O_2 concentrations

The setup discussed in section 2.3.2 was used for flowing the oxygen-nitrogen mixtures through the Hartmann tube. The time required to reach a uniform oxygen concentration in the tube *i.e* the time required at the lowest point to reach the desired oxygen content was measured at each different oxygen-nitrogen mixture. The purge time required for different oxygen concentrations are observed in Table 3. The time required at the lowest point in the tube to reach the desired flow oxygen content is more for 12% O_2, balance N_2 than that required for 21% O_2, balance N_2. This is understandable as the Hartmann tube already contains atmospheric oxygen content ~ 20.8 vol. % O_2 requiring longer purge times the further the flow concentration is from this value. Thus, the experimental time required to reach the oxygen was observed to decrease with increasing oxygen content.

Table 3 Experimental purge time required at different O_2 concentrations in purge

O_2 % in the purge	Experimental time required to reach O_2 % (s)
12	39
15	38
16	34
18	31
21	15

2.5.2 Experimental and simulated oxygen drop in tube during purging

The decrease in the oxygen concentration in the Hartmann tube during purging was monitored using an oxygen sensor at points 1, 2 and 3 in the tube and is observed in Figure 12. Experimentally, the time required to reach the desired oxygen concentration of 12.03% was observed to be 39 ± 3 seconds. Thus, the experimental measurements (Figure 12) confirm that the purge time of ~ 21 seconds [38] is not sufficient and can result in higher oxygen concentrations than desired.

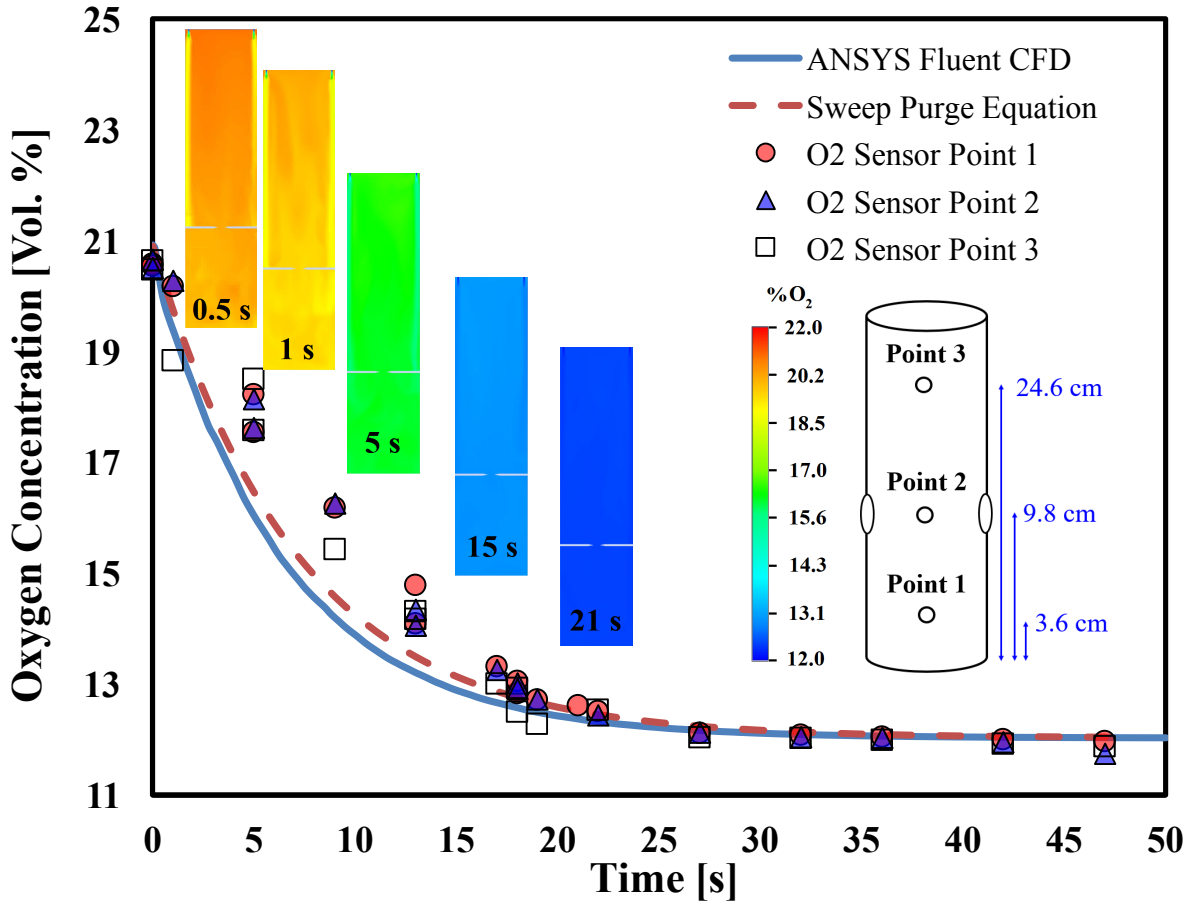

Figure 12 : Oxygen concentration during purge (12.03 % O_2, 87.97 % N_2), ANSYS Fluent simulations showing average oxygen concentration and the sweep purge model [33]

An average of the oxygen concentration simulated by the CFD at the points 1, 2 and 3 in the tube was calculated. The CFD model in Figure 12 shows this averaged oxygen concentration as a function of time. The oxygen concentration drops from 20.9 to 12.05 volume percent in 39 seconds when purged with 12.03 volume percent oxygen. Thus, the oxygen concentration obtained through the CFD model agrees with the experimentally measured oxygen content. Figure 12 shows CFD concentration distributions in the MIE tube as a function of time. There is considerable mixing of purge gas in the tube due to the purge system design and flow rate for up to 5 seconds.

After this time the gas composition becomes uniform with a gradual change in oxygen concentration throughout the tube.

The sweep through purge equation [80] was used to calculate the oxygen concentration in the Hartmann tube as a function of time:

$$t = \frac{V}{Qv} \ln \frac{(C_1 - C_0)}{(C_2 - C_0)} \quad (1)$$

where, t is time (s), V is Hartmann tube volume (m^3), Q_v is the purge volumetric flow rate (m^3/s), C_1 is the initial oxidant concentration in the tube (mol/m^3), C_0 is the purge gas oxidant concentration tube (mol/m^3), C_2 is the desired oxidant concentration after purging (mol/m^3).

The assumptions for sweep through purge equation are: (i) the volumetric flow rate of the inlet and outlet streams are equal into the tube; (ii) the purge gas always remains at atmospheric pressure and (iii) perfect mixing inside the vessel.

Ideally, sweep through purging should be conducted with the purge gas and the exit location located as far apart as possible to avoid short circuiting the purge. In this work the entrance and exit are near the top of the tube. The results agree well with the CFD model and the experimental measurements. However, both the CFD and sweep equation predict lower oxygen concentration in the first 15 seconds of purging. This difference is likely due to the fact that the sweep through purge model and the CFD equations assume the system to be perfectly mixed, while in reality it is less than perfect. More importantly, after 15 seconds the CFD, sweep equation, and the experimental measurements have strong agreement.

The close agreement between the CFD model and the experimental oxygen measurements also suggest that the add-on purging device used in this study and described by Chaudhari and Mashuga (2017) is properly designed and operated [38].

An important conclusion can be made from the modeling and oxygen measurements. For the oxygen concentrations in this study, the tube needs to be purged for at least 40 seconds before MIE testing. It is important to know the minimum purge time required while conducting experiments as the purge time defines the oxygen content in the tube. Thus, for the range of oxygen concentrations used in this study (12 - 21.05 vol. %), the purge time for all the MIE tests was maintained at 60 seconds, which ensured the tube reached the desired oxygen content.

2.6 Summary

In this section, the first research objective of designing a device and defining a method for MIE measurements has been addressed. A novel add-on purge device to the MIKE3 MIE testing apparatus has been designed and patented. The purge time for partial inerting testing has been defined and experimentally determined for the range of oxygen concentrations used in this research. The experimentally determined purge time was compared with the sweep through purge flow equation used in literature and was found to be in good agreement with it. CFD modeling of the gas flow (O_2-N_2 mixture) in Hartmann tube was conducted which agreed well with the experimentally determined time and the sweep through purge equation.

The effective purge time for partial inerting to an oxygen concentration of 12 % was determined to be at least 40 seconds through both CFD and experiments. Therefore, to be on a more conservative side, the partial inerting tests in this research were conducted after purging the tube for 1 minute. Thus, these findings provide a basis for conducting partial inerting MIE testing for combustible dusts.

3 PARTIAL INERTING OF COMBUSTIBLE DUSTS USING A MODIFIED STANDARD MINIMUM IGNITION ENERGY DEVICE*

3.1 Introduction

Partial inerting is an important but underutilized mitigation technique in which minimum ignition energy (MIE) of a dust cloud is increased through inerting, reducing the risk of an accidental dust explosion or more accurately, a dust deflagration. This technique has wide application potential in numerous chemical and general manufacturing industries. The Kühner MIKE3 is the predominant apparatus for measurement of the minimum ignition energy (MIE) of combustible dusts worldwide. The current version of the MIKE3 device is not specifically designed to measure partial inerting minimum ignition energies. The purpose of this work is to demonstrate that a properly designed add on purge device and technique can accurately produce partial inerting MIE results with an existing MIE device.

*Parts of this section have been reprinted with permission from: P. Chaudhari, B. Ravi, P. Bagaria, C. Mashuga, "Improved partial inerting MIE test method for combustible dusts and its CFD validation", Process Safety and Environmental Protection 2019, vol. 122, pp. 192-199, 2019, Copyright 2019 by Chaudhari et al.[33] and P. Chaudhari, and C. Mashuga, "Partial inerting of dust clouds using a modified standard minimum ignition energy device", Journal of Loss Prevention in the Process Industries, vol. 48, pp. 145-150, 2017, Copyright 2019 by Chaudhari and Mashuga [38].

The purge device ensures complete purging of the Hartman dust dispersion tube with the desired gas concentration before experimentation. The same gas is then pulsed into the dispersion tube producing the dust dispersion for ignition testing. This approach leads to uniform testing conditions in the tube with respect to gas concentration which is essential for producing proper measurements. Additionally, experiments show the turbulence generated by the purging technique did not significantly affect the MIE measurements. Therefore, an important finding of this work is that purging the tube before partial inerting MIE testing results in a proper characterization of the relationship between the MIE and oxygen for the dust. The findings therefore demonstrate the need to amend existing or develop new standards for this type of dust testing. The effect of these modifications and techniques are demonstrated by the experimental determination of the partial inerting curve for Niacin (CaRo15) using the MIKE3 apparatus. This test method of purging before MIE experimentation was first implemented for conducting partial inerting tests for Niacin dust to demonstrate the difference in MIE values with and without purging method. Further, this test method was extended to conduct partial inerting testing for lycopodium, calcium stearate and anthraquinone.

3.2 Materials

Combustible dust Niacin (CaRo15), a material used for participation in the international round robin comparing minimum ignition energy devices has been used to demonstrate the effect of MIE test method on MIE values. Niacin is also commonly known as Vitamin B_3 or Nicotinic acid ($C_6H_5NO_2$) and is a favorable calibration material due to its pharmaceutical level of chemical purity, low moisture absorbance, consistent particle size, and its low MIE ($\sim$1.7 mJ) at atmospheric conditions [81-82]. The Niacin dust was obtained from Kühner AG pre-milled, homogenized and

stored in an airtight package. The dust was tested as received, as is recommended in the Kühner international round robin.

For this work, Niacin (CaRo15) dust was tested as received from Kühner in accordance with the ASTM E2019-03 standard testing procedures (ASTM E-2019-03, 2013). Before MIE testing, niacin dust was characterized for its particle size in the Beckmann Coulter Particle Size Analyzer LS 13320 device (see Figure 13), where the d_{50} was observed to be 22.21 μm as shown in Figure 14.

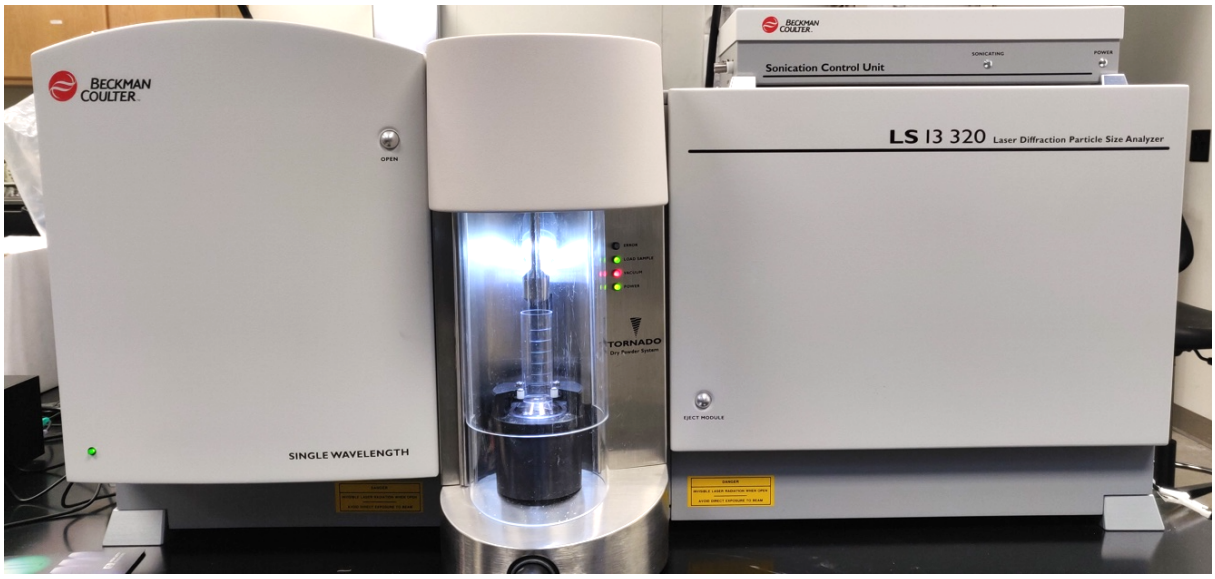

Figure 13 : Beckman Coulter LS 13 320 Particle Size Analyzer

In order to capture the MIE–oxygen behavior of different dust types, lycopodium *clavatum*, calcium stearate and anthraquinone were tested in this study. Lycopodium *clavatum* is a naturally occurring plant spore and has been used by researchers as a reference material due to its dispersibility, flowability, combustibility, and monodispersity. Its naturally occurring monodisperse size distribution (narrow range of particle size distribution) results in consistent

explosion characteristics [83-85]. Industrially relevant dusts such as calcium Stearate and anthraquinone were chosen not only because of the concerns associated with safe handling and processing, but also because their MIE values in air (O_2 = 21%) are < 10 mJ which makes them suitable for partial inerting MIE testing in the energy range of 1–1000 mJ provided by the MIKE3 device.

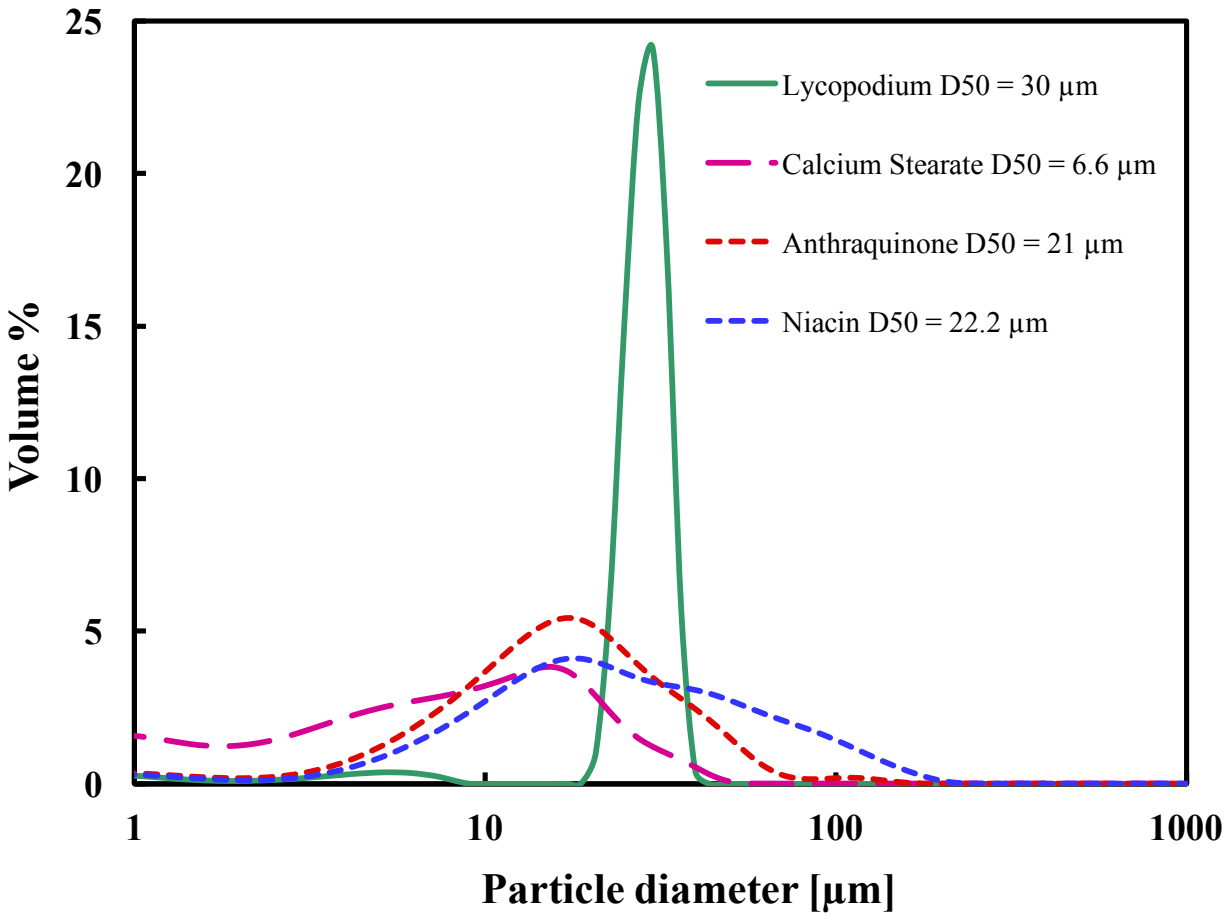

Figure 14 : Particle size distribution for Niacin d_{50} = 22.2 µm, Calcium stearate d_{50} = 6.6 µm, Lycopodium d_{50} = 30 µm and Anthraquinone d_{50} = 21 µm [38]

3.3 Methodology

3.3.1 MIE testing

This partial inerting study was conducted using the MIKE3 MIE device discussed in detail in section 2. The device consists of a Hartmann explosion tube and electrodes which generate spark in the explosion tube. The 1.2 L Hartmann tube was purged from the top at a flow rate of 10 L/min for 1 minute to control the pre-ignition atmosphere in the tube. The dust was dispersed for ignition immediately (≤ 1 second) after the stopping the purge flow. Any residual turbulence when shutting off the purge gas flow was observed to have no impact on the dust MIE [33]. The lab temperature and humidity were monitored during every test and were maintained at 70 ± 5 ^{o}F, and 50 ± 5 % relative humidity.

One of the parameters that can be adjusted in the MIKE3 device is the inductance (can be set at ≤ 0.025 mH or 1mH). The presence of an inductance while testing is known to result in lower measured MIE values. The MIE testing for calcium stearate, lycopodium and anthraquinone was conducted at an inductance of L = 1 mH to enable better comparison with data available in literature. The electrode gap was maintained at 6 mm for all the tests. A 120 ms ignition time delay was selected for this study as it corresponds to a turbulence level at which there is limited influence on the MIE [22]. Ignition delay times > 100 ms are known to result in more conservative (lower) MIE values for various dusts [22, 81]. In this study, for a given gas composition (N_2-O_2 mixture), the dust concentration was varied from 125 to 3000 g/m^3 and the energy levels varied from 1 to 1000 mJ. A visual confirmation of ignition or no ignition was noted for 10 consecutive tests at a particular energy level. If an ignition was observed at an energy level, tests were conducted at the next lower energy at varying concentrations. Thus, testing was shifted to lower energy levels until an energy level was reached where no ignition is observed for all concentrations.

Figure 15 shows the typical ignition energy and dust concentration relationship for a dust. In Figure 15, each test point corresponds to a given energy level and concentration. Each no ignition point (blue circle) consists of 10 consecutive no ignition tests. The ignition points (red square) are indicated at different concentrations. The MIE of the dust is between the ignition energy level and the no ignition level. Therefore, determination of MIE requires extensive testing over a wide range of energy levels and concentrations.

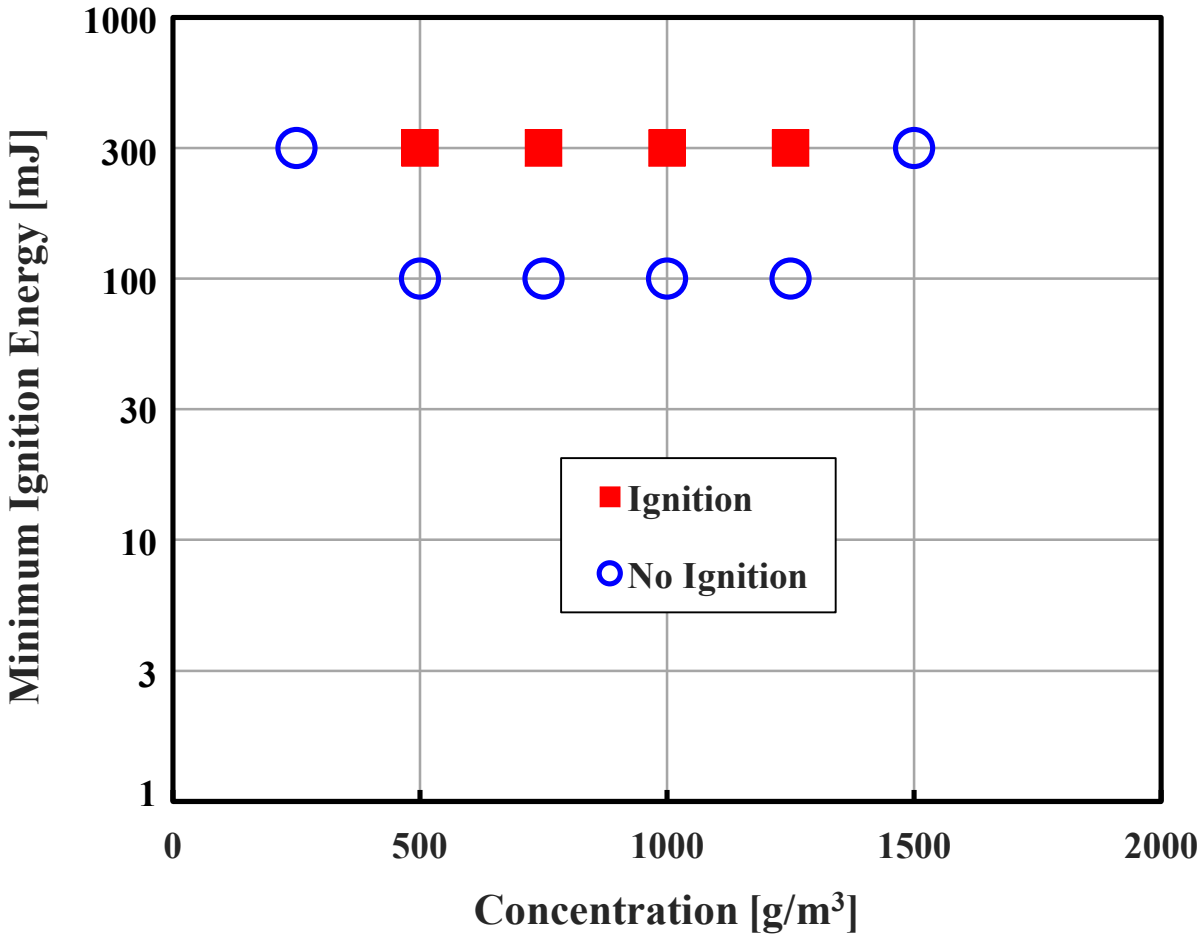

Figure 15 : Typical MIE data observed during testing in the MIKE3 device. E_2 = 300 mJ and E_1= 100 mJ [33]

For every energy level, tests were conducted at different dust concentrations until the energy level was bracketed with no ignition points on both sides as is typical experimental practice. For example, in Figure 15 at 300 mJ, no-ignition tests were conducted at 300 and 1500 g/m^3 to close off the energy level. After every dispersion, a polyester brush was used to clean the Hartman tube wall and the electrodes, returning the dust to the bottom for re-dispersion. In this study, the sample was replaced after 3 consecutive dispersions with no ignition observed. The dust MIE was calculated using the following equation [81]:

$$\mathbf{MIE} = \mathbf{10}^{\frac{(\log \mathbf{E2} - \mathbf{I[E2]}.(\log \mathbf{E2} - \log \mathbf{E1})}{((\mathbf{NI+I})[\mathbf{E2}]+1)}} \quad (2)$$

where E_2 is the energy level at which ignition is observed and E_1 is the energy level below E_2 where no ignition was observed after 10 tests. $I[E_2]$ corresponds to the number of tests having ignition at the energy E_2 and $(NI+I)[E_2]$ represents the total number of tests at E_2. For MIE calculations, $(NI+I)[E_2] \geq 5$.

3.3.2 Particle size reduction of combustible dust

To capture the MIE-oxygen behavior for different particle sizes, acetaminophen was selected for this study. Acetaminophen is a common pharmaceutical dust used to make over-the-counter medicines for pain and fever relief (Food and Drug Administration, 2017). Since it is processed in capsule or tablet form, concerns associated with safe handling and processing can arise. Acetaminophen possesses low MIE values, which makes it particularly suitable for partial inerting MIE testing in the MIKE3 device. Since different particle size samples are necessary for this study, acetaminophen's high breakability index score indicated it would be an excellent candidate for rotary milling to obtain additional particle sizes [86].

Three different particle sizes of Acetaminophen dust were generated to study the effect of particle size on partial inerting characteristic of dust MIE. The particle sizes of the three samples were made different while ensuring that the samples had near similar polydispersities for each particle size through rigorous milling, sieving and back blending processes. Dust polydispersity is an important parameter that is known to affect the explosive properties of dust [87]. Dust polydispersity (σ) can be defined as:

$$\sigma = \frac{\mathbf{d_{90} - d_{10}}}{\mathbf{d_{50}}} \quad (3)$$

where,

σ is the polydispersity, d_{90} is the diameter below which 90% of the dust mass can pass through, d_{10} is the diameter below which 10% of the dust mass can pass through, d_{50} is the diameter below which 50% of the dust mass can pass through.

The Acetaminophen dust as received from the supplier had a d_{50} of 55 µm, a polydisperisity of 3.4. To obtain a d_{50} of 4.5µm, the 55 µm dust was milled using the Retsch rotary mill (sieve ring size of 0.08 mm at 12,000 rpm) and then sieved through the Retsch sieve shaker. The mill and the sieve shaker used for particle size reduction in this study are observed in Figure 16 and Figure 17 respectively. Milling resulted in changing the particle size distribution of the dust and sieving ensured its polydispersity was relatively similar. Acetaminophen with d_{50} = 125 µm dust was obtained and milled and sieved to obtain d_{50} of 99 µm and a polydisperity of 4.6.

Figure 16 : Retsch ZM 200 rotary mill

Figure 17 : Retsch AS 300 sieve shaker

The particle size distributions (PSD) of the acetaminophen dust samples were characterized using the Beckman Coulter Particle Size Analyzer LS 13320 which operates on the principle of laser diffraction. The particle size distributions of the three samples are seen in Figure 18. The polydispersity of the samples is observed in Table 4.

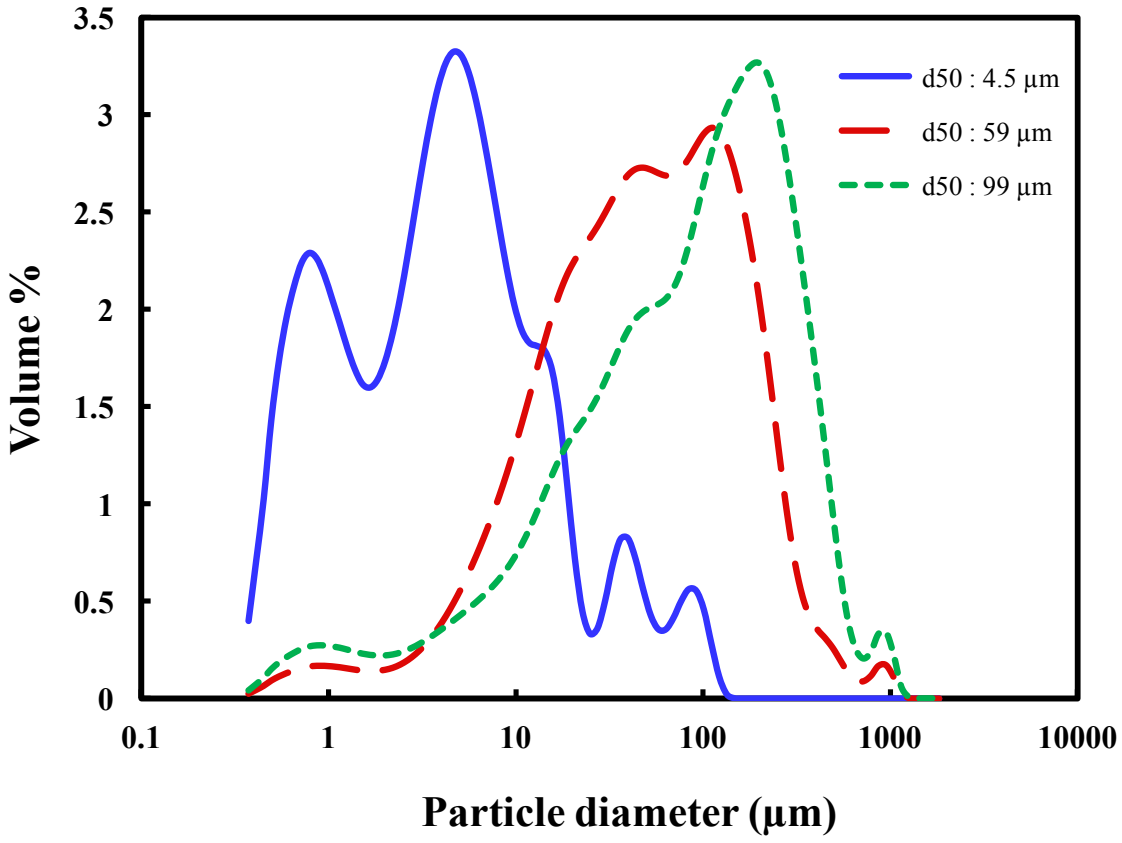

Figure 18 : Particle size distribution of acetaminophen samples of different sizes used in this study

Table 4 Particle size and polydispersity of acetaminophen samples used in this study

Acetaminophen particle size d_{50} (µm)	Polydispersity
99	3.4
55	3.9
4.5	4.2

Before MIE testing the three particle size samples were dried at 60 ^{o}C in the nitrogen atmosphere, where moisture content was monitored with time. After drying, it was observed that there was no significant loss in weight (+/- 1%), no change in PSD, and no impact on polydispersity.

3.4 Results

3.4.1 Effect of improved test method on MIE

As discussed above, two different methods for partial inerting have been investigated to underscore the importance of test method employed. Method (a) Not purging the tube before dust dispersion and ignition. Method b) Purging the tube from top before dust dispersion and ignition. Figure 19 shows the MIE values of Niacin (CaRo15) for various experimental approaches to partial inerting in the Kühner MIKE3. In Figure 19, curve (a) was obtained without purging the Hartman tube, while inerted air was used to disperse the dust. The gas composition used for dust dispersion was different from the composition present in the tube which is atmospheric. Curve (b) was obtained by using the purge device at the top of the Hartman tube, purged for 21 s at 10 L/min. A 1 s delay ($t_{purge-ign.}$) was allowed between shutting off the purge flow and attempting ignition. In experiment (b) no modifications were made to seal the flapper vent valve at the top of the tube. Once the delay time lapsed, the same inerted air used for purging was used to disperse the dust into the tube. In experiment (b) the diffusion of atmospheric oxygen into the tube is mitigated by purging, resulting in higher MIE values for lower oxygen levels. The change in the MIE values between experiments (a) and (b) demonstrates the necessity of tube purging and the purge device.

The experiment shown in Figure 19, curve (c) is the same experiment as curve (b) with the addition of a seal around the flapper valve at the top of the tube, intended to maintain the desired tube gas composition. Comparison of experiments (b) and (c) show at lower oxygen concentrations the sealed tube has slightly higher MIE values. This indicates that the purging was slightly improved by the seal, preventing atmospheric oxygen from diffusing into the tube. At higher oxygen concentrations (21% O_2) the MIE value lowered, indicating the seal helped hold the oxygen level in the tube, which is higher than the atmosphere.

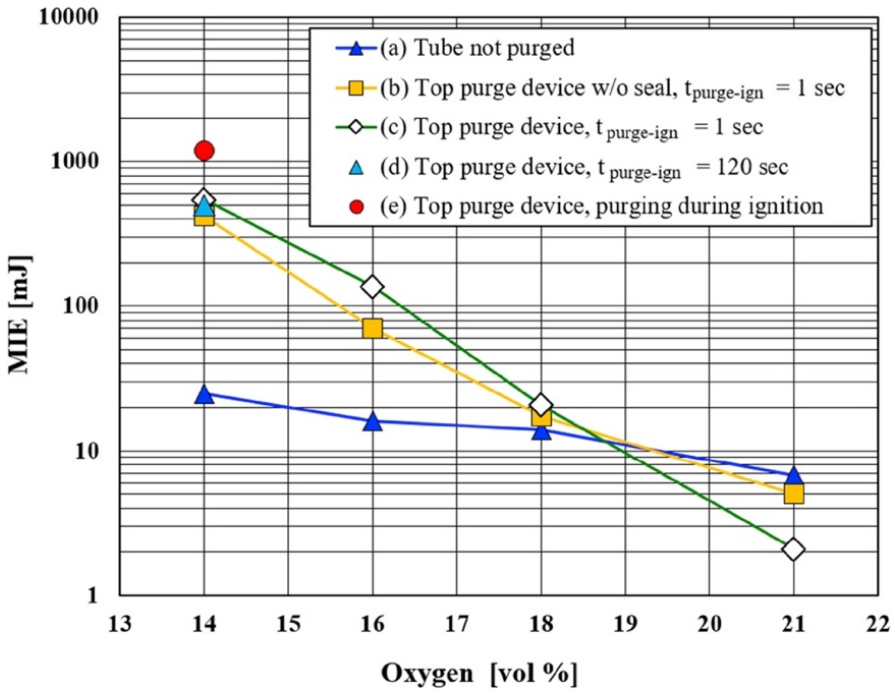

Figure 19 : MIE (L = 0 mH) and oxygen concentration for various experimental approaches to the purging of Niacin dust (CaRo15): (a) Without purging, (b) With purge device, w/o seal, $t_{purge-ign.}$ = 1 s (c) With purge device, w/seal, $t_{purge-ign.}$ = 1 s (d) With purge device, w/o seal, $t_{purge-ign.}$ = 120 s (e) With purge device, w/o seal, purging during ignition. [38]

For tests in air (i.e. 21% O_2, 79% N_2), the MIE values with the purge device in case (b) are slightly lower than case (a). This is because the purge gas, which is also the dispersion gas, has slightly higher oxygen content than atmospheric air. For case (a), the dispersion gas is diluted by atmospheric oxygen present in the tube, resulting in lower than 21% oxygen leading to higher MIE values. For case (b), the tube is purged with the dispersion gas before testing resulting in 21% oxygen, which leads to slightly lower MIE values than case (a). This effect is more pronounced for case (c) where the seal further prevents any atmospheric oxygen from diffusing into the tube and maintains the testing conditions at 21% oxygen. These results justify the need for purging and maintaining the desired gas composition with respect to the external atmosphere.

In Figure 19, the greatest difference in MIE values occurs at 14% oxygen for a non-purged (a) and purged experiment (c). At this composition the concentration driving force is the highest for oxygen to diffuse into and nitrogen to diffuse out of the dispersion tube. It is believed if turbulence from purging has an impact on the MIE values, then the maximum effect should be found where the concentration driving force is largest, that is, at low oxygen concentration. Therefore, the potential turbulence effect was analyzed only at this particular composition. Figure 19 shows experimental point (d) in which the delay between stopping the purge and attempting ignition was 120 s. This time delay was chosen to determine if a longer delay time allowed purging induced turbulence to dissipate, resulting in a change in the MIE value. The results of this test at 14% oxygen show no significant difference between experiments (c) and (d) with delay times of 1 and 120 s respectively. This indicates that turbulence 1 s after purging ceases does not significantly affect the MIE and that the dispersion tube can maintain the desired gas concentration over this period of time. Experimental point (e) in Figure 19 shows the MIE value at 14% oxygen with purge gas flowing during an ignition attempt. The influence of the continuous purging

turbulence increases the MIE value. These results are in accordance with literature where it is observed that turbulence makes ignition more difficult and therefore raises the MIE [88-90].

From these experiments and the above discussion, it is believed that experiment (c) is an acceptable way to conduct partial inerting MIE tests. Experiment (c) consists of a purging device, a seal around the flapper valve, and a 1 s delay between purging shut off and an ignition attempt. With this approach, the slope of the partial inerted MIE curve is much steeper, resulting in a proper representation of the impact of inert on the MIE values. At higher inerting levels, the resulting MIE is higher and the dust becomes less hazardous. Hence, without tube purging and the purging device, the characteristic partial inerting curve for dusts can lead to overestimation of the hazards posed in manufacturing facilities.

It is important to keep in mind that the recommended relationship for Niacin dust observed in case (c) represents the worst case scenario near atmospheric oxygen concentrations (from O_2 ~ 19% - 21% O_2), but does not represent the worst case scenario at lower oxygen concentrations (O_2 < 19%). However, at lower oxygen concentrations, it signifies a true MIE measurement, which can differ significantly from those reported in literature, if there is no purging. In an industrial application of partial inerting, accurate knowledge of MIE values at lower oxygen concentrations are of particular interest. If not determined accurately, an overestimation of the risks involved can occur leading to improper design.

3.4.2 Effect of inerting on dust MIE for different combustible dusts

After the purge time was determined experimentally and validated through CFD, partial inerting measurements of the dusts (lycopodium clavatum, calcium stearate and anthraquinone) were conducted in the modified MIKE3 device using the improved test method with a purge time of 1 minute.

The partial inerting curve measured for calcium stearate is observed in Figure 20. The MIE value of 3.7 mJ obtained in air for calcium stearate is in agreement with reported values (3-10 mJ) in literature for this material [91].

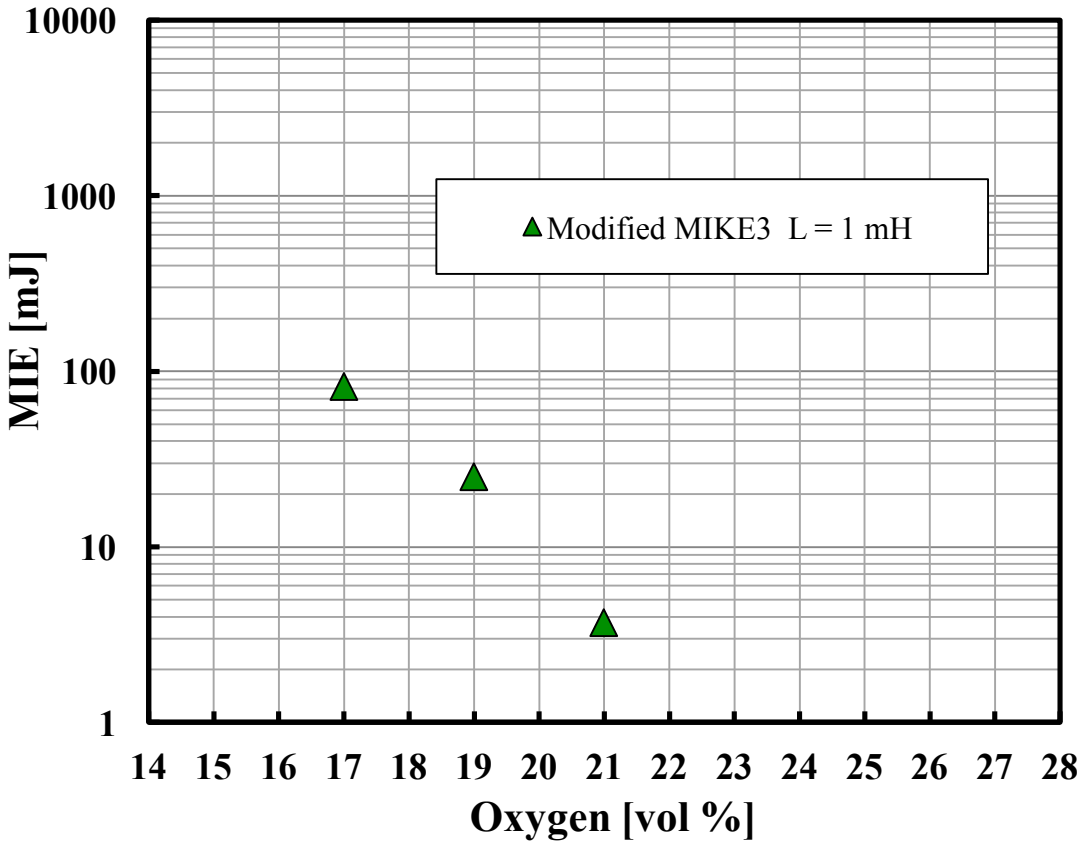

Figure 20 : MIE-O_2 for calcium stearate obtained in the MIKE3 device [33]

For lycopodium, this work is compared with the existing literature and is shown in Figure 21. The MIE-oxygen relationship for lycopodium in this work is in close agreement to that reported by Choi *et al.* [26] and Glor and Schwenzfeuer [19]. These two studies have pre-purged the tube before experimentation and conducted testing with the presence of inductance in the circuit (L = 1 mH).

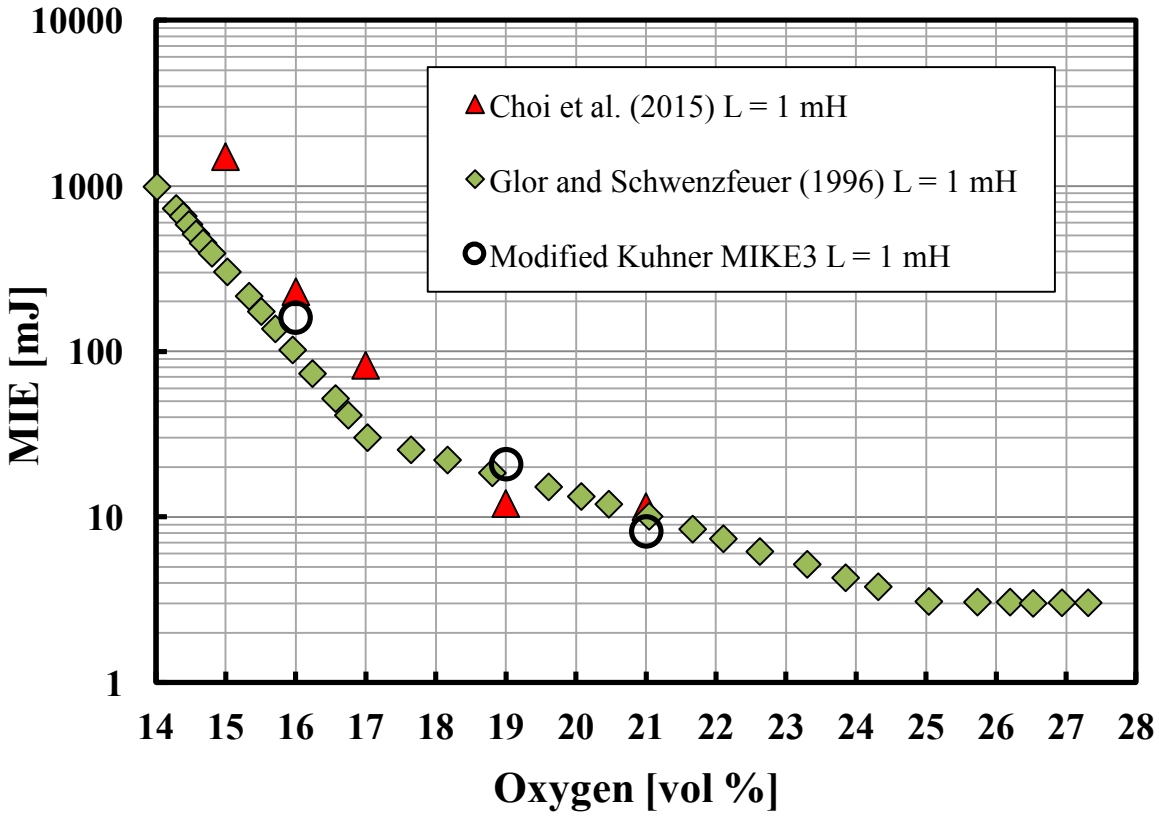

Figure 21 : MIE-O_2 for lycopodium in MIKE3 device compared with literature [33]

Similarly, for anthraquinone the MIE-O_2 experimental relationship observed in this study is similar to that reported by Glor and Schwenzfeuer [19] (see Figure 22). For studies that have reported purging the 1.2 L Hartmann tube before MIE testing [19, 26], the effective purge flow

rate and time have not been mentioned. This can result in not knowing the exact oxygen concentration while MIE testing. It is highly possible that the above two studies were conservative and purged for more than the required time. However, the purge flow rate and time should be stated (along with parameters such as ignition delay time, inductance) when reporting partial inerting MIE values as this would make the reported literature more useful for future reference.

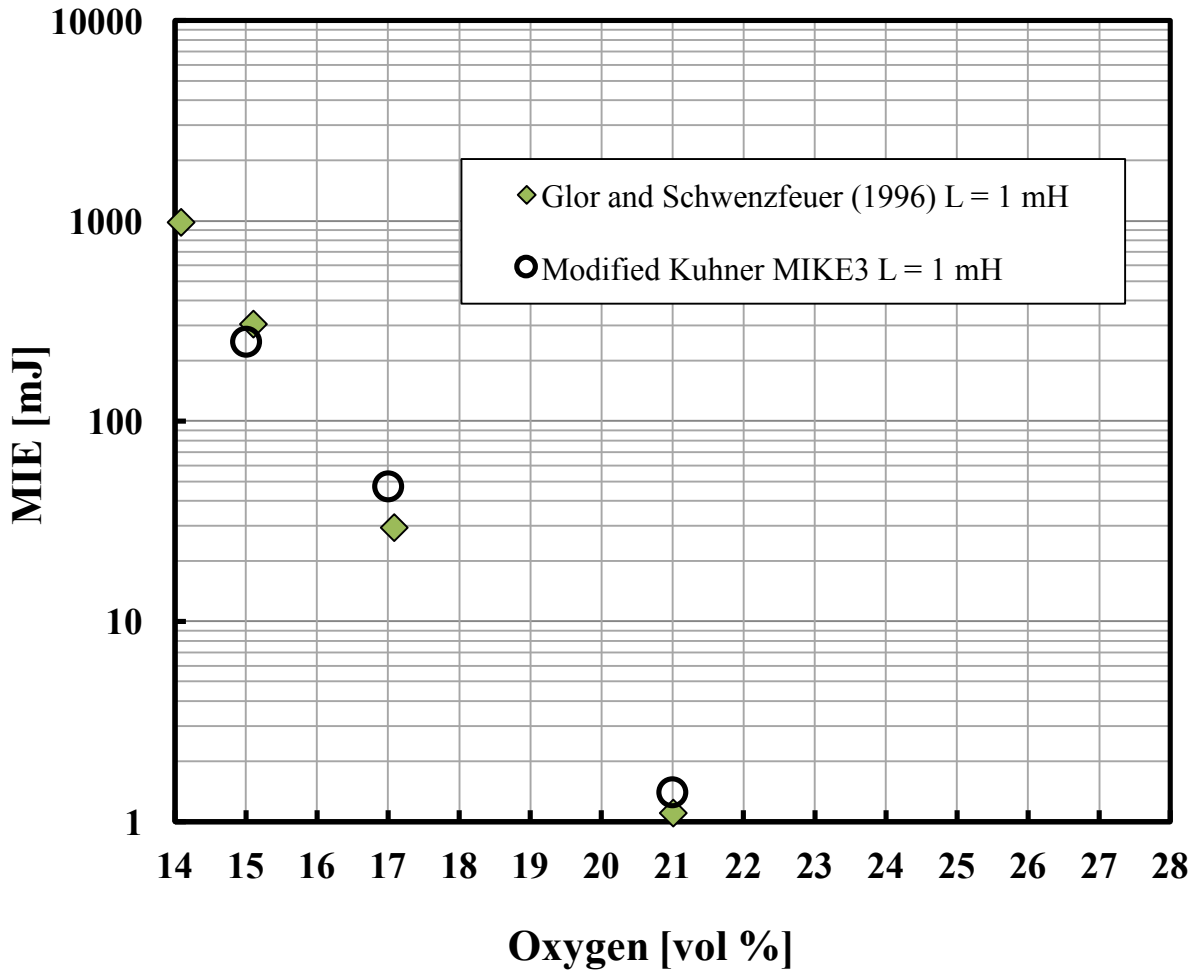

Figure 22 : MIE-O_2 anthraquinone in MIKE3 device compared with literature [33]

3.4.3 Mathematical variation of MIE with changing O_2 content

Schwenzfeuer *et al.* have qualitatively stated that the MIE-O_2 relationship for any dust can be defined by a curve with the oxygen content on the X-axis and the Minimum Ignition Energy (MIE) on the Y-axis [92]. The curve has two asymptotes – the Limiting Oxygen Concentration (LOC) and the Lowest Minimum Ignition Energy (LMIE), which is the MIE in pure oxygen. Where the x = LOC is the asymptote parallel to the Y-axis and the y = LMIE will be a line parallel to X-axis where LMIE is the Lowest Minimum Ignition Energy of dust in pure oxygen (see Figure 23).

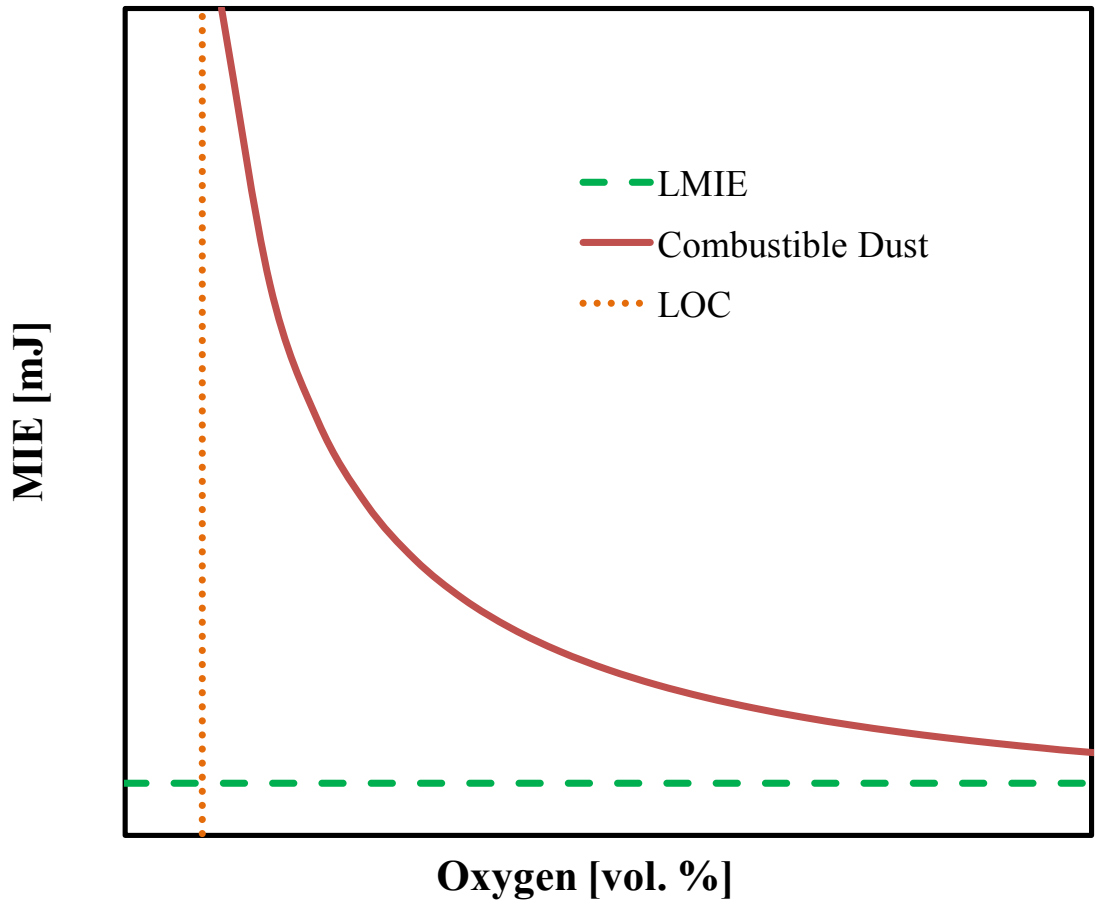

Figure 23 : MIE–oxygen relationship for typical dust displaying two asymptotes - Limiting oxygen concentration (LOC) and the lowest minimum ignition energy (LMIE) as qualitatively proposed by Schwenzfeuer *et al.* (2001)[33]

Using their qualitative study, for any particular dust, a curve that has the two asymptotes - LOC and LMIE can be described by the following equation:

$$(y - \text{LMIE}) = \frac{A'}{(x-\text{LOC})^{B'}} \qquad (4)$$

where A' and B' are constants for that particular dust.

Because the LMIE of a dust will be very low, it was assumed that LMIE ~ 0

Equation (3) can be further simplified and described as:

$$y = \frac{A'}{(x\text{-}LOC)^{B'}} \tag{5}$$

Solving for A' (at O_2 = 21 %, y = MIE_{21} (MIE of dust in air), can be expressed in the following way:

$$\mathbf{MIE(O_2) = MIE_{21}\left(\frac{21-LOC}{O_2-LOC}\right)^{B'}} \tag{6}$$

where

MIE (O_2) = MIE of dust at a given oxygen concentration (mJ),

MIE_{21} = MIE of dust in air (mJ),

LOC = Limiting Oxygen Concentration (vol. %),

O_2 = oxygen concentration (vol. %),

B' > 0 and is a coefficient varying with the dust type.

The LOC for anthraquinone, calcium stearate and lycopodium were obtained from literature [1, 3, 92-93] and are given in Table 5. The MIE of these three dusts in air (O_2 = 21 %) was obtained experimentally in this study. The B' coefficient which resulted in the best fit for the experimental MIE data at O_2 = 21% was calculated for each dust (see Table 5).

Table 5 LOC values and the calculated best fit coefficient B' values for the dusts

Dust	LOC	Coefficient B'
Calcium Stearate	12	5.28
Lycopodium	6	6.72
Anthraquinone	11	5.66

Although, B' for these dusts is observed to vary only between 5 to 6, this coefficient being an exponent (See equation 6), slight variation in its values can significantly change the predicted MIE values. A similar prediction equation form was developed by Ackroyd *et al.* (see equation 7 below), where they have used a single coefficient (B' = 3.75) which gave a best fit to all their experimental data [25].

$$\mathbf{MIE(O_2) = MIE_{21}\left(\frac{21-LOC}{O_2-LOC}\right)^{3.75}} \quad (7)$$

Figures 24-26 show a comparison of the experimental MIE values (lycopodium *clavatum*, anthraquinone, calcium stearate) found in this study to the proposed MIE prediction equation (equation 6) with dust specific coefficients and with the fixed coefficient (B' = 3.75) as proposed by Ackroyd *et al.* [25]. Additionally, a comparison of the experimental MIE has been made with the prediction equation proposed by Glor and Schwenzfeuer [19]:

$$\mathbf{MIE(O_2) = MIE_{21}\exp^{\left(23.2-\frac{23.2}{21}\right)O_2}} \quad (8)$$

From Figures 24-26, a fixed coefficient for any dust (B' = 3.75) proposed by Ackroyd *et al.* deviated significantly from the experimental data [25]. Thus a fixed value of coefficient B' does not satisfactorily describe all the experimental MIE behavior of all dusts but the value B' can be dependent on the type of dust. Similarly, equation 8 was observed to deviate significantly from experimental values in this study and over-predicted the MIE values (See Figures 24 - 26). A similar observation has been reported by Ackroyd *et al*. [25], where equation 8 failed to agree with experimental MIE values for the dusts tested in their study.

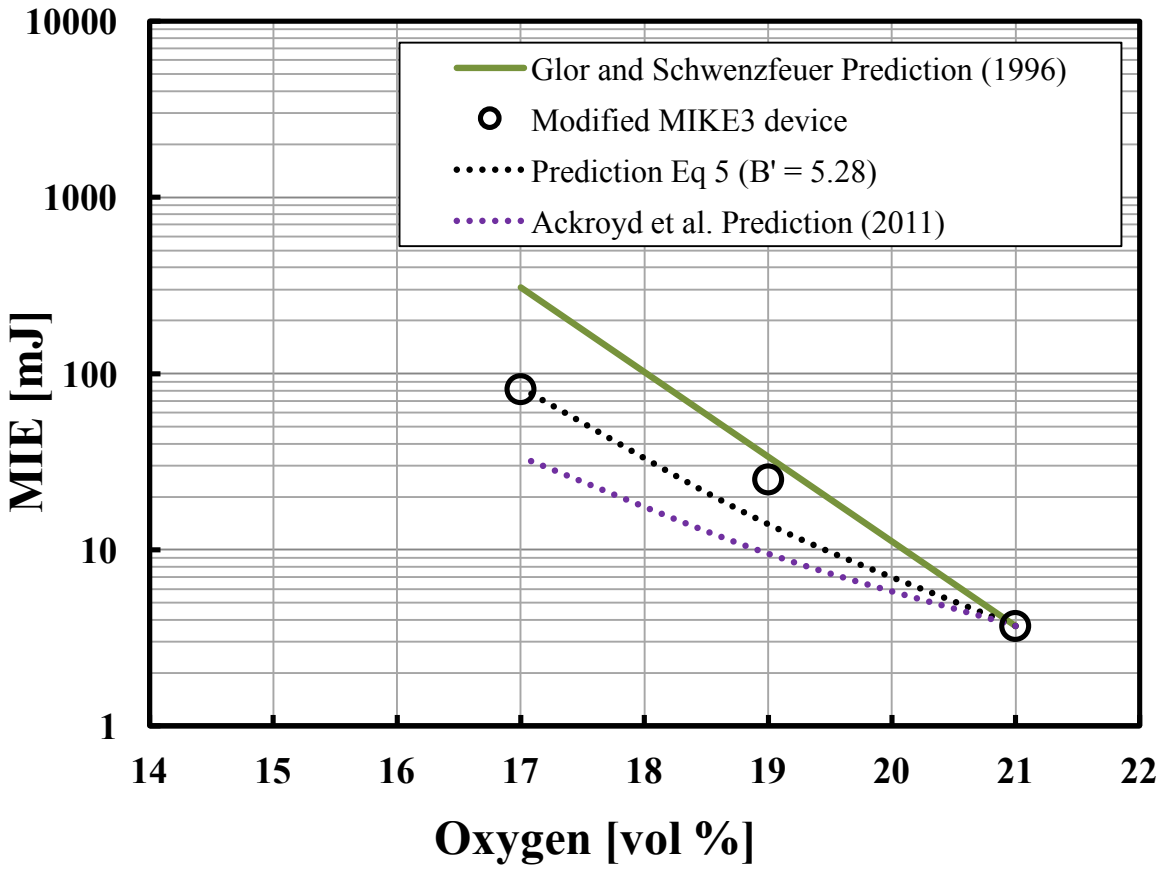

Figure 24 : Comparison of experimental MIE values of calcium stearate with MIE prediction equations adapted from Glor and Schwenzfeuer [19] and Ackroyd *et al.* [25] and the prediction equation (6) with B' = 5.28 in this work [33]

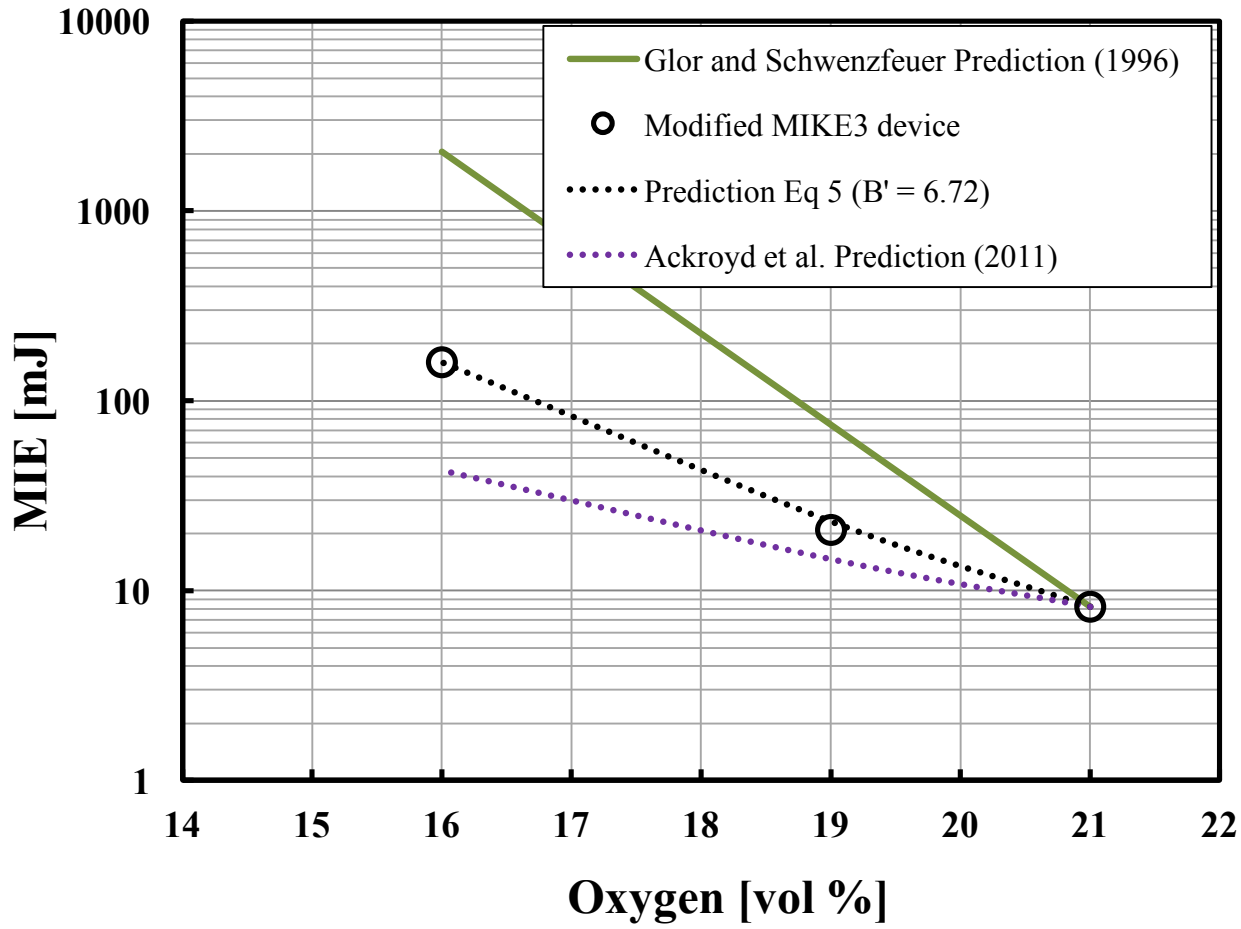

Figure 25 : Comparison of experimental MIE values of lycopodium with MIE prediction equations adapted from Glor and Schwenzfeuer [19], Ackroyd *et al.* [25] prediction equations and the prediction equation (6) with B' = 6.72 in this work [33]

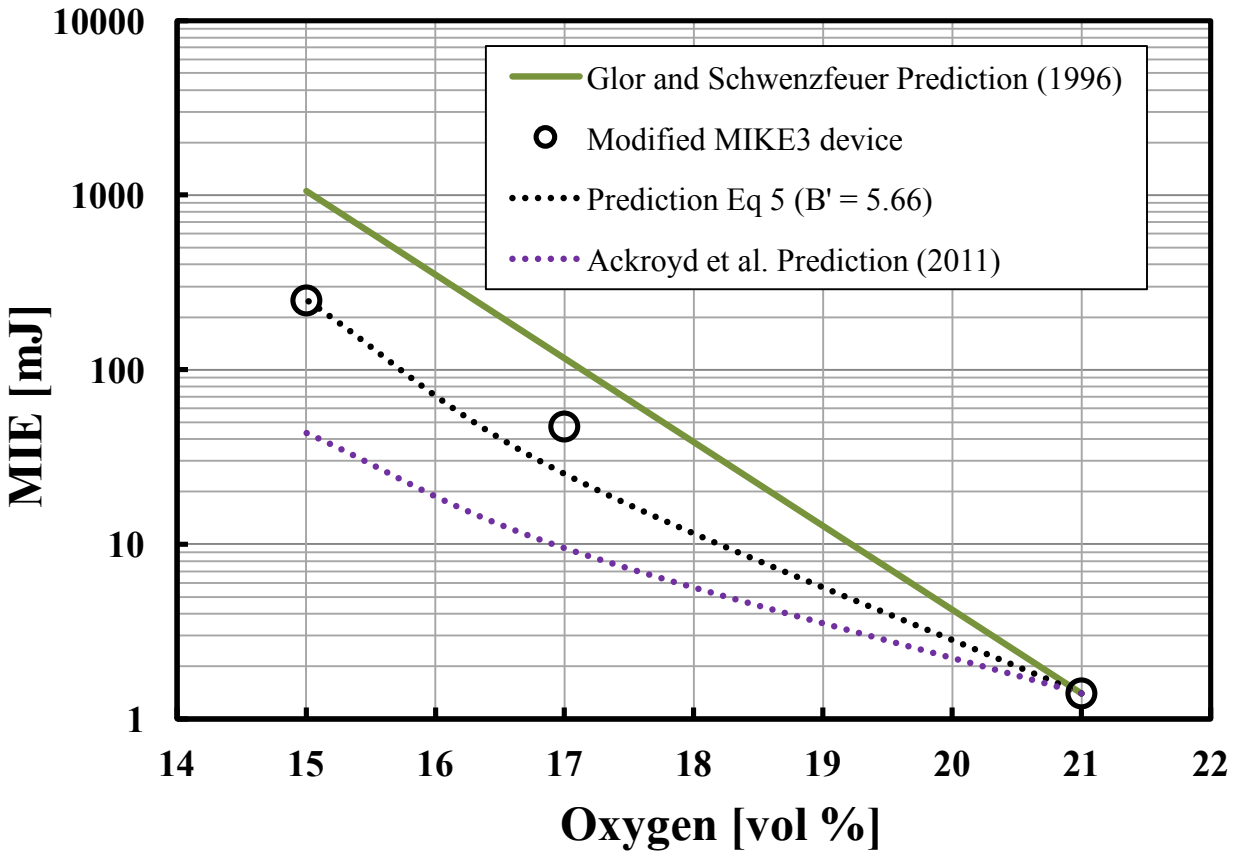

Figure 26 : Comparison of experimental MIE values of anthraquinone with MIE prediction equations adapted from Glor and Schwenzfeuer [19], Ackroyd *et al.* [25] prediction equations and the prediction equation (6) with B' = 5.66 in this work [33]

Therefore, it is observed that the MIE-O_2 relationship is well described by an equation of the form in equation 6, rather than the exponential form proposed in equation 8. This is an important observation and supports the observations of Ackroyd *et al*. about the mathematical nature of the MIE-O_2 relationship [25]. Moreover, a generic equation describing the MIE-O_2 relationship for all dusts cannot be described without considering specific dust parameters exclusive to that dust (B' = 3.75 does not describe dust behavior well). However, determination of B' is complex and it can depend on some of the fundamental and physical properties of dust such as dust particle size, morphology, conductivity, heat of combustion, and bond strength. Additional

experimental investigation and modeling is required to further explore the effect of dust properties on the coefficient B'.

3.4.4 Effect of particle size on partial inerting MIE characteristic of combustible dust

While, the effect of particle size on dust MIE is known [39], the effect of particle size on partial inerting characteristic curve of the dust remains unexplored. The three acetaminophen samples having different particle sizes were tested at a range of different oxygen concentrations to obtain their partial inerting characteristic curves. The effect of particle size on partial inerting MIE-O_2 behavior for acetaminophen (paracetamol) dust is observed in Figure 27. As there is little resolution in the MIE values for oxygen concentrations of 18 % and 21 %, that zone is zoomed in further in the Figure 27.

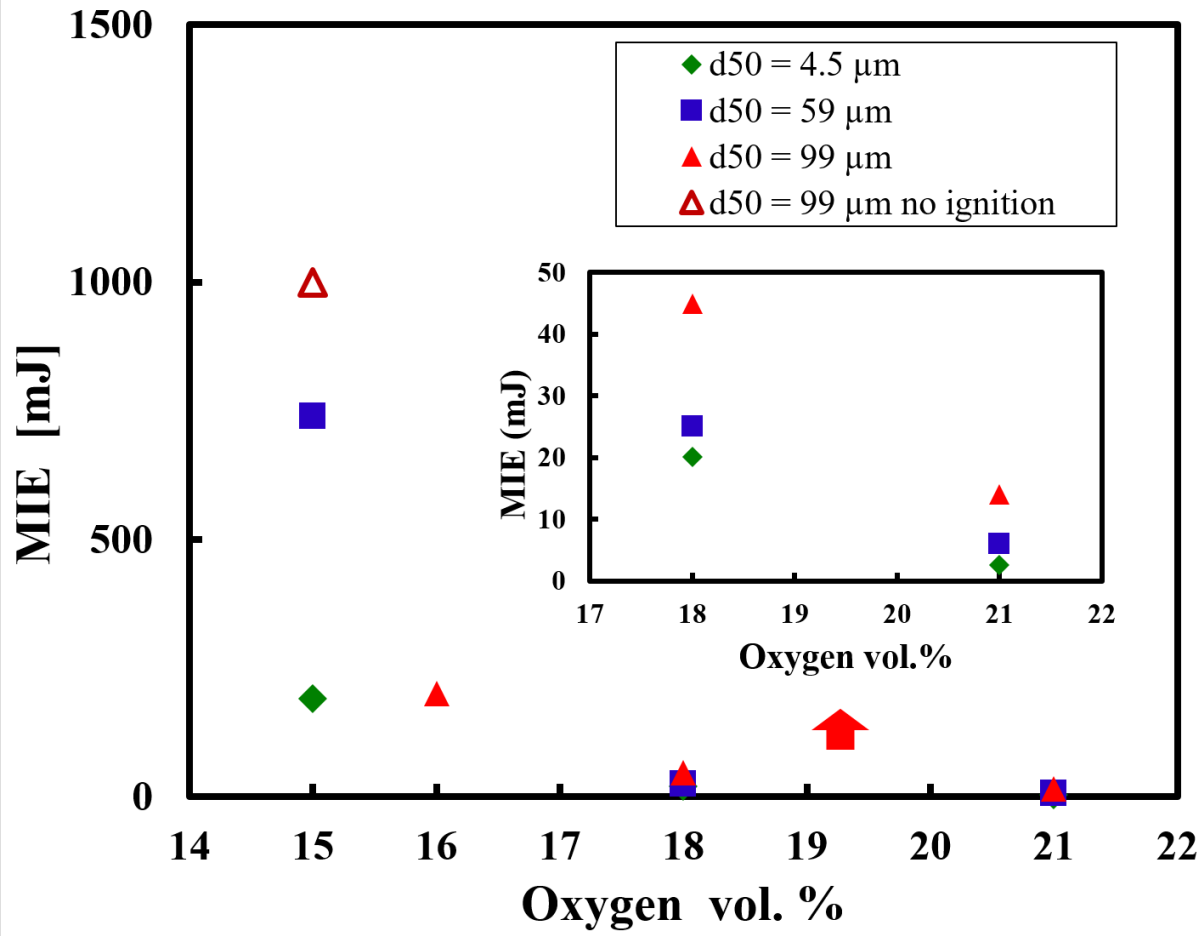

Figure 27 : Experimental partial inerting characteristics of acetaminophen (paracetamol) dust at different diameters (d_{50} = 4.5 µm, d_{50} = 55 µm and d_{50} = 99 µm)

It can be observed from Figure 27 that the particle size has an effect on the partial inerting characteristic of acetaminophen dust. As expected from literature and also observed in Figure 27, the MIE raises with increasing particle diameter. At each oxygen concentration where MIE testing was conducted (O_2 = 15 vol. %, 18 vol. % and 21 vol.%), it can be observed that the MIE of the dust with bigger particle size is higher. This effect becomes more significant at lower oxygen concentrations where MIE significantly rises with increase in particle size. At O_2 = 15 % the MIE rise was so high that the dust did not ignite at the highest testing energy level of 1000 mJ provided by the MIKE3 device. The sudden rise in the MIE at lower oxygen concentrations for high particle

size can be explained by the fact that for a bigger particle diameter the surface area available for reaction at lower oxygen concentrations is much less as compared to smaller particle diameter. This lower availability of surface area for reaction is further compounded by the fact that much less oxygen is available for reaction, raising the dust MIE.

This information can be very valuable in combustible dust handling facilities where the partial inerting of the processes can be determined based on the particle size of the dust. For example, a facility that handles large particle sizes of acetaminophen can determine the amount of partial inerting in processes (the percent O_2 that can be maintained which raises the dust MIE significantly. While these results present a compelling case that the partial inerting characteristics are affected by the particle diameter this aspect needs further investigation for other combustible dusts.

3.5 Summary

In summary, the improved test method proposed earlier was successfully implemented to develop partial inerting data and equation. The improved test method significantly influenced the measured partial inerting MIE values (displayed through Niacin dust) resulting in more accurate MIE measurements. Thereafter, this test method was used to generate MIE-O_2 data for various different combustible dusts. The MIE equation which predicted the MIE with changing oxygen content agreed with the empirical MIE-O_2 relationship available in literature. Additionally, the effect of particle size on MIE-O_2 of acetaminophen dust was investigated to observe that particle size affects MIE more significantly at lower oxygen concentrations.

4 MIE PREDICTION USING QSPR AND MACHINE LEARNING

4.1 Introduction

Gas and dust explosions pose a serious hazard to process industries, resulting in loss of life, property and resources[3, 10, 94-95].Experimental determination of MIE can be costly, risky, tedious (time intensive) and resource limiting process [96-97]. Therefore, prediction of MIE of compounds provides an alternative to experimental testing and there is a need to explore this prospect further. Based on the accuracy of the prediction models, important risk assessment decisions can be made.

Several studies in literature have employed Quantitative Structure-Property Relationship (QSPR) models relating molecular structures to the physical properties of compounds such as boiling point [53,54], flash point temperature [55] and auto-ignition temperature [56,57-58].
Recent QSPR studies have employed a variety of algorithms for MIE, K_{st}, P_{max} and UFL predictions [44-45, 49, 98-99]. QSPR models using machine learning algorithms have been developed extensively in literature [45, 49, 69-74, 98, 100]. Yuan *et al*. have utilized machine learning algorithms support vector machine (SVM), k-Nearest-Neighbors (KNN), and random forest (RF) to predict the upper flammability limit (UFL) of pure organic compounds [98]. For combustible dusts, Reyes *et al.* predicted explosion severity parameters (K_{st} and P_{max}) through QSPR using Genetic Function Approximation (GFA) algorithm [44].

Baati (2016) has developed MIE prediction models of dusts, liquids and gases. Their most robust prediction model for dusts in this study consisted of 27 parameters, making it unfeasible due to large input parameters [60]. However, they did not have any conclusive outcome whether molecular structures influence material MIE. Wang *et al*.[44,49] have developed robust QSPR models

for MIE prediction of liquid and gas hydrocarbon fuels employing Multiple Linear Regression (MLR) and Support Vector Machine (SVM) methods [44,49]. Owolabi *et al.* [99] have estimated the MIE of chemical compounds using hybrid model of Support Vector Regression (SVR) and Gravitational Search Algorithms (GSA), stating that their hybrid GSA-SVR model outperforms the prediction model developed by Wang *et al.* [44,49].

Based on the existing literature, machine learning techniques employing Artificial Neural Networks (ANN), Random Forests (RF), Decision Tree (DT) algorithms for MIE prediction need to be investigated further. Additionally, as Genetic Function Approximation (GFA) algorithm was observed to be promising for explosive property prediction (K_{st} and P_{max}) by Reyes *et al*., it was deemed worthwhile to investigate this algorithm for MIE prediction of compounds [44].

In this research, machine learning algorithms were employed to develop QSPR models for MIE prediction of 60 flammable compounds. The molecular descriptors are obtained through the QSPR module in the BIOVIA Materials Studio software [101]. Machine learning models were developed on this dataset using Scikit learn [102] for RF, DT and TensorFlow [103] for Artificial Neural Networks (ANN) respectively. Random Forests (RF) has been used to determine the 10 most important molecular descriptors influencing MIE prediction accuracy adding more deterministic value to the machine learning model developed. Additionally, GFA algorithm in Materials Studio was used to develop a 10 parameter MIE prediction equation.

Once the model was validated on the first dataset, the RF and DT models were implemented on another dataset consisting of 64 pharmaceutically relevant combustible dusts.

4.2 Methodology - MIE prediction for liquid and gas hydrocarbons

4.2.1 MIE dataset

The first dataset used in this study consisted of 60 flammable liquid and gas fuels obtained from Calcote *et al*. study of spark ignition of stoichiometric fuel-air mixtures (Appendix A) [104]. The dataset was divided into training set (80%) for model development and test set (20%) for model validation.

4.2.2 Geometry optimization and determination of molecular descriptors

The molecular structures of the compounds used in this study were obtained through PubChem database [105]. Energy minimization of molecular structures is an important step in QSPR, dictating the quality of the model developed. Geometry optimization of the molecular structures was conducted using Gaussian 09 [106] at the B3LYP (Becke, 3-paramater, Lee, Yang, Parr) density functional theory method and the 6-31(d) basis set. B3LYP at 6-31(d) was selected based on its consistently successful performance in literature for a number of different systems [107-109]. Vibrational frequency calculations were performed to ensure optimization to minimum energy level (*i.e*. no imaginary modes) and the convergence of the optimization was checked to determine successful completion of the optimization.

After conducting geometry optimization, the molecular descriptors for each of these compounds were calculated from the QSPR models available in the Materials Studio software. The descriptors used in this study are quantum chemical, fast descriptors, atomistic descriptors and topological descriptors. Molecular descriptor reduction was conducted first by removing the null values and then by removal of descriptors having high degree of correlation. A reduced set of descriptors were used as input parameters for model development for the RF (see Table 6). The RF algorithm was used to identify the top descriptors amongst the list in Table 6 (those affecting MIE prediction accuracy > 1%) which were used as an input in the DT, ANN and GFA algorithms.

Table 6 List of descriptors used for RF model development

Molecular descriptor	Type of descriptor	Description
Total molecular mass	Atomistic	Molecular weight
Dipole Moment	Electronic	Dipole moment
HOMO	Electronic	Energy of the highest occupied molecular orbital
LUMO	Electronic	Energy of the lowest unoccupied molecular orbital
Chemical Potential (μ^2)	Electronic	$\frac{\text{HOMO} + \text{LUMO}}{2}$
Electrophilicity Index (η)	Electronic	HOMO - LUMO
Hardness (ω)	Electronic	$\frac{\mu^2}{2\eta}$
# of C atoms	Atomistic	Number of C atoms in the molecule
# H atoms	Atomistic	Number of H atoms in the molecule
# of O atoms	Atomistic	Number of O atoms in the molecule
# of N atoms	Atomistic	Number of N atoms in the molecule
# of S atoms	Atomistic	Number of S atoms in the molecule
# of halogen atoms	Atomistic	Number of X atoms in the molecule
E-state keys (counts): N_sCH_3	Fast	Number of C bonded to 3 H and 1 single bond
E-state keys (counts): N_ssCH_2	Fast	Number of C bonded to 2 H and 2 single bonds
E-state keys (counts): N_tCH	Fast	Number of C bonded to 1 H and 1 triple bond
E-state keys (counts): N_sNH_2	Fast	Number of N bonded to 2 H and 1 single bond

4.2.3 Model development and validation

QSPR models for this dataset were developed employing RF, DT, ANN and GFA algorithms. Machine learning methods such as RF and ANN have employed regression for model development. A decision tree (DT) gives a visual representation and categorization of the compounds based on the important descriptors values [75-76]. RF has used multiple such decision trees for model development [75-76]. A shortcoming of machine learning algorithms is that an explicit prediction equation is generally not obtained which can limit understanding and interpretation of the parameters affecting the material properties. Therefore, in this study, the RF algorithm was used to determine 10 most important molecular descriptors influencing MIE prediction. The 10 descriptors obtained through RF were further used for model development in ANN and GFA methods to see the effect of initial selection on model prediction. The RF and DT models were developed using the programming language Python employing the module Scikit-learn [102]. The ANN model was developed in Python using TensorFlow [103].

Additionally, a separate MIE prediction equation through GFA algorithm available through Materials Studio software [101] was developed. GFA was used in this study because it has been proven to be an effective method for large parameter spaces and small datasets [109-113].

The developed models were validated using the following:

$$\text{Coefficient of determination } R^2 = \frac{\sum_{i=1}^{n}(\hat{y}_i-\bar{y})^2}{\sum_{i=1}^{n}(y_i-\bar{y})^2} \quad (9)$$

$$\text{Root-Mean-Square Error RMSE} = \sqrt{\frac{\sum_{i=1}^{n}(\hat{y}_i-y_i)^2}{n}} \quad (10)$$

where $\hat{y}_i$ is the predicted value, y_i is the observed value in the data set, $\bar{y}$ is the mean of the observed values, and n is the number of observations in the data set.

Leave-One-Out cross-validation $Q^2_{LOO} = 1 - \frac{\sum_{i=1}^{training}(y_i - \hat{y}_i)^2}{\sum_{i=1}^{training}(y_i - \bar{y})^2}$ (11)

where y_i, $\hat{y}_i$, and $\bar{y}$ are the observed, predicted and mean experimental values of the training set, respectively.

Co-relation coefficient of external validation predictive ability

$$Q^2_{ext} = 1 - \frac{\sum_{i=1}^{test}(y_i - \hat{y}_i)^2}{\sum_{i=1}^{test}(y_i - \bar{y}_{tr})^2} \quad (12)$$

where $y_i$and $\hat{y}_i$ are the observed and predicted MIE values in the test set and $\bar{y}_{tr}$ is the mean observed MIE values of data in the training set.

4.3 Results - MIE prediction of liquid and gas hydrocarbons

4.3.1 Random Forest (RF) algorithm

Random Forest regression was conducted through the Python Scikit-Learn module using the Random Forest Regressor [102]. The number of decision trees used in the random forest algorithm were 1000. Figure 28 shows the comparison between the predicted and experimental MIE values for this algorithm for the training and test set. The Random Forest based QSPR model has the following values: R^2 = 0.84, RMSE = 2.15, AAE = 1.92 for the test set displaying an excellent goodness of fit through Q^2_{LOO} = 0.89 and Q^2_{ext} = 0.84. Figure 29 shows the residual plots of the training and test set.

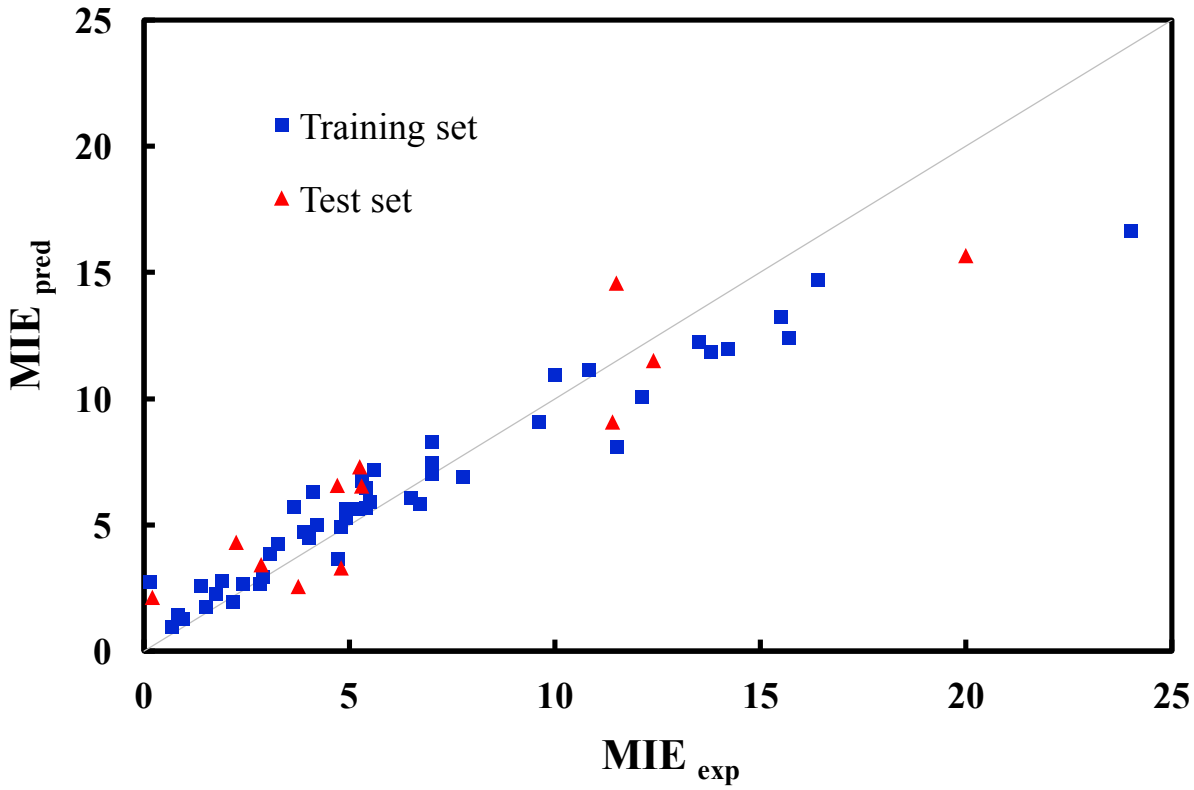

Figure 28 : Experimental versus predicted MIE values through Random Forest (RF) algorithm for training and test set

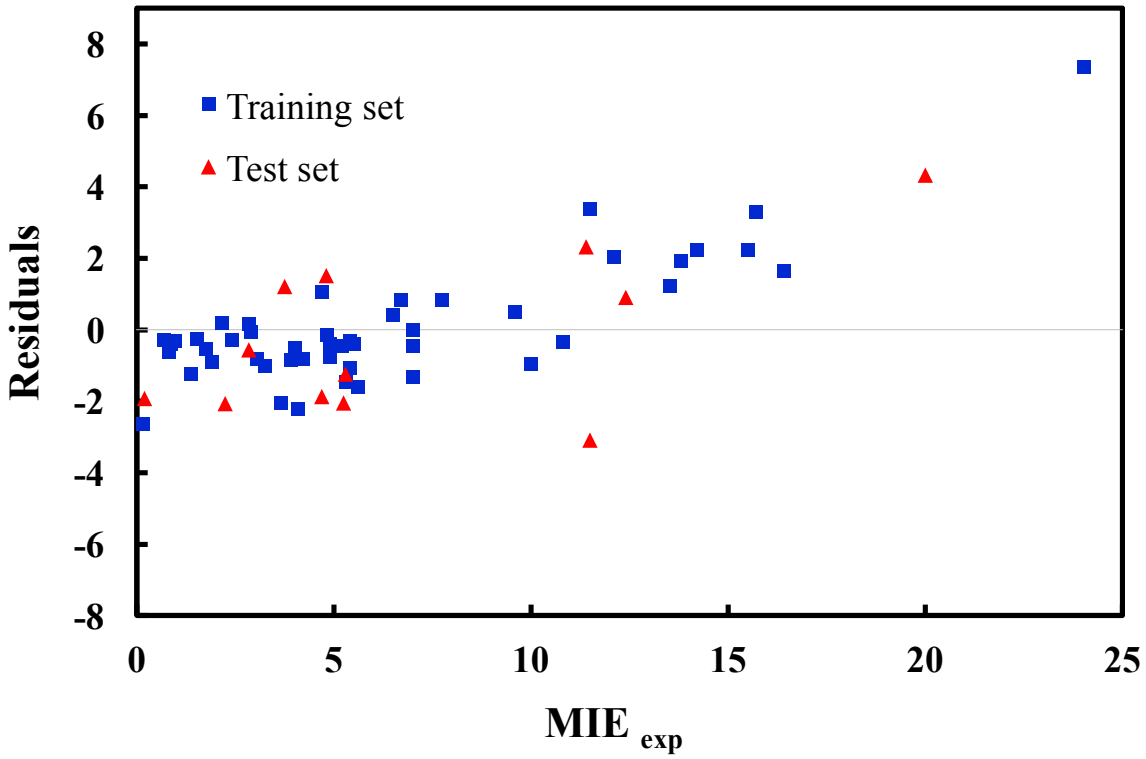

Figure 29 : Experimental MIE versus residuals through Random Forest (RF) algorithm for training and test set

Figure 30 below shows a training set plot of the list of the molecular descriptors having the most effect on MIE prediction accuracy. Thus, the Figure 30 represents the decrease in mathematical performance of the RF algorithm prediction on removal of the specific descriptor. For example, removal of the descriptor 'Total molecular mass' affects MIE prediction the maximum by 27.21 %.

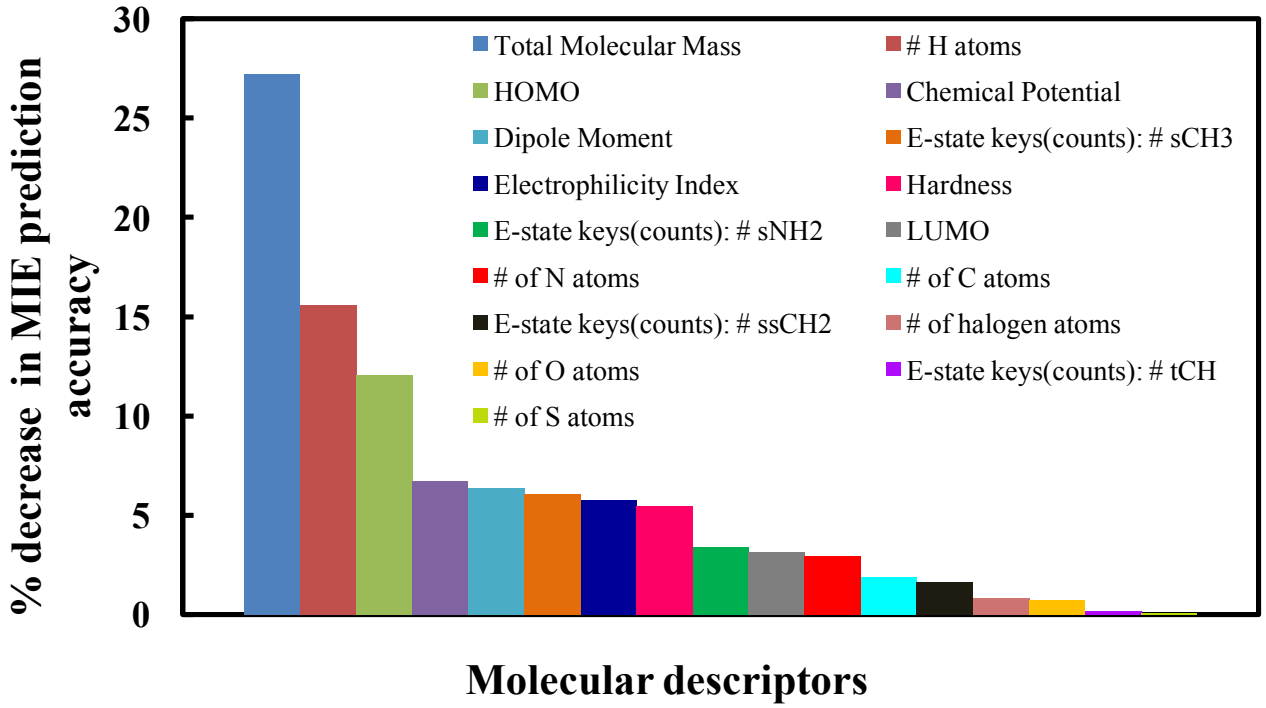

Figure 30 : Relevance of descriptors based on mean decrease in MIE prediction accuracy determined from RF algorithm for liquids and gases

Amongst this list, the descriptors having < 1% contribution to MIE prediction accuracy were considered as having a negligible effect on MIE. Thus, the DT, ANN and GFA algorithms only utilized the 13 descriptors (influencing MIE >1%), reducing the parameter space used for

model development. The % contribution by descriptors to MIE (>1%) is observed in Table 7 below.

Table 7 List of descriptors having > 1% effect on MIE prediction accuracy

Molecular Descriptors	% decrease in MIE prediction
Total molecular mass	27.21
# H atoms	15.58
HOMO	12.05
Chemical Potential	6.72
Dipole Moment	6.39
E-state keys (counts): N_sCH3	6.04
Electrophilicity Index	5.77
Hardness	5.47
E-state keys (counts): N_sNH2	3.39
LUMO	3.13
# of N atoms	2.97
# of C atoms	1.85
E-state keys (counts): N_ssCH2	1.63

It was observed that the molecular mass contributes the greatest amongst all the descriptors (27.21 %) to the MIE and is a key factor determining the MIE. This can be explained by the fact that higher molecular mass makes it more difficult to ignite the compound thereby increasing its MIE. The quantum chemical parameters such as HOMO, LUMO, chemical potential, hardness, electrophilicity index and dipole moment were observed to be importance factors in MIE

determination. This can also be confirmed from previous works on MIE where quantum chemical parameters and molecular mass have surfaced as important descriptors determining MIE [45, 49]. Another important factor influencing MIE was observed to be the # of H atoms. This can be explained by the fact that the number of hydrogens in the compound influence the accessibility of the molecule for ignition. The more the stearic hindrance provided by H atoms, the difficult it becomes to access the molecule, thereby raising its MIE.

The E-state keys (counts) are an important parameter which are related to the electrostatics of the compounds. From the data set it can be deduced that compounds having methyl and amine groups have higher electrostatic properties which influences the MIE values.

4.3.2 Decision Tree (DT) algorithm

DT regression was employed on the hydrocarbon dataset to develop a more interpretable visual model. The 13 descriptors identified through RF were used as the input parameters for the decision tree algorithm. Often, DT having high predictability are extremely complex to interpret. In this work, a DT with a max depth = 3 was developed for ease of interpretation. The DT based QSPR model had the following test set values: $R^2 = 0.85$, RMSE = 2.59, AAE = 1.95 along with excellent internal robustness displayed by $Q^2_{LOO} = 0.63$ and external validation $Q^2_{ext} = 0.85$. Figure 31 shows the comparison between the predicted and experimental MIE values for this algorithm for the training and test set and Figure 32 shows the residual plots of the same.

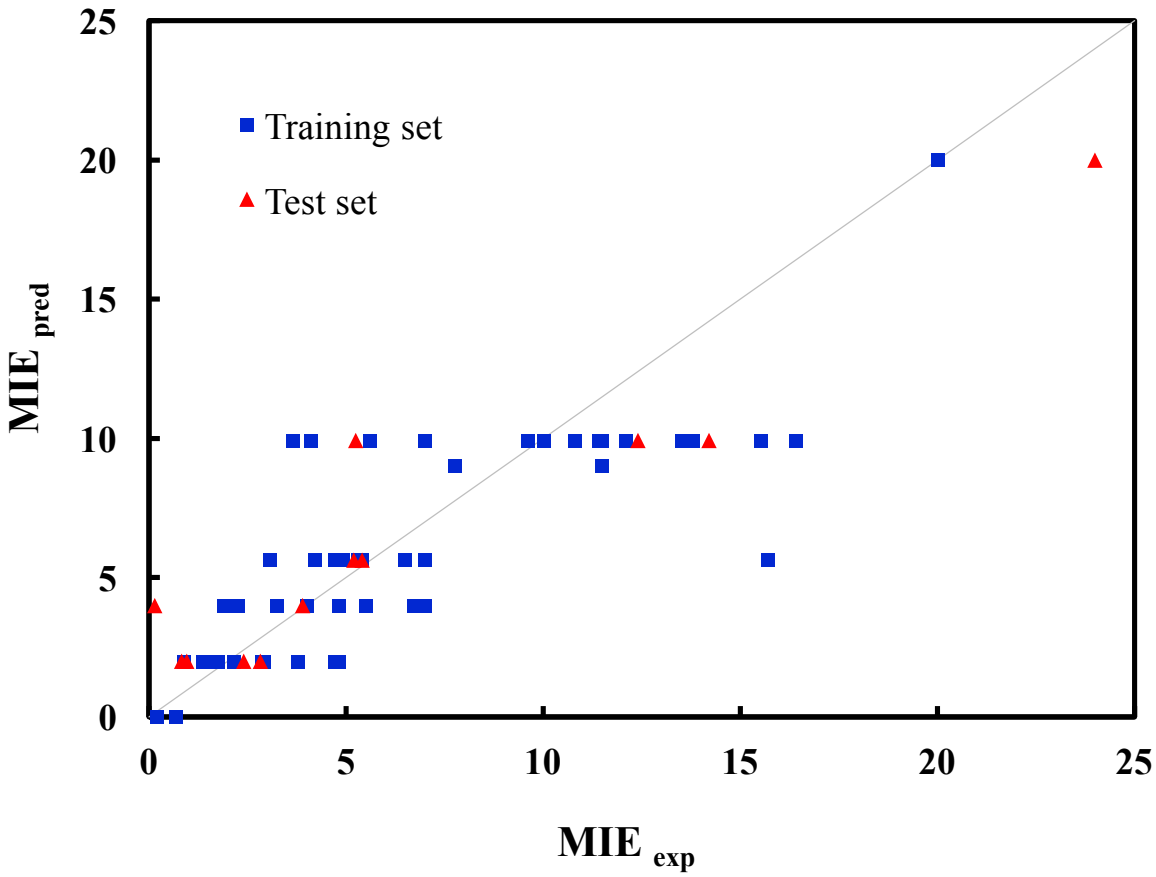

Figure 31 : Experimental versus predicted MIE values through Decision Tree (DT) algorithm for training and test set

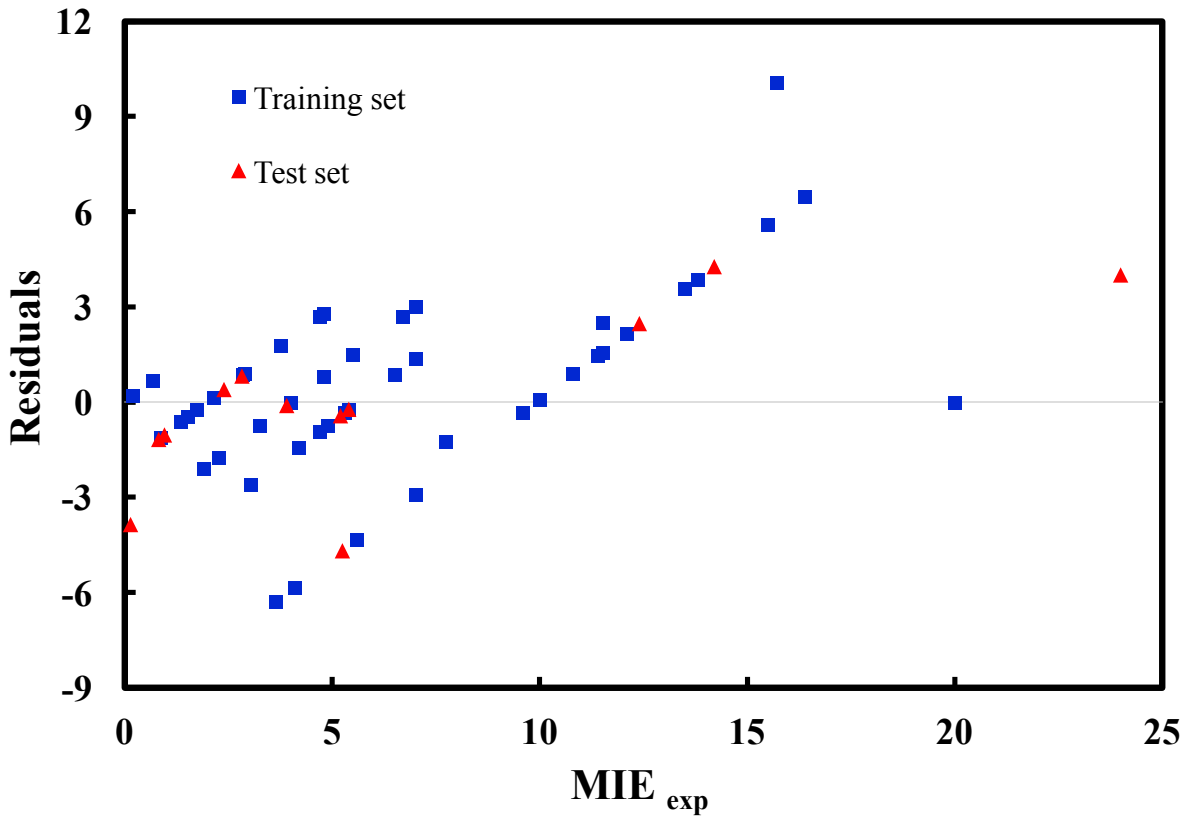

Figure 32 : Experimental MIE versus residuals through Decision Tree (DT) algorithm for training and test set

Figure 33 depicts the decision tree representation for the dataset. The molecular descriptors used in the decision tree are E-state keys (counts): # of CH_3 (X_8), Total molecular mass (X_0) ,# of C atoms (X_{12}) and dipole moment (X_1). The 'mse' represents the mean square error, samples represents the number of compounds and the value represents the MIE value. The first level allows for a True/False decision based on the value of descriptor X_8, followed by the second level which allows decision making based on descriptors X_0 and X_{12}. While, the third level minimizes the error and enables making decisions based on value of descriptors X_8, X_1 and X_0, thereby dividing the total training set into different MIE categories. A drawback of the decision tree can be the black-

box nature of the descriptor and their magnitudes used for the nodes of the tree. However, for quick data representation and understanding it can prove to be a useful method.

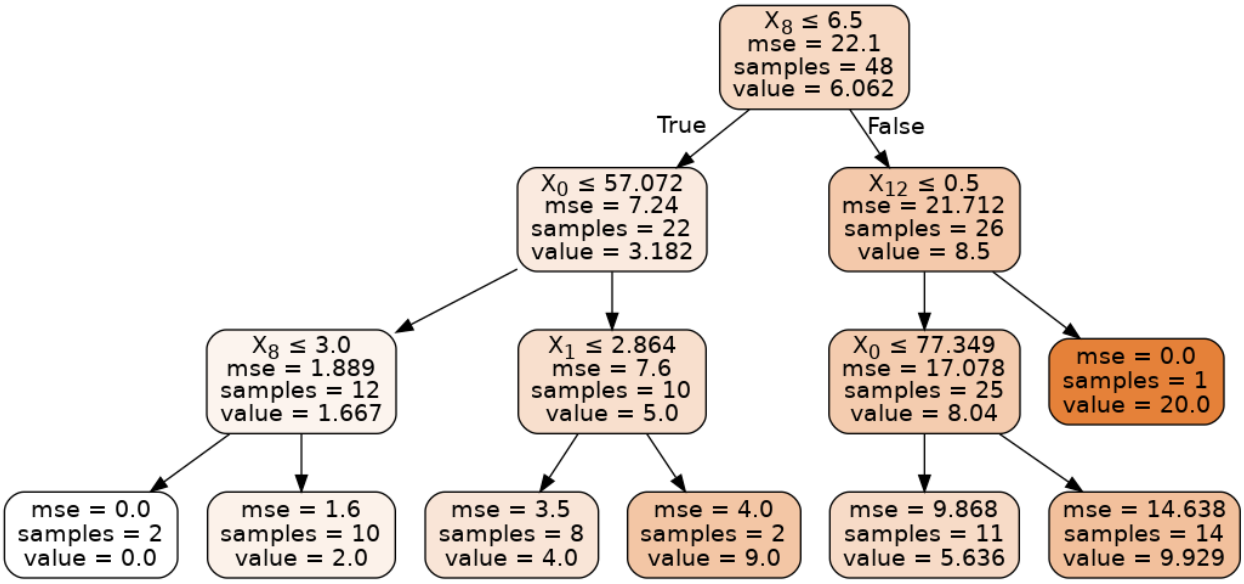

Figure 33 : Decision tree representation of training set, where X_8, X_0, X_{12} and X_1 are E-state keys (counts) # of CH_3, Total molecular mass, # of C atoms and dipole moment respectively

4.3.3 Artificial Neural Networks (ANN) algorithm

ANN regression was conducted through Python library keras, TensorFlow [103]. The ANN used the sequential model with 5 dense layers, activation relu function and the AdamOptimizer. The first ANN model was developed using the 13 molecular descriptors in Table 8 resulting in test set $R^2 = 0.52$, RMSE = 0.26 and $Q^2_{ext} = 0.57$ displaying bad predictability.

An additional input parameter namely Structure Parameter (SP) for the model was introduced which resulted in significantly improved predictability of the model. The concept of structure parameter has been introduced by Calcote *et al.,* where they have assigned a numerical value for each functional group [104]. Further, this parameter was also successfully by Wang *et*

al. to develop QSPR MIE prediction models [45,49]. The Structure Parameter (SP) is a numerical number assigned to different functional groups and discussed in literature [102, 45, 49]. The SP for different functional groups is observed in Table 8.

Table 8 Structure parameter for different functional groups

Functional group	SP	Functional group	SP
alkane	2.0	tertiary amine	2.0
alkene	-0.3	aldehyde	2.0
alkyne	-3.0	ketone	2.6
alcohol	2.1	ester	5.0
sulfur alcohol	1.0	ether	2.1
chloride	3.0	sulfur ether	1.5
primary amine	5.0	cyclic compound	0.5
secondary amine	3.0	inorganic substance	0

The second ANN model was developed using the molecular descriptors selected through the random forest algorithm and the additional input parameter-SP. This resulted in test set R^2 = 0.75, RMSE = 0.2, AAE = 0.17 and Q^2_{ext} = 0.75 with excellent internal robustness of Q^2_{LOO} = 0.67. From this, it can be deduced that addition of the structure parameter significantly improved the model predictability, making it an important parameter to be considered during model development. Figure 34 shows the predicted and experimental MIE values for training and test set

using the ANN model using the 13 input descriptors identified through RF and the structure parameter. The residual plots for the training and test set are observed in Figure 35.

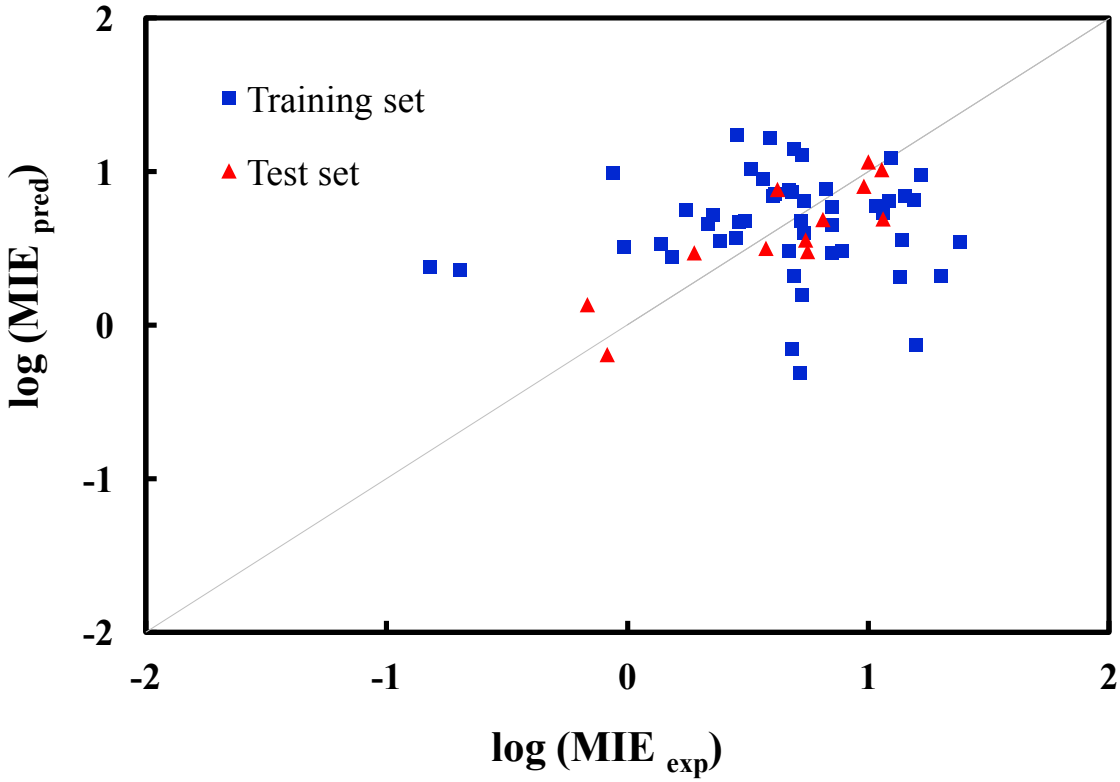

Figure 34 : Experimental versus predicted MIE values through ANN algorithm for training and test set

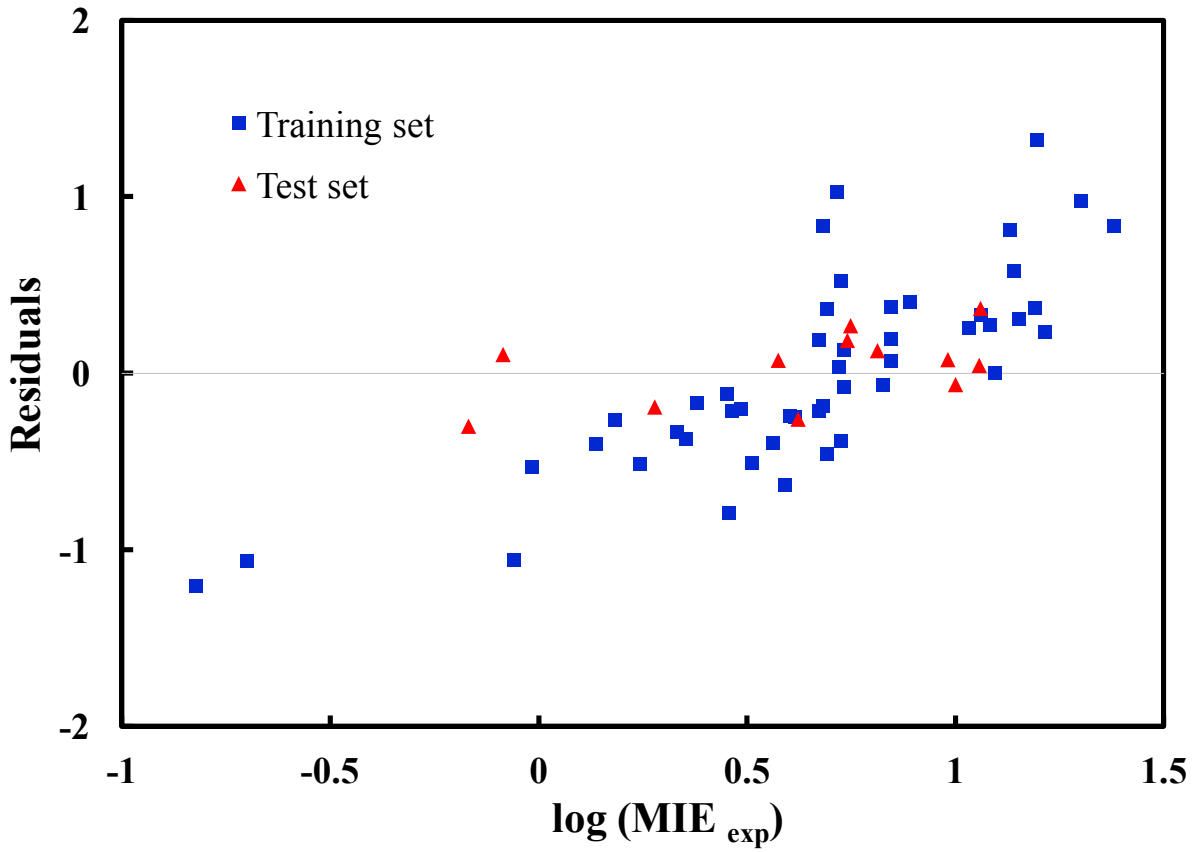

Figure 35 : Experimental MIE versus residuals through ANN algorithm for training and test set

4.3.4 Genetic Function Approximation (GFA) algorithm

The GFA algorithm was employed for model development through the Materials Studio software [101]. It allows selection of a number of parameters required for model development using all the descriptors, creating multiple models. The dataset was divided into training set (80%) and test set (20%). The most significant 13 descriptors influencing MIE identified through RF algorithm were used as an input for the GFA algorithm. Similar to section 3.2, two cases were considered during model development. In the first case, GFA model was developed with the 13 descriptors identified through RF resulting in test set R^2 = 0.54, indicating bad predictability. In

the second case, GFA model was developed with the 13 descriptors with the addition of the SP parameter. In this case, the model displayed very good predictive ability and external and internal robustness through test set: R^2= 0.72, RMSE = 0.25, AAE = 0.19 and Q^2_{LOO} = 0.82 and Q^2ext = 0.70. QSPR models were considered acceptable if they satisfied the following conditions: for the training set, $Q^2_{LOO} > 0.5$; for the test set, $R^2 > 0.6$ [114]. Therefore, similar to the ANN model, addition of structure parameter to the parameters, resulted in significantly better model predictability. Figure 36 shows the predicted and experimental MIE values for training and test set and Figure 37 displays the residual plots for the case including SP as a parameter.

The MIE prediction equation including SP determined through GFA is:

$$Y = 0.003\,(X1) + 0.112\,(X2) - 8.347\,(X3) + 23.097\,(X4) + 0.121\,(X5) + 0.0836\,(X6) + 0.066\,(X7) + 0.298\,(X8) - 0.173\,(X9) - 0.097\,(X10) - 0.785 \quad (13)$$

where,

X1: Total molecular mass, X2: Dipole moment,

X3: Chemical Potential, X4: Electrophilicity Index,

X5: SP, X6: # of C atoms,

X7: # H atoms, X8: # of N atom,

X9: E-state keys (counts): N_sCH_3, X10: E-state keys (counts): N_ssCH_2

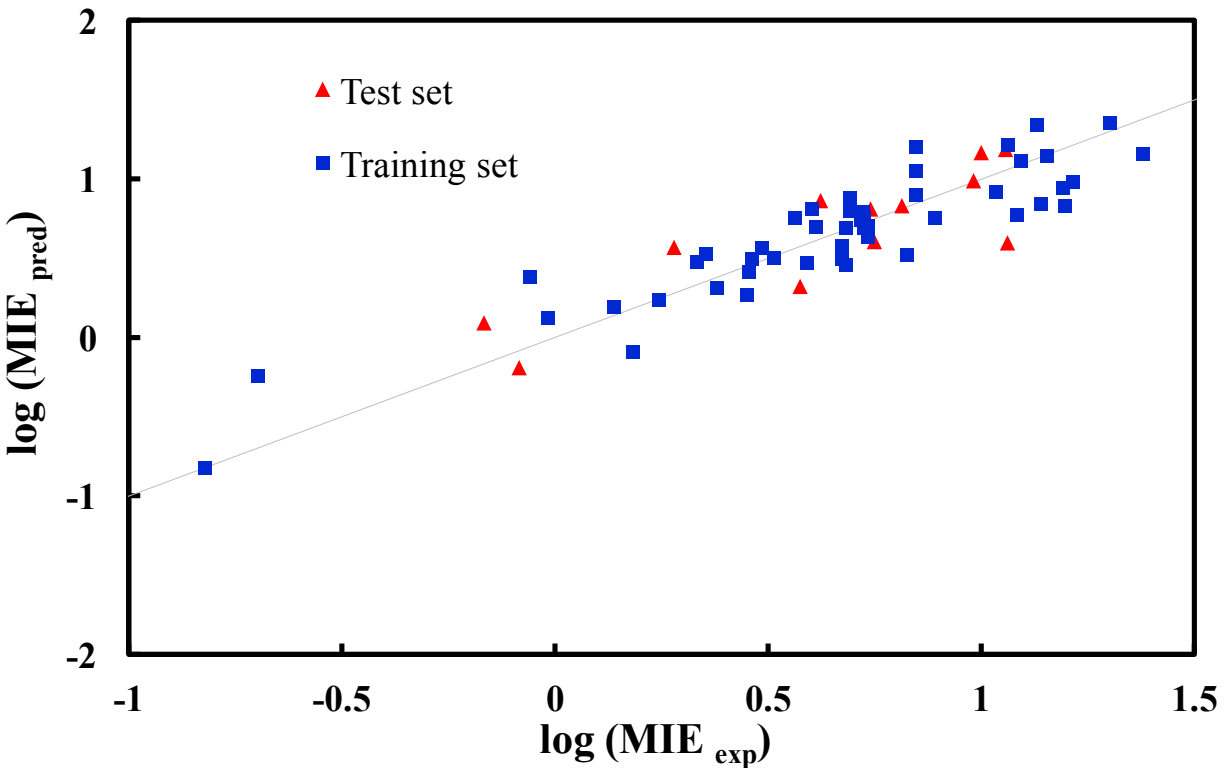

Figure 36 : Experimental versus predicted MIE values through GFA algorithm for training and test set

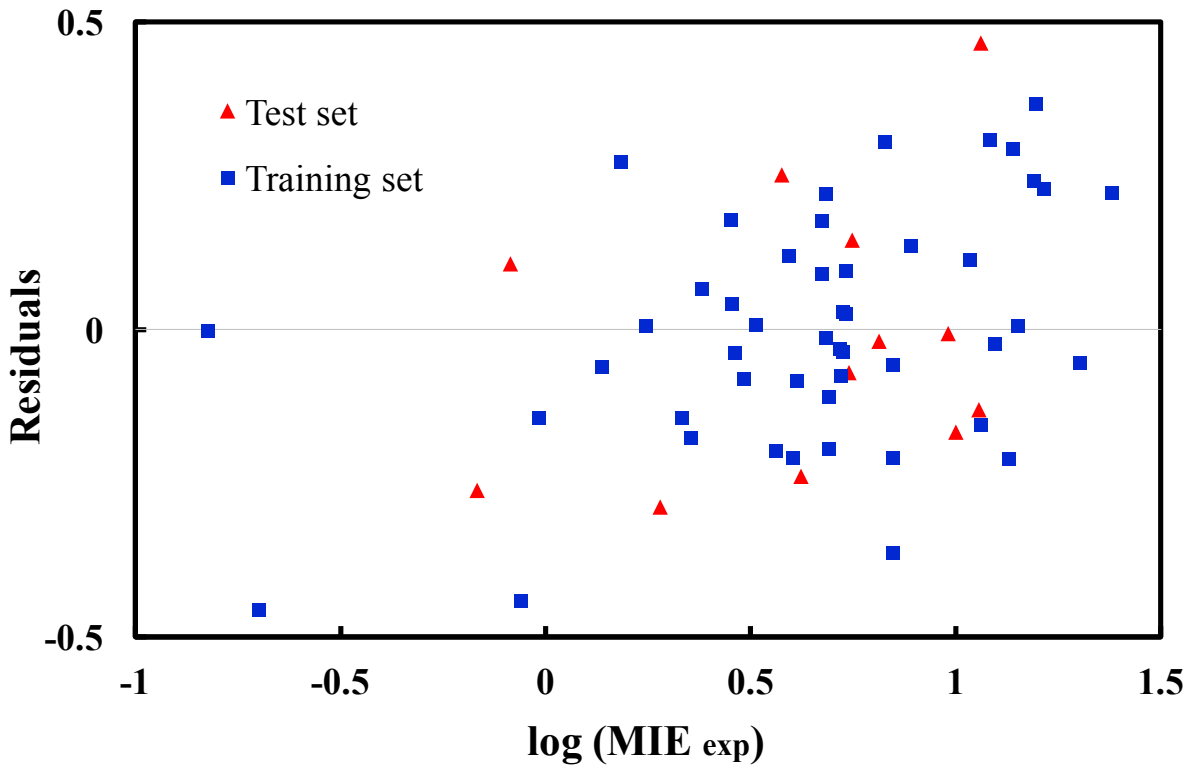

Figure 37 : Experimental MIE versus residuals through GFA algorithm for training and test set

4.4 Methodology - MIE prediction for combustible dusts

4.4.1 MIE dataset

The second dataset used for model development consists of 64 combustible dusts obtained through the GESTIS DUST-EX database [115]. It is known that the macroscopic properties of dusts such as its particle size, polydispersity and shape affect its ignition properties. While, there are numerous different MIE databases are available in literature, this work has only used the MIE data from the GESTIS Database to maintain consistency in the dataset. The combustible dusts in this dataset were selected such that the molecular structures consisted of cyclic or aromatic ring to maintain similarity in the dataset. The d_{50} (mean diameter) of the combustible dusts in this dataset

has been used as a parameter in model development as particle diameter is known to have a significant effect on MIE values. While the first dataset consisting of liquid and gaseous compounds has used point MIE values for model development, the second dataset has used MIE ranges for model development. In the second dataset, the MIE values for the combustible dusts have been classified as MIE < 10 mJ and MIE > 10 mJ. The < 10 mJ has been assigned the classifier '0' and the compounds having MIE >10 mJ have been assigned the classifier '1' (Appendix A)

4.4.2 Geometry optimization and molecular descriptors

The molecular structures of the compounds used in this study were obtained through PubChem database [105]. Energy minimization of molecular structures is an important step in QSPR, dictating the quality of the model developed. Geometry optimization of the molecular structures was conducted using the Gaussian [106] at the B3LYP (Becke, 3-paramater, Lee, Yang, Parr) density functional theory method and the 6-31(d) basis set. Vibrational frequency calculations were performed to ensure optimization to minimum energy level (i.e. no imaginary modes) and the convergence of the optimization was checked to determine successful completion of the optimization.

After conducting geometry optimization, the molecular descriptors for each of these compounds were calculated from the QSPR models available in the Materials Studio software. The descriptors used in this study are quantum chemical, fast descriptors, atomistic descriptors and topological descriptors. In addition to the regular quantum chemical descriptors, the experimental mean diameter (d_{50}) of the dusts obtained through the GESTIS DUST-EX database was also included as a descriptor for model development. Molecular descriptor reduction was conducted first by removing the null values and then by removal of descriptors having high degree of correlation.

4.4.3 Model development and validation

The RF and DT algorithms were observed to give good predictability for the liquid and gas hydrocarbon databases and therefore, have been implemented for model development for the dusts. As the dusts have been classified into two different categories on the basis of their MIE ranges, the RF and DT have used the binary classification for model development. The Random Forest algorithm was used to rank the descriptors in their order of importance for MIE prediction. This reduced set of descriptors were used as an input to develop the decision tree.

For binary classification problems, confusion matrix and the Receiver Operator Characteristic (ROC) curve is used to evaluate the model performance [116,117]. A typical confusion matrix is seen below in Figure 38.

		Actual values	
		Positive (1)	**Negative (0)**
Predicted values	**Positive (1)**	True Positive (TP)	False Positive (FP)
	Negative (0)	False Negative (FN)	True Negative (TN)

Figure 38 : Confusion matrix - actual and predicted positives and negatives

Based on the confusion matrix above, the ROC curve is the plot of True Positive Rate (TPR) versus the False Positive Rate (FPR) at different threshold probabilities. The threshold probability is defined as the probability of separation of the positive and negative categories of the dataset.

The True Positive Rate (TPR) is represented by:

$$TPR = \frac{TP}{TP+FN} \quad (14)$$

The False Positive Rate (FPR) can be represented by:

$$FPR = \frac{FP}{TN+FP} \quad (15)$$

An ROC curve for a random model will be a diagonal TPR versus FPR curve (having 50% probability of correct prediction) [116,117]. While, a better performing model's ROC curve will be on the upper side of the random diagonal curve indicating a better prediction of true positive values as compared to false positive values. A defining metric of the ROC curve which signifies model performance is the area under the ROC curve also termed as Area Under Curve (AUC). The AUC can also be interpreted as the measure of seperability between the positive and negative values in predictability of the dataset. The AUC value for the binary classification model falls between the range 0 to 1, where AUC = 0 indicates bad model predictability and AUC of 1 or closer to 1 indicates good model predictability and separation between the positive and negative categories.

4.5 Results - MIE prediction of combustible dusts

4.5.1 Random Forests (RF) algorithm

Random Forest binary classification model was developed through the Python Scikit-Learn module using the RandomForestClassifier [102]. The number of decision trees used to develop this random forest algorithm were 1000. The model displayed excellent predictability indicated by the AUC of 0.94 as seen in Figure 39. Thus, the model shows remarkable performance and much better predictability than a random 50 % chance.

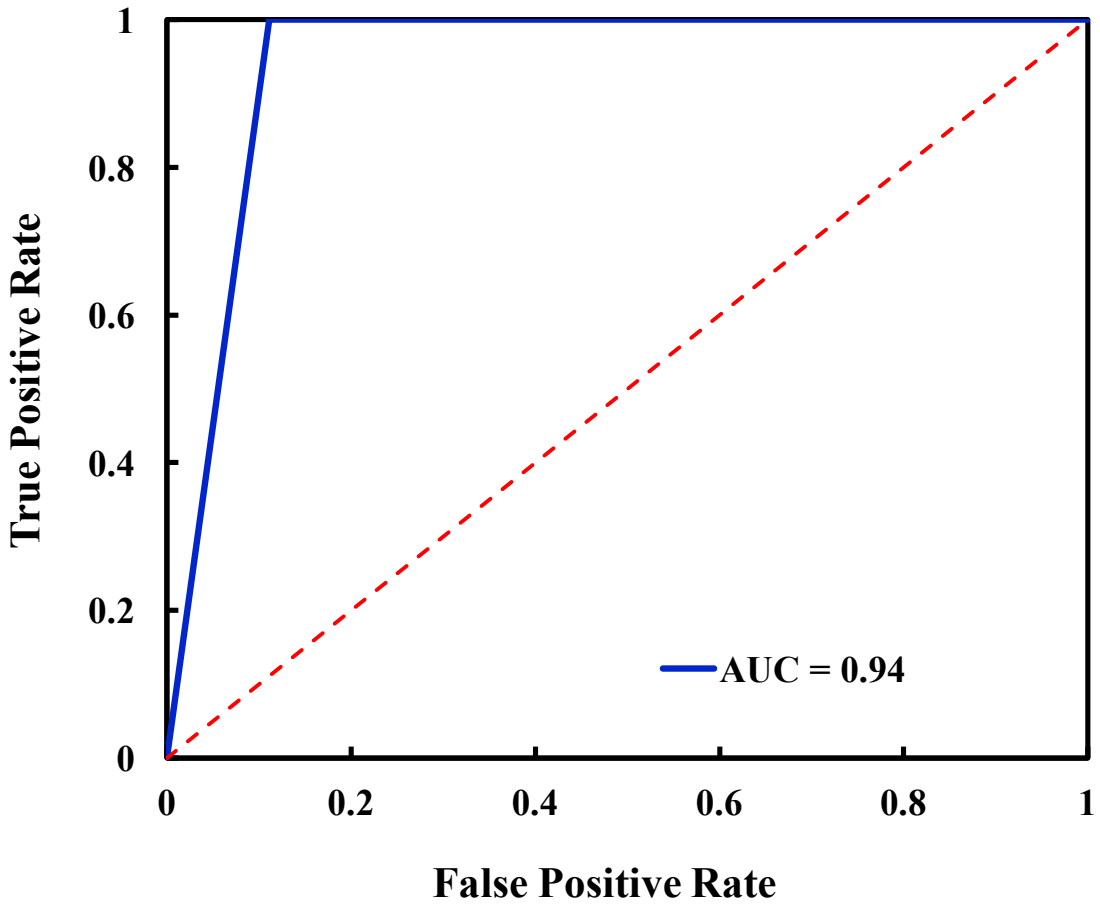

Figure 39 : ROC-AUC curve with AUC of 0.94 for RF model for combustible dusts

Figure 40 below shows a training set plot of the list of the top 13 molecular descriptors having the most influence on MIE. In order to discern the effect of those descriptors which impact the MIE most, the molecular descriptors having < 3% contribution to MIE accuracy were considered to be negligent. Thus, the DT algorithm described in the following section utilized the 13 descriptors (influencing MIE >3%), reducing the parameter space used for model development.

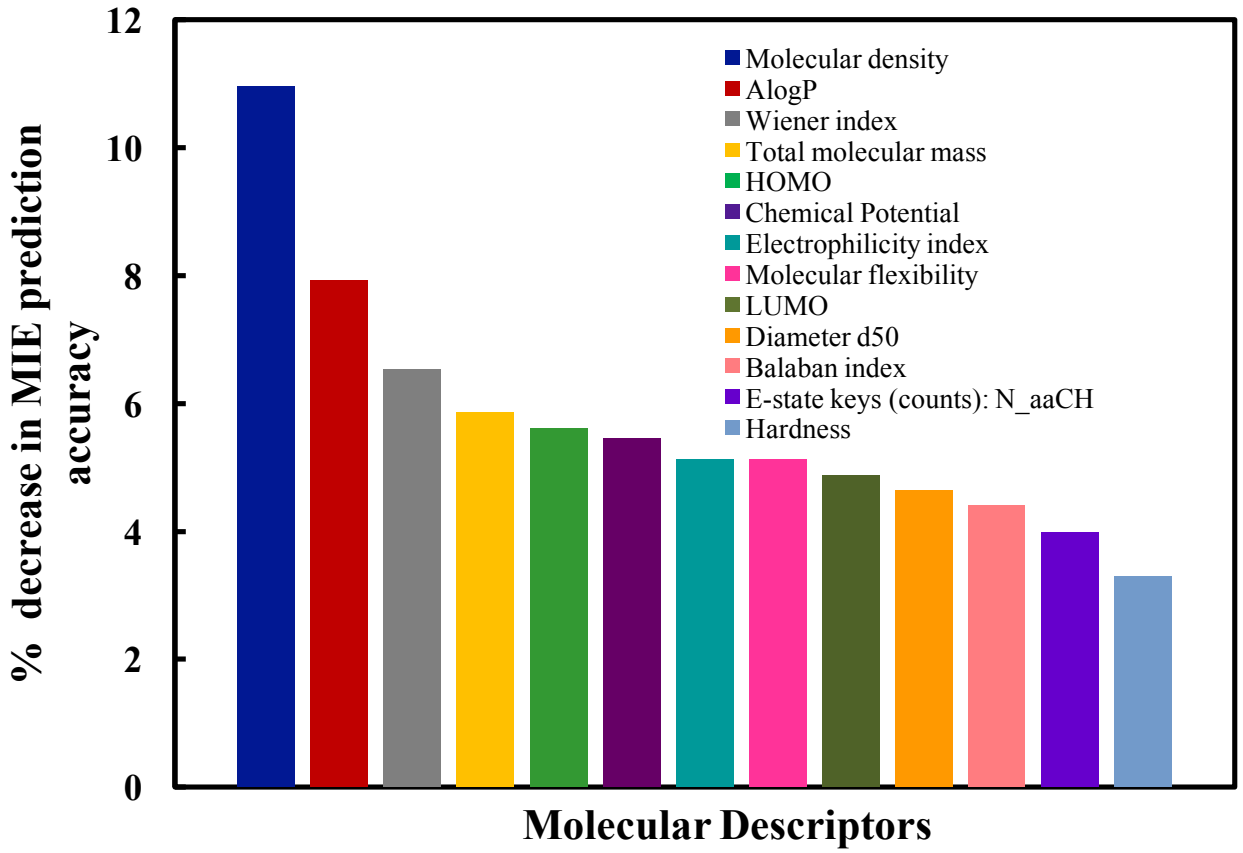

Figure 40 : Relevance of descriptors based on mean decrease in MIE prediction accuracy determined through RF algorithm for combustible dusts

The % contribution by descriptors to MIE (>3%) is observed in Table 9 below. It was observed that the molecular density has the greatest impact on MIE amongst all the descriptors (~11 %). This can be explained by the fact that dense packing of the molecule which is the molecular density makes it difficult to ignite increasing the MIE.

Table 9 List of descriptors having > 3% effect on MIE prediction accuracy

Molecular Descriptors	% effect on MIE prediction
Molecular density	10.95
AlogP	7.92
Wiener index	6.53
Total molecular mass	5.86
HOMO	5.61
Chemical Potential	5.45
Electrophilicity index	5.13
Molecular flexibility	5.13
LUMO	4.88
Diameter d_{50}	4.65
Balaban index	4.41
E-state keys (counts): N_aaCH	3.99
Hardness	3.30

The second most influential descriptor for MIE was the AlogP (~8%) which is a thermodynamic parameter. AlogP is the n-octanol /water partition co-efficient for a molecule which depicts its hydrophobicity. In context of the dusts, AlogP would have a significant effect on the polarity of the molecules which can affect MIE. The Wiener index (~ 6 % effect on MIE prediction) is the sum contribution of the connecting bonds in a molecule and is defined by [52]:

$$W = \frac{1}{2} \sum_{i=1}^{N} \sum_{j=1}^{N} \delta_{ij} \quad (16)$$

where N is the number of vertices or atoms and δ_{ij} is the distance matrix of the shortest possible path between vertices i and j.

For dusts, the Weiner index can be indicative of the branching in the molecule and can have an effect on MIE. The total molecular mass of the molecule can also understandably affect the MIE as molecules having higher molecular weight can be difficult to ignite and can have high MIE values. The quantum chemical descriptors such as the Highest Occupied Molecular Orbital (HOMO), chemical potential, electrophilicity index, Lowest Unoccupied Molecular Orbital (LUMO) and Hardness were observed to be importance factors influencing MIE prediction accuracy. As the HOMO and LUMO contain the molecular orbital energies, these descriptors are closely related to reactivity of the molecule and therefore can be strongly co-related with the MIE of combustible dusts. The quantum chemical descriptors such as HOMO, LUMO and their combinations have resurfaced in the MIE model developed by Wang *et al*. (2017), thus reconfirming their importance for MIE prediction.

Another interesting descriptor was observed to be the Balaban index (known to affect MIE ~ 4 %). Balaban index can be described by the following [52]:

$$J = \frac{M}{\mu+1} \sum_{\text{all edges}} (\delta_i \, \delta_j)^{-0.5} \quad (17)$$

where M is the number of edges, μ represents the cyclomatic number, $\delta_{I \text{ and }} \delta_j$ are the vertex-distance degrees of adjacent vertices and δ_i is defined as $\delta_i = \sum_{j=1}^{A} \delta_{ij}$.

For dusts, the Balaban index can be indicative of the edges which can be correlated to the surface of the molecule and the cyclic rings in the molecule thereby influencing reactivity and

MIE. The E-state keys (counts) # of aaCH (indicates the number of times CH is attached to aromatic bonds in the molecule) was observed to affect MIE ~ 4 %. This observation is well in line as the dataset consists of only aromatic / cyclic compounds, therefore the aromatic rings in molecules can influence the reactivity of the compound eventually influencing its MIE.

The experimental mean diameter (d_{50}) values of the particle, which was also included as a parameter in the dataset was considered as an input parameter along with other parameters. It was observed that the particle diameter did surface in the top 13 parameters that influence MIE having an effect of ~ 4% on MIE. Thus, an interesting observation of is that while, macroscopic properties of combustible dusts are known to influence MIE significantly, from this work the particle diameter was observed to not have a significant effect on MIE as compared to other descriptors determined through molecular structure information. From literature d_p is known to increase MIE cubically [39]. Thus it can be deduced that the descriptors above dust diameter in this list can have a pronounced effect on dust MIE. While such an effect can only be deduced through this work, an experimental verification is necessary.

4.5.2 Decision Tree (DT) algorithm

A binary classification model was employed to develop a Decision Tree through the DecisionTreeClassifier available through the Python Scikit learn [102]. The decision tree was developed to obtain a more visually interpretable model for dusts. The top 13 descriptors identified through RF algorithm were used as the input parameters for the decision tree algorithm. Often, decision trees can be very complex due to the branching. In this work, a DT with a max depth = 5 was developed and required for complete resolution of the dataset into either of the two categories. Figure 41 shows the decision tree representation for the dataset. The molecular descriptors used in decision making in Figure 41 are the dust diameter d_{50} (X_0), Lowest Unoccupied Molecular Orbital

(X_2) = LUMO, Electrophilicity index (X_4), Molecular mass (X_6), Wiener index (X_{10}), E-state keys (counts) : N_aaCH (X_{11}) and Molecular density (X_{12}). These descriptors are also amongst the top few descriptors that significantly influence dust MIE predictability as identified through the RF algorithm. The Decision Tree algorithm identifies the most important descriptors and their values which reduce the error. Each node of the decision tree enables making a decision based on the descriptor value and helps in categorizing the MIE values of compounds. The 'gini' in each node represents the entropy at each level which represents the chaos in the optimization and the samples represents the number of compounds and the value represents the MIE value. The numbers in value [x,y] in each node are represented by: x - the number of compounds classified under the MIE category of '0' (MIE <10 mJ), y - the number of compounds classified under MIE category '1' (MIE > 10mJ). The first level allows for a True/False decision based on the value of descriptor X_{12}, followed by the second level which allows decision making based on descriptors X_{10} and X_4 and so on. The second level minimizes the 'gini' to 0 thereby dividing the total training set into the two different MIE categories. The decision tree can be a useful graphical representation for categorizing the data by just using the information from certain molecular descriptor values.

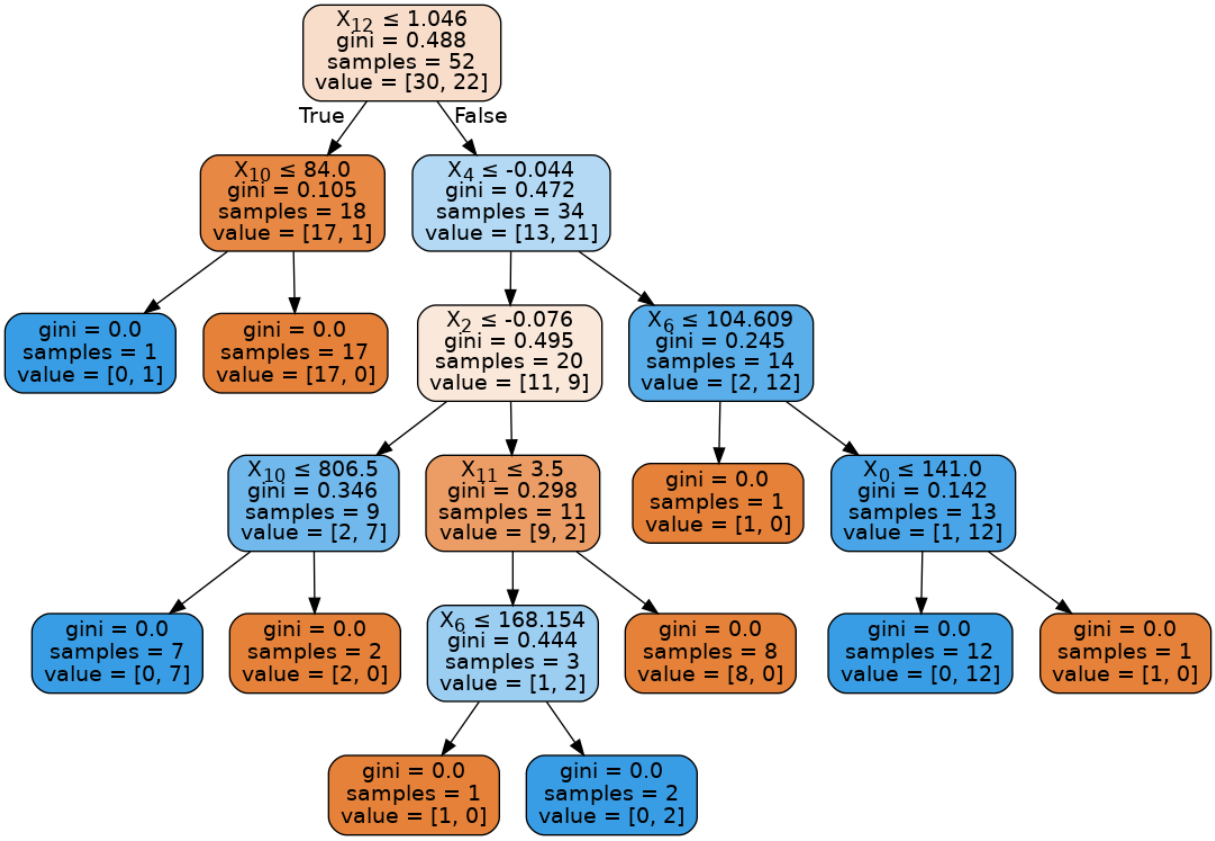

Figure 41 : Decision tree representation of training set, where X_0 = d_{50}, X_2 = LUMO, X_4 = Electrophilicity index, X_6 = Molecular mass, X_{10} = Wiener index, X_{11} = E-state keys (counts) : N_aaCH and X_{12} = Molecular density

The DT showed excellent predictability for the test set displayed through AUC of 0.95 seen in Figure 42. This essentially means that the probability of correctly predicting the MIE category in the test set is 95%.

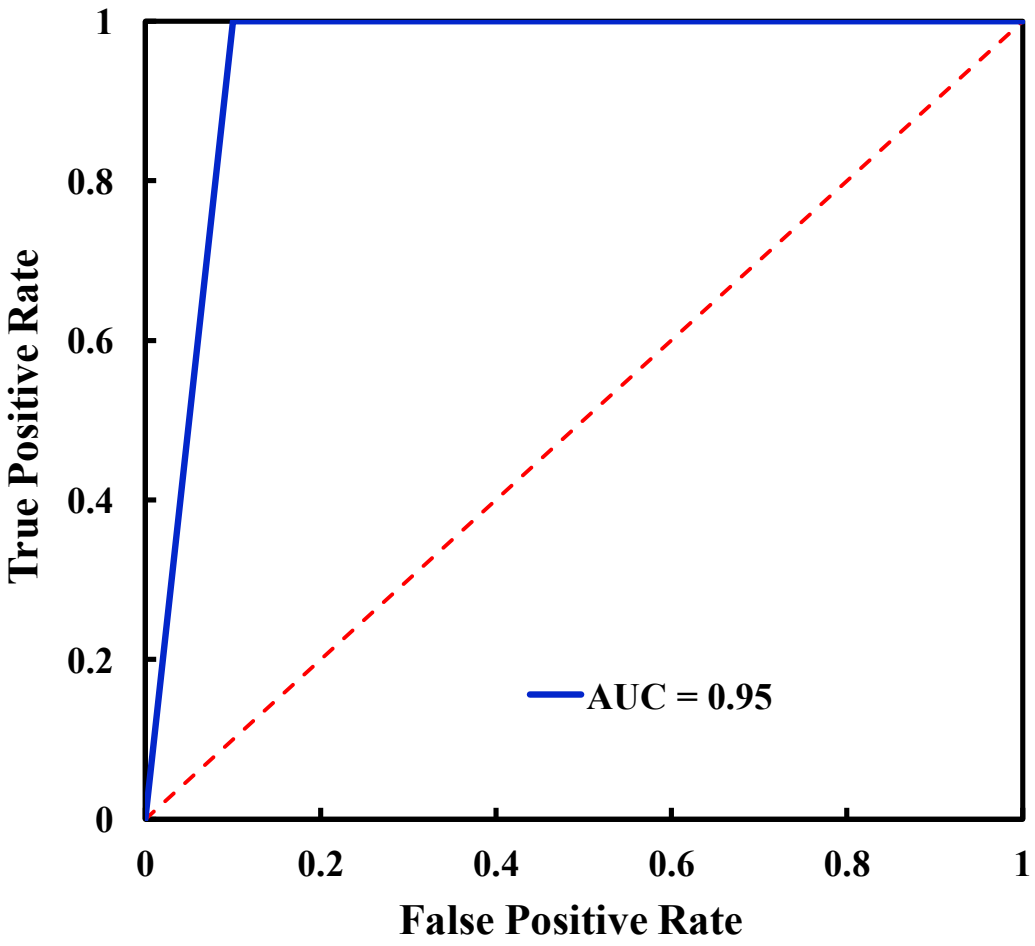

Figure 42 : ROC-AUC curve with AUC of 0.95 for DT model for combustible dusts

4.6 Summary

To summarize, QSPR models for a liquid and gas hydrocarbon dataset were developed using RF, DT, ANN and GFA algorithms. The machine learning algorithms such as RF and DT were observed to give a better predictability over the ANN and GFA algorithms. A similar framework was extended to a combustible dust dataset and RF and DT models were developed. The models displayed excellent predictability for the combustible dusts and helped in identification of the parameters most influencing the dust MIE prediction.

5 CONCLUSIONS AND FUTURE WORK

5.1 Conclusions

Through a series of experiments and modeling, this study has quantified several approaches to partial inerting Minimum Ignition Energy (MIE) measurement and MIE prediction.

Section 1 has discussed dust explosions and provided a comprehensive literature review of MIE testing and prediction for combustible dusts, underscoring the unexplored areas and defining the objectives of this research.

In section 2, an improved MIE test method and its CFD validation have been discussed in detail. This research on partial inerting has demonstrated a proven approach and provided a detailed experimental validation which has not been realized previously in literature. This section has discussed purge turbulence as a parameter that can influence MIE of dust. However, the effect of controlling parameters (such as dust particle size, shape, and conductivity) on the dust MIE needs to be further investigated. Currently, MIE device manufacturers worldwide such as TUV-SUD, Chilworth, and ANKO do not have such purging capability integrated into their instruments. This study provides the ground work for proper measurement of partially inerted MIE values. It is recommended that the work presented here be incorporated into a best practice approach to accompany ASTM E2019-03 (2013) or as a standalone ASTM standard.

In this section, Hartmann tube purging was conducted prior to partial inerting MIE experimentation. The purge time required was determined experimentally and simulated using CFD. For consistency in literature and to facilitate easy comparison amongst different studies, it is recommended from this research that partial inerting studies employ pre-purging and mention the purge flow rate and time along with other relevant testing parameters. Based on this study, for

12–21 volume % oxygen the minimum purge time was determined to be 40 s through CFD which was further validated experimentally.

In section 3, the improved test method was used to demonstrate the effect of MIE test method on its measurement. The partial inerting MIE curves for an international round robin material (Niacin, CaRo15) were presented to demonstrate the effectiveness of the purging device and the various approaches. The experiments demonstrate that pre-purging of the minimum ignition energy dispersion tube is essential for maintaining a controlled concentration of inerted air for the ignition energy measurements. In addition, the importance of sealing the flapper value at the top of the Hartman tube proved necessary in order to produce the most accurate results at higher oxygen concentrations.

It is important to note that for a valid MIE comparison of a given dust at a specific oxygen-nitrogen composition, the parameters of particle size, size distribution, dust moisture, ignition delay time, test temperature, gas humidity, and turbulence must remain consistent. In this work, the only parameter changing between purging and non-purging cases is the purge-induced turbulence. The potential influence of purging turbulence on the MIE measurements was examined. The MIE values were found to be nearly identical for experiments in which the ignition was attempted 1 s and 120 s after the purging was stopped. This validates the time saving method of halting the tube purging followed by an immediate ignition attempt. Experiments were also conducted in which an ignition attempt was made while purge gas was flowing. This experiment produced a higher MIE value as expected due to turbulence in the ignition zone.

Finally, partial inerting data (MIE-O_2) was generated for different combustible dusts. A MIE-O_2 equation was developed and verified through experimental partial inerting studies. While previous studies have used a single coefficient in the MIE-O_2 equation for all dusts, this work has

proposed the coefficient be dust dependent. The last part of this section included the investigation of particle size on partial inerting characteristic of Acetaminophen (Paracetamol) dust. The preliminary finding from this work that the particle size had a more significant impact on dust MIE at lower oxygen concentrations would prove to be useful for facilities handling combustible dusts.

Thus, the sections 2 and 3 have provided a scientific basis for inclusion of purging and purge parameters into partial inerting MIE testing. This work through affecting combustible dust MIE measurements can influence handling of processes in partially inerted atmospheres and hybrid systems (combustible dust-flammable gas-air) in industries. Currently, the MIE testing standards do not mention purging (or its specifications) which can result in inconsistency in comparison of partial inerting MIE values in literature. Thus, based on the test method in this work, it is recommended that the ASTM E2019-03 standard include these provisions.

In section 3, MIE prediction models were developed using QSPR and machine learning algorithms. Two different datasets - liquids/gas hydrocarbons and combustible dusts have been used for model development. For the liquids and gases, the QSPR models were developed using Random Forests (RF), Decision Trees (DT), Artificial Neural Networks (ANN) and Genetic Function Approximation (GFA) regression algorithms. RF algorithm was used to identify the most important descriptors affecting MIE which were used as input parameters in the DT, ANN and GFA algorithms. The RF and DT algorithms were observed to yield excellent predictability as compared to the ANN and GFA algorithms. The molecular mass of the hydrocarbons and the quantum chemical descriptors such as Highest Occupied Molecular Orbital (HOMO), Chemical potential, Electrophilicity index were identified to affect the MIE values the most. An interesting observation from this work has been that the Structure Parameter which has been discussed in

literature before was observed to significantly improve MIE predictability when ANN and GFA algorithms were used for model development.

The framework for model development used for the hydrocarbon dataset, was extended to the combustible dust dataset which consisted of compounds containing aromatic rings. For combustible dusts, a binary classification model was developed with the classifiers '0' indicating MIE <10 mJ and '1' indication MIE > 10 mJ. The RF and DT classification algorithms for the combustible dust dataset showed excellent predictability. The top few descriptors that affected the combustible dust MIE were molecular density, AlogP (octanol/ water partition co-efficient), Wiener index, Molecular mass of the dust, quantum chemical descriptors such as Homo, LUMO, Chemical Potential, Electrophilicity index and Hardness, Molecular flexibility, Balaban index, E–state key counts and dust diameter. An interesting observation from this work has been that the dust diameter (d_{50}) which is a macroscopic property did not affect the MIE as significantly as other descriptors. Thus based on this study, the machine learning algorithms RF and DT provided better predictability. The GFA has traditionally been used for prediction of datasets with large parameters and small datasets but in this work was observed to result in less robust models as compared to the machine learning algorithms RF and DT.

Based on this work, QSPR models using DT and RF can be successfully applied for combustible dust MIE prediction. Knowledge of the exact descriptors influencing dust MIE can facilitate quick risk assessment in solids handling facilities through molecular structure information of the dust. Thus, MIE predictions conducted in this way can result in lowering testing costs, time and any hazards involved in the process.

5.2 Future work

While this research has attempted to address some of the existing gaps in literature, there are some ideas for future work resulting from this work that have been elucidated below:

1) A preliminary investigation of the effect of particle size on partial inerting characteristics has been demonstrated through the study on acetaminophen dust. It would be interesting to extend this to a number of different combustible dusts. Further, quantification of this effect in a single mathematical equation which consists of MIE, oxygen concentration and particle size would be very beneficial to industry and help in navigation of safe conditions to be maintained in processes.
2) The Hartmann tube used for MIE testing can also influence the measured MIE values. Conventionally, MIE testing has been conducted in the glass tube or steel tubes by device manufacturers. The existing device manufacturers recommend that the test sample be changed after every 4 dispersions. Each combustible dust has a different sticking ability which can further change depending on the explosion tube material. The effect of explosion tube material, the electrostatics between the combustible dust and the tube on measured MIE is worth investigating.
3) In this work, CFD modeling of the purge flow for N_2-O_2 mixture in the Hartmann tube has been conducted to determine the purge time for partial inerting case. This can be extended to hybrid dust-gas systems where CFD modeling of the flow of flammable gas-air mixture in Hartmann tube can be simulated and the purge time required can be determined. This information will be useful when testing hybrid systems MIE.
4) In this work, the MIE prediction of combustible dusts has been conducted on a dataset consisting of 65 compounds. This dataset has also used the particle diameter d_{50} as one of

the parameters for model development. Dust diameter (d_{50}) has been used in this work due to easy availability of data. However, a more holistic representation of particle diameter is D (3,2) which represents the volume to surface area ratio for any particle. Inclusion of a more inclusive parameter such as D (3,2) on the MIE prediction would be a useful addition to the model. Thus QSPR and machine learning model development with a more comprehensive dust dataset which can include a wide range of MIE values (rather than just two MIE categories) and D(3,2) as one of the parameters would be valuable.

5) Reactivity of the dusts can have a large influence on its MIE. To study this, the correlation between onset temperatures and heat of combustion to MIE needs to be investigated in detail. This endeavor will require rigorous literature search of combustible dusts for their reaction onset temperature, heat of combustion along with MIE values or it can also include generation of such a dataset including these properties. Therefore, such an experimental and modeling study of developing trends between onset temperature T_{onset} behaviors to MIE would be beneficial for fundamental understanding of dust MIE.

6) This work has developed models for dusts that have a common functional characteristic of aromatic ring in their molecular structure. The effect of different functional groups on MIE prediction and the descriptors can be important. It is highly possible that different functional groups require different molecular descriptors for MIE prediction. Thus MIE prediction models for each different function group should be developed and compared for better understanding. This knowledge can be useful to understand which parameters affect dust MIE the most based on their functional groups.

REFERENCES

[1] W. Bartknecht and G. Zwahlen, *Dust-explosions*. Berlin: Springer-Verlag, 1989.

[2] K. Cashdollar and M. Hertzberg, *Industrial dust explosions*. Philadelphia, Pa: American Society for Testing and Materials, 1987.

[3] R. Eckhoff, *Dust explosions in the process industries (3rd ed.)*. Boston, USA: Gulf Professional Publishing/Elsevier, 2003.

[4] Z. Yuan, N. Khakzad, F. Khan, P. Amyotte, "Dust explosions: A threat to the process industries", *Process Safety and Environmental Protection*, vol. 98, pp. 57-71, 2015.

[5] P. Bagaria, J. Zhang, C. Mashuga, "Effect of dust dispersion on particle breakage and size distribution in the minimum ignition energy apparatus", *Journal of Loss Prevention in the Process Industries*, vol. 56, pp. 518-523, 2018.

[6] Combustible Dust: Safety and Injury Prevention, Awareness Training Program, Instructors Manual. Kirkwood Community College Community Training and Response Center. Susan Harwood Grant Number SH-17797-08-60-F-19.

[7] U.S Chemical Safety and Hazard Investigation Board (USCSB). Sugar Dust Explosion and Fire. Report 2008-05-I-GA, 2009.

[8] U.S Chemical Safety and Hazard Investigation Board (USCSB). West Pharmaceutical Services Dust Explosion and Fire, 2004.

[9] P.R. Amyotte, M.P. Clouthier, F.I. Khan, "Dust explosions: An overview", *Methods in Chemical Process Safety*, In press, 2019.

[10] T. Abbasi, and S.A. Abbasi, "Dust explosions-Cases, causes, consequences, and control", *Journal of Hazardous Materials*, vol. 140, pp. 7-44, 2007.

[11] P. Amyotte, and R. Eckhoff, "Dust explosion causation, prevention and mitigation: An overview", *Journal of Chemical Health and Safety*, vol. 17, pp. 15-28, 2010.

[12] R. Eckhoff, "Understanding Dust Explosions. The Role of Powder Science and Technology", *KONA Powder and Particle Journal*, vol. 15, pp. 54-67, 1997.

[13] R. Eckhoff, "Prevention and mitigation of dust explosions in the process industries: A survey of recent research and development", *Journal of Loss Prevention in the Process Industries*, vol. 9, pp. 3-20, 1996.

[14] T. Hoppe and N. Jaeger, "Reliable and effective inerting methods to prevent explosions", *Process Safety Progress*, vol. 24, pp. 266–272, 2005

[15] P. Amyotte, "Some myths and realities about dust explosions", *Process Safety and Environmental Protection*, vol. 92, pp. 292–299, 2014.

[16] P. Amyotte*, An Introduction to Dust Explosions: Understanding the Myths and Realities of Dust Explosions for a Safer Workplace*. Boston: Butterworth-Heinemann, 2013.

[17] R. Eckhoff, "Partial inerting-an additional degree of freedom in dust explosion protection", *Journal of Loss Prevention in the Process Industries*, vol. 17, pp. 187–193, 2004.

[18] R. Eckhoff, "Dust Explosion Prevention and Mitigation, Status and Developments in Basic Knowledge and in Practical Application", *International Journal of Chemical Engineering*, pp. 1-12, 2009.

[19] M. Glor and K. Schwenzfeuer, "Einfluss der Sauerstoffkonzentration auf die Mindestzündenergie von Staüben", *VDI. Berichte*, vol. 1272, pp. 119–134, 1996.

[20] J. P. Zeeuwen, "Dust explosion protection of grinding installations", Proceedings of 2nd World Seminar on the Explosion. Phenomenon and on the Application of Explosion Protection. Techniques in Practice, Gent, Belgium Kontich, Belgium: EuropEx., 1996.

[21] CREDIT, "Dust explosions: protecting people, equipment, buildings and environment", Proceedings of Conference in London, October 11–12, 1995, IBC Technical Services, London, UK, 1995.

[22] T. Glarner, "Mindestzundenergie - Einfluss der Temperatur", *VDI. Berichte*, vol. 494, pp. 109–118, 1984.

[23] M. Devlikanov, D. Kuzmenko, N. Poletaev, "Nitrogen dilution for explosion of nutrient yeast dust-air mixture", *Fire Safety Journal*, vol. 25, pp. 373, 1995.

[24] R. A. Ogle, "Dust Explosion Dynamics", Boston: Butterworth-Heinemann, 2017.

[25] G. Ackroyd, M. Bailey and R. Mullins, "The effect of reduced oxygen levels on the electrostatic ignition sensitivity of dusts", *Journal of Physics: Conference Series*, vol. 301, pp. 12034, 2011.

[26] K. Choi, K. Choi, K. Nishimura, "Experimental study on the influence of the nitrogen concentration in the air on the minimum ignition energies of combustible powders due to electrostatic discharges", *Journal of Loss Prevention in the Process Industries*, vol. 34, pp. 163-166, 2015.

[27] ASTM E2019-03: Standard Test Method for Minimum Ignition Energy of a Dust Cloud in Air; ASTM: West Conshohocken, 2013.

[28] K. Choi, H. Sakasai, H. Nishimura, "Minimum ignition energies of pure magnesium powders due to electrostatic discharges and nitrogen's effect", *Journal of Loss Prevention in the Process Industries,* vol. 41, pp. 144-146, 2016.

[29] Y. Chunmiao, P. Amyotte, M.N. Hossain, C. Li, "Minimum ignition energy of nano and micro Ti powder in the presence of inert nano TiO_2 powder", *Journal of Hazardous Materials*, vol. 274, pp. 322-330, 2014.

[30] I. Iarossi, P. Amyotte, F.I. Khan, L. Marmo, A.G. Dastidar, R. Eckhoff, "Explosibility of polyamide and polyester fibers", *Journal of Loss Prevention in the Process Industries*, vol. 26, pp. 1627-1633, 2013.

[31] L. Marmo and D. Cavallero, "Minimum ignition energy of nylon fibers", *Journal of Loss Prevention in the Process Industries*, vol. 21, pp. 512-517, 2008.

[32] H. C. Wu, R. C. Chang, H. C. Hsiao, "Research of minimum ignition energy for nano Titanium powder and nano Iron powder", *Journal of Loss Prevention in the Process Industries*, vol. 22 , pp. 21-24, 2009.

[33] P. Chaudhari, B. Ravi, P. Bagaria, C. Mashuga, "Improved partial inerting MIE test method for combustible dusts and its CFD validation", *Process Safety and Environmental Protection* 2019, vol. 122, pp. 192-199, 2019.

[34] E. Randeberg and R. Eckhoff, "Measurement of minimum ignition energies of dust clouds in the < 1mJ region", *Journal of Hazardous Materials*, vol. 140, pp. 237-244, 2007.

[35] E.K. Addai, D. Gabel, M. Kamal, U. Krause, "Minimum ignition energy of hybrid mixtures of combustible dusts and gases", *Process Safety and Environmental Protection*, vol. 102, pp. 503-512, 2016.

[36] G. Pellmont, "Minimum ignition energy of combustible dusts and explosion behavior of hybrid mixtures", 3rd International Symposium on Loss Prevention and Safety Promotion in the Process Industries, vol. 3, pp. 851-862, 1980.

[37] H. Franke, "Determination of the minimum ignition energy of coal dust-methane-air mixtures (hybrid mixtures)", *Erdöl und Kohle, Erdgas. Petrochem*, vol. 33, pp. 283, 1980.

[38] P. Chaudhari, and C. Mashuga, "Partial inerting of dust clouds using a modified standard minimum ignition energy device", *Journal of Loss Prevention in the Process Industries*, vol. 48, pp. 145-150, 2017.

[39] W. Jost, "Theory of flame velocity, III. Elementary considerations on spark ignition", *Zeitschrift für physikalische Chemie*, 1950.

[40] N. Kalkert and H. Schecker, "Theoretische Überlegungen zum Einfluß der Teilchengröße auf die Mindestzündenergie von Stäuben", *Chemie Ingenieur Technik*, vol. 51, pp. 1248–1249, 1979.

[41] E. I. Gubin and I.G. Dik, "Ignition of a Dust Cloud by a Spark", *Combustion, Explosion and Shock Waves*, vol. 22, pp. 135-141, 1986.

[42] M. Bidabadi, M. Mohammadi, A.K. Poorfar, S. Mollazadeh, S. Zadsirjan. "Modeling combustion of aluminum dust cloud in media with spatially discrete sources", *Heat and Mass Transfer*, vol. 51, pp. 837–845, 2015.

[43] S. Bernard, K. Lebecki, P. Gillard, L. Youinou, G. Baudry, "Statistical method for the determination of the ignition energy of dust cloud-experimental validation", *Journal of Loss Prevention in the Process Industries*, vol. 23, pp. 404–411, 2010.

[44] A. Wähner, G. Gramse, T. Langer, M. Beyer, "Determination of the minimum ignition energy on the basis of a statistical approach", *Journal of Loss Prevention in the Process Industries*, vol. 26, pp. 1655–1660, 2013.

[45] O.J. Reyes, S. J. Patel, M.S. Mannan, "Quantitative Structure Property Relationship Studies for Predicting Dust Explosibility Characteristics (Kst, Pmax) of Organic Chemical Dusts", *Industrial & Engineering Chemistry Research*, vol. 50, pp. 2373–2379, 2011.

[46] B. Wang, L. Zhou, K. Xu, Q. Wang, "Prediction of Minimum Ignition Energy from Molecular Structure Using Quantitative Structure–Property Relationship (QSPR) Models", *Industrial & Engineering Chemistry Research,* vol. 56, pp. 47–51, 2017.

[47] D. Frenkel, B. Smit and M. Ratner, "Understanding Molecular Simulation: From Algorithms to Applications", *Physics Today*, vol. 50, pp. 66-66, 1997.

[48] J.N. Israelachvili, *Intermolecular and Surface Forces*. London: Elsevier Academic Press, 2015.

[49] D. Tabor, *Gases, Liquids and Solids: And Other States of Matter*. Cambridge: University Press, 1991.

[50] B. Wang, L. Zhou, K. Xu, Q. Wang, "Fast prediction of minimum ignition energy from molecular structure using simple QSPR model", *Journal of Loss Prevention in the Process Industries*, vol. 50, pp. 290-294, 2017.

[51] A. Katritzky, V. Lobanov, M. Karelson, "QSPR: the correlation and quantitative prediction of chemical and physical properties from structure", *Chemical Society Reviews*, vol. 24, pp. 279, 1995.

[52] M. Dehmer, K. Varmuza, D. Bonchev, *Statistical modelling of molecular descriptors in QSAR/QSPR*. Weinheim: Wiley-Blackwell, 2012.

[53] K. Roy, S. Kar, R. Das, *Understanding the basics of QSAR for applications in pharmaceutical sciences and risk assessment*. Amsterdam: Academic Press, an imprint of Elsevier, 2015.

[54] A. Katritzky, I. Stoyanova-Slavova, K. Tämm, T. Tamm, M. Karelson, "Application of the QSPR Approach to the Boiling Points of Azeotropes", *The Journal of Physical Chemistry A*, vol. 115, pp. 3475-3479, 2011.

[55] V. Zare-Shahabadi, M. Lotfizadeh, A. Gandomani, M. Papari, "Determination of boiling points of azeotropic mixtures using quantitative structure–property relationship (QSPR) strategy", *Journal of Molecular Liquids*, vol. 188, pp. 222-229, 2013.

[56] F. Gharagheizi and R. Alamdari, "Prediction of Flash Point Temperature of Pure Components Using a Quantitative Structure–Property Relationship Model", *QSAR & Combinatorial Science*, vol. 27, pp. 679-683, 2008.

[57] Y. Pan, J. Jiang, R. Wang, H. Cao, J. Zhao, "Prediction of auto-ignition temperatures of hydrocarbons by neural network based on atom-type electrotopological-state indices", *Journal of Hazardous Materials*, vol. 157, pp. 510-517, 2008.

[58] T. Borhani, A. Afzali, M. Bagheri, "QSPR estimation of the auto-ignition temperature for pure hydrocarbons", *Process Safety and Environmental Protection*, vol. 103, pp. 115-125, 2016.

[59] S. Saraf, W. Rogers, M.S. Mannan, "Prediction of reactive hazards based on molecular structure", *Journal of Hazardous Materials*, vol. 98, pp. 15-29, 2003.

[60] N. Baati, "Predictive Models for Thermal Stability and Explosive Properties of Chemicals from Molecular Structure", Ph.D. Thesis, Ećole Polytechnique Feďeŕale De Lausanne, 2016.

[61] B. Henrique, V. Sobreiro and H. Kimura, "Literature review: Machine learning techniques applied to financial market prediction", *Expert Systems with Applications*, vol. 124, pp. 226-251, 2019.

[62] J. McCoy and L. Auret, "Machine learning applications in minerals processing: A review", *Minerals Engine*ering, vol. 132, pp. 95-109, 2019.

[63] J. Wu and Y. Zhao, "Machine learning technology in the application of genome analysis: A systematic review", Gene, vol. 705, pp. 149-156, 2019.

[64] Y. Pan, J. Jiang, R. Wang, H. Cao and Y. Cui, "A novel QSPR model for prediction of lower flammability limits of organic compounds based on support vector machine", *Journal of Hazardous Materials*, vol. 168, no. 2-3, pp. 962-969, 2009.

[65] Y. Pan, J. Jiang, R. Wang, H. Cao and J. Zhao, "Quantitative Structure-Property Relationship Studies for Predicting Flash Points of Organic Compounds using Support Vector Machines", *QSAR & Combinatorial Science*, vol. 27, no. 8, pp. 1013-1019, 2008.

[66] Y. Pan, J. Jiang, R. Wang and H. Cao, "Advantages of support vector machine in QSPR studies for predicting auto-ignition temperatures of organic compounds", *Chemometrics and Intelligent Laboratory Systems*, vol. 92, no. 2, pp. 169-178, 2008.

[67] P. He, Y. Pan and J. Jiang, "Prediction of the self-accelerating decomposition temperature of organic peroxides based on support vector machine", *Procedia Engineering*, vol. 211, pp. 215-225, 2018. Available: 10.1016/j.proeng.2017.12.007.

[68] X. Yu, "Support vector machine-based QSPR for the prediction of glass transition temperatures of polymers", *Fibers and Polymers*, vol. 11, no. 5, pp. 757-766, 2010.

[69] N. Goudarzi and M. Goodarzi, "Prediction of the acidic dissociation constant (pKa) of some organic compounds using linear and nonlinear QSPR methods", *Molecular Physics*, vol. 107, no. 14, pp. 1495-1503, 2009.

[70] C. Xue, R. Zhang, H. Liu, X. Yao, M. Liu, B. Fan, "An Accurate QSPR Study of O—H Bond Dissociation Energy in Substituted Phenols Based on Support Vector Machines.", *ChemInform*, vol. 35, no. 25, 2004.

[71] M. Shen, Y. Xiao, A. Golbraikh, V. Gombar and A. Tropsha, "Development and Validation ofk-Nearest-Neighbor QSPR Models of Metabolic Stability of Drug Candidates", *Journal of Medicinal Chemistry*, vol. 46, no. 14, pp. 3013-3020, 2003.

[72] D. Palmer, N. O'Boyle, R. Glen and J. Mitchell, "Random Forest Models To Predict Aqueous Solubility", *Journal of Chemical Information and Modeling*, vol. 47, no. 1, pp. 150-158, 2006.

[73] A. Rodgers, H. Zhu, D. Fourches, I. Rusyn and A. Tropsha, "Modeling Liver-Related Adverse Effects of Drugs UsingkNearest Neighbor Quantitative Structure–Activity Relationship Method", *Chemical Research in Toxicology*, vol. 23, no. 4, pp. 724-732, 2010.

[74] A. Teixeira, J. Leal and A. Falcao, "Random forests for feature selection in QSPR Models - an application for predicting standard enthalpy of formation of hydrocarbons", *Journal of Cheminformatics*, vol. 5, no. 1, 2013. Available: 10.1186/1758-2946-5-9.

[75] T. Mitchell, *Machine learning*, McGraw Hill: New York, 2017.

[76] M. Mohammed, M. Khan, E. Bashier, *Machine learning*. CRC Press: Boca Raton, Florida, 2016.

[77] C. Mashuga and P. Chaudhari, "Method and Apparatus for Minimum Ignition Energy Testing Using Partial Inerting". U.S. Patent Application No.62 436 247, December 19, 2016.

[78] ISO/IEC 80079-20-2, Explosive Atmospheres-Part 20-2: Material Characteristics-Combustible Dusts Test Methods, 2016.

[79] Ansys, ANSYS Fluent Release 18.2. User's Guide; ANSYS Inc.: Canonsburg, PA, 2017.

[80] D. Crowl and J. Louvar, *Chemical process safety*, New Jersey: Prentice Hall: Upper Saddle River, 2014.

[81] A. Kühner, C. Cesana, R. Siwek, Operating Manual MIKE 3.4. Kühner AG: CH-4127 Birsfelden, Switzerland, 2010.

[82] R. Sanchirico, P. Russo, V. Di Sarli, A. Di Benedetto, "On the explosion and flammability behavior of mixtures of combustible dusts", *Process Safety and Environmental Protection*, vol. 94, pp. 410-419, 2015.

[83] International Standard (ISO), 6184-1. Explosion protection systems—part 1: determination of explosion indices of combustible dusts in air, 1985.

[84] P. Amyotte and M. Pegg, "Lycopodium dust explosions in a Hartmann bomb: effects of turbulence", *Journal of Loss Prevention in the Process Ind*ustries, vol. 2, pp. 87–94, 1989.

[85] O.S. Han, M. Yashima, T. Matsuda, H. Matsui, A. Miyake, T. Ogawa, "Behavior of flames propagating through lycopodium dust clouds in a vertical duct", *Journal of Loss Prevention in the Process Ind*ustries, vol. 13, pp. 449–457, 2000.

[86] P. Bagaria, Q. Li, A. Dastidar, C. Mashuga, "Classification of particle breakage due to dust dispersion", *Powder Technology*, vol. 342, pp. 204-213, 2019.

[87] D. Castellanos, V. Carreto-Vazquez, C. Mashuga, R. Trottier, A. Mejia and M. Mannan, "The effect of particle size polydispersity on the explosibility characteristics of aluminum dust", *Powder Technology*, vol. 254, pp. 331-337, 2014.

[88] P. Amyotte, S. Chippett, M. Pegg, "Effects of turbulence on dust explosions", *Progress in Energy and Combustion Science*, vol. 14, pp. 293-310, 1988.

[89] M. Hertzberg, R. S. Conti, K. Cashdollar, "Spark ignition energies for dust-air mixtures: temperature and concentration dependences", *Symposium on Combustion*, vol. 20, pp. 1681-1690, 1985.

[90] C.C. Swett. NACA Report 1287, 1956.

[91] A. Janes, J. Chaineaux, D. Carson, P. Le Lore. MIKE 3 versus HARTMANN apparatus: Comparison of measured minimum ignition energy (MIE). *Journal of Hazardous Materials*, vol. 152, pp. 32-39, 2008.

[92] K. Schwenzfeuer, M. Glor, A. Gitzi, "T5-16- relation between ignition energy and limiting oxygen concentration for powders", Loss prevention and safety promotion in the process industries. Proceedings of the 10th Internatinoal Symposium, pp. 909-916, 2001.

[93] U. Krause, E. K. Addai, D. Gabel, "Determination of the limiting oxygen con-centration of dust/air and hybrid mixtures based on thermochemical properties", 11th International Symposium on Hazards, Prevention, and Mitigation of Indus-trial Explosion (ISHPMIE), 1–11, 2016.

[94] B. Lewis B, G. Von Elbe, *Combustion, Flames And Explosions Of Gases*. Saint Louis: Elsevier Science, 2014.

[95] U. Maas and J. Warnatz, "Ignition processes in hydrogen-oxygen mixtures", *Combustion and Flame*, vol. 74, no. 1, pp. 53-69, 1988.

[96] Q. Wang, J. Wang, M. Larranaga, "Simple relationship for predicting onset temperatures of nitro compounds in thermal explosions", *Journal of Thermal Analysis and Calorimetry*, vol. 111, no. 2, pp. 1033-1037, 2012.

[97] Q. Wang, W. Rogers, M. Mannan, "Thermal risk assessment and rankings for reaction hazards in process safety", *Journal of Thermal Analysis and Calorimetry*, vol. 98, no. 1, pp. 225-233, 2009.

[98] S. Yuan, Z. Jiao, N. Quddus, J. Kwon and C. Mashuga, "Developing Quantitative Structure–Property Relationship Models To Predict the Upper Flammability Limit Using Machine Learning", *Industrial & Engineering Chemistry Research*, vol. 58, no. 8, pp. 3531-3537, 2019.

[99] T. Owolabi, M. Suleiman, H. Adeyemo, K. Akande, J. Alhiyafi, S. Olatunji, "Estimation of minimum ignition energy of explosive chemicals using gravitational search algorithm based support vector regression", *Journal of Loss Prevention in the Process Industries*, vol. 57, pp.156-163, 2019.

[100] Y. Zhang and C. Ling, "A strategy to apply machine learning to small datasets in materials science", *npj Computational Materials*, vol. 4, no. 1, 2018.

[101] Dassault Systèmes BIOVIA, Materials Studio, 17.1, San Diego: Dassault Systèmes, 2017.

[102] F. Pedregosa, G. Varoquaux, A. Gramfort, V. Michel, B. Thirion, O. Grisel, M. Blondel, P. Prettenhofer, R. Weiss, V. Dubourg, J. Vanderplas, A. Passos, D. Cournapeau, M. Brucher, M. Perrot, É. Duchesnay, "Scikit-Learn: Machine Learning in Python", *Journal of Machine Learning Research*, vol. 12, pp. 2825– 2830, 2011.

[103] M. Abadi, P. Barham, J. Chen, Z. Chen, A. Davis, J. Dean, M. Devin, S. Ghemawat, G. Irving, M. Isard, M. Kudlur, J. Levenberg, R. Monga, S. Moore, D.G. Murray, B. Steiner, P. Tucker, V. Vasudevan, P. Warden, M. Wicke, Y. Yu, X. Zheng, G. Brain. TensorFlow: a system for large-scale machine learning. 12th USENIX Symposium on Operating Systems Design and Implementation (OSDI '16), pp. 265-284, 2016.

[104] H. Calcote, C. Gregory, C. Barnett and R. Gilmer, "Spark Ignition. Effect of Molecular Structure.", *Industrial & Engineering Chemistry*, vol. 44, no. 11, pp. 2656-2662, 1952.

[105] NCBI. PubChem Project. Retrieved from: https://pubchem.ncbi.nlm.nih.gov/(accessed May 2019)

[106] M. J. Frisch, G. W. Trucks, H. B. Schlegel, G. E. Scuseria, M. A. Robb, J. R. Cheeseman, G. Scalmani, V. Barone, G. A. Petersson, H. Nakatsuji, X. Li, M. Caricato, A. Marenich, J. Bloino, B. G. Janesko, R. Gomperts, B. Mennucci, H. P. Hratchian, J. V. Ortiz, A. F. Izmaylov, J. L. Sonnenberg, D. Williams-Young, F. Ding, F. Lipparini, F. Egidi, J. Goings, B. Peng, A. Petrone, T. Henderson, D. Ranasinghe, V. G. Zakrzewski, J. Gao, N. Rega, G. Zheng, W. Liang, M. Hada, M. Ehara, K. Toyota, R. Fukuda, J. Hasegawa, M. Ishida, T. Nakajima, Y. Honda, O. Kitao, H. Nakai, T. Vreven, K. Throssell, J. A. Montgomery, Jr., J. E. Peralta, F. Ogliaro, M. Bearpark, J. J. Heyd, E. Brothers, K. N. Kudin, V. N. Staroverov, T. Keith, R. Kobayashi, J. Normand, K. Raghavachari, A. Rendell, J. C. Burant, S. S. Iyengar, J. Tomasi, M. Cossi, J. M. Millam, M. Klene, C. Adamo, R. Cammi, J. W. Ochterski, R. L. Martin, K. Morokuma, O. Farkas, J. B. Foresman, and D. J. Fox, Gaussian 09, Revision A.02. Gaussian, Inc: Wallingford CT, 2016.

[107] R. Zhu, D. Zhang, J. Wu, C. Liu, "A DFT study on the mechanism and regioselectivity of the tandem O-nitroso aldol/Michael reaction of nitrosobenzene and cyclohexenone", *Journal of Molecular Structure: THEOCHEM*, vol. 815, no. 1-3, pp. 105-109, 2007.

[108] J. Tirado-Rives and W. Jorgensen, "Performance of B3LYP Density Functional Methods for a Large Set of Organic Molecules", *Journal of Chemical Theory and Computation*, vol. 4, no. 2, pp. 297-306, 2008.

[109] D. Rogers and A. Hopfinger, "Application of Genetic Function Approximation to Quantitative Structure-Activity Relationships and Quantitative Structure-Property Relationships", *Journal of Chemical Information and Modeling*, vol. 34, no. 4, pp. 854-866, 1994.

[110] L. Shi, Y. Fan, J. Lee, M. Waltham, D. Andrews, U. Scherf, K. Paull, J. Weinstein, "Mining and Visualizing Large Anticancer Drug Discovery Databases", *Journal of Chemical Information and Computer Sciences*, vol. 40, no. 2, pp. 367-379, 2000.

[111] Y. Fan, L. Shi, K. Kohn, Y. Pommier, J. Weinstein, "Quantitative Structure-Antitumor Activity Relationships of Camptothecin Analogues: Cluster Analysis and Genetic Algorithm-Based Studies", *Journal of Medicinal Chemistry*, vol. 44, no. 20, pp. 3254-3263, 2001.

[112] T. Hou, Y. Li, W. Zhang, J. Wang, "Recent Developments of In Silico Predictions of Intestinal Absorption and Oral Bioavailability", *Combinatorial Chemistry & High Throughput Screening*, vol. 12, no. 5, pp. 497-506, 2009.

[113] D. Couling, R. Bernot, K. Docherty, J. Dixon, E. Maginn, "Assessing the factors responsible for ionic liquid toxicity to aquatic organisms via quantitative structure–property relationship modeling", *Green Chemistry*, vol. 8, no. 1, pp. 82-90, 2006.

[114] A. Golbraikh and A. Tropsha, "Beware of q2!", *Journal of Molecular Graphics and Modelling*, vol. 20, no. 4, pp. 269-276, 2002.

[115] IFA. GESTIS-DUST-EX. Database Combustion and explosion characteristics of dusts. Retrieved from: http://www.dguv.de/ifa/en/gestis/expl/index.jsp (accessed May 2019).

[116] T. Fawcett, "ROC graphs with instance-varying costs", *Pattern Recognition Letters*, vol. 27, no. 8, pp. 882-891, 2006.

[117] J. Mandrekar, "Receiver Operating Characteristic Curve in Diagnostic Test Assessment", *Journal of Thoracic Oncology*, vol. 5, no. 9, pp. 1315-1316, 2010.

APPENDIX A

DATABASES USED FOR MIE PREDICTION

Table A1 Liquid and gas MIE (Dataset 1 - taken from Calcote *et al.* [104])

Liquids and gases	**MIE (10^{-4} J)**
Ethane	2.85
Propane	3.05
Methane	4.7
n-Pentane	4.9
Isobutane	5.2
Isopentane	7
n-Heptane	7
Triptane	10
Isooctane	13.5
2,2-Dimethylpropane	15.7
2,2-Dimethylbutane	16.4
Acetylene	0.2
Vinylacetylene	0.822
Ethylene	0.96
Methylacetylene	1.52
1,3-Butadiene	1.75
Propylene	2.82
1-Heptyne	5.6
2-Pentene	4.7
Diisobutylene	9.6
Methanol	2.15
Isopropylmercaptan	5.3
Isopropylalcohol	6.5
Allylchloride	7.75
n-Propylchloride	10.8
Triethylamine	11.5
n-Butylchloride	12.4
Isopropylchloride	15.5
Isopropylamine	20
Ethylamine	24
Acrolein	1.37

Table A1 Continued

Propionaldehyde	3.25
Acetaldehyde	3.76
Methylethylketone	5.3
Acetone	11.5
Methylformate	4
Vinylacetate	7
Ethylacetate	14.2
Dimethylether	2.9
Dimethoxymethane	4.2
Diethylether	4.9
Diisopropylether	11.4
Dimethylsulfide	4.8
Di-tert-butylperoxide	4.1
Furan	2.25
Thiophene	3.9
Benzene	5.5
Ethyleneoxide	0.87
Propyleneoxide	1.9
Cyclopropane	2.4
Dihydropyran	3.65
Ethylenimine	4.8
Cyclohexene	5.25
Cyclopentane	5.4
Tetrahydrofuran	5.4
Cyclopentadiene	6.7
Tetrahydropyran	12.1
Cyclohexane	13.8
Carbondisulfide	0.15
Hydrogensulfide	0.68

Table A2 Combustible dust MIE (Dataset 2 compounds from GESTIS DUST-EX [115])

Combustible dust	Dust diameter d_{50}	MIE range (mJ)	MIE category
Naphthalene	95	<1	0
1,1'-Binaphthalene-2,2'-diol	16	3/10	0
1,4-cyclohexanedicarboxylic acid	29	10/30	1
1-Phenyl-3-(1,2,3-thiadiazol-5-yl)-urea	17	1/3	0
Povidone	65.2	300/1000	1
2,2-Methylene-bis-(4-methyl-6-tert-butyl-p-phenol)	23	<10	0
2,6-Dichlorobenzonitrile	70	>1000	1
2-(2H-Benzotriazol-2-yl)-4,6-bis(1-methyl-1-phenylethyl)phenol	15.5	<1	0
2-Amino-4-methoxy-6-methyl-s-triazine	10	10/100	1
2-Anilino-4,6-dimethyl pyridine	150	<1	0
2-Ethoxy-4,6-dihydroxy pyrimidine	25	<10	0
2-Naphthol	10	>5	1
2-phenyl-2-imidazoline	10	1/3	0
4-Morpholinepropanesulfonic acid	10	30/100	1
4,4´,4"-(Ethane-1,1,1-triyl)triphenol	34	10/30	1
4-Aminobenzamidin-dihydrochlorine	21	>1000	1
4-Pyridylethansulfonicacid	38	30/100	1
Acetanilide	31	3/10	0
Acetoguanamine	10	>1000	1
Acetylsalicylic acid	39	<10	0
Aminotriazole	22	<10	0
Anthracene	102	4/8	0
Antioxidant (1-(2-hydroxy-3-sulfopropyl)-pyridinium-betaine)	35	100/1000	1
Antioxidant (2,2'-(2-methylpropylidene)-bis-(4,6-di-methylphenol))	10	<10	0
Antioxidant (2,5-di-tert.-amyl hydroquinone)	13	<10	0
Antioxidant (3-(3,5-di-tert.-butyl-4-hydroxyphenyl)-propionic-acid methyl ester)	40	<10	0
4,4'-Thiobis(6-tert-butyl-m-cresol)	30	<10	0
Antioxidant (octadecyl-3-(3,5-di-tert.-butyl-4-hydroxy-phenyl)-propionate)	33	<10	0
1,2-Bis(3,5-di-tert-butyl-4-hydroxyhydrocinnamoyl)hydrazine	10	1/3	0
Antioxidantie Tris(4-tert-butyl-3-hydroxy-2,6-dimethylbenzyl)isocyanurat	22	1/3	0
Azacycloheptane-2,2-diphosphonic acid	10	10^5	1
Benzoguanamine	18	<10	0
Benzoic acid	22	1/3	0

Table A2 Continued

Bis(2,6-Diisopropylphenyl)carbodiimide	32.4	1/3	0
Bisphenol A	63	<4	0
Caprinoguanamine	33	<10	0
Carbamazepine	15	2/5	0
Cinnamic acid	36	<10	0
Dextrose	132	>1000	1
Benzenesulfonic acid, 4,4'-oxybis-, 1,1'-dihydrazide	10	3/10	0
Dibenzo[b,k][1,4,7,10,13,16]hexaoxacyclooctadecin	10	1/3	0
Carbazole	150	< 3	0
Sodium diclofenac	28	>10000	1
Dimethyl terephthalate	27	>2	1
Estradiol valerianate	10	< 1	0
Enalapril	100	300/1000	1
Ethinyl estradiol	10	1/3	0
Felodipine	80	30/100	1
Guanine	22	300/1000	1
Isophthalic acid	32	1/3	0
Naphthalic acid anhydride	16	> 3	1
Nicotinic acid	15	1/3	0
Nifedipine	24	<10	0
Pentoxifylline	14	<10	0
Phenytoin	26	<10	0
Quinine benzoate	33	1/3	0
Salicylic acid	36	3/10	0
Sucrose	34	10/30	1
Terephthalic acid	40	10/30	1
Tetramethylpiperidine	21	1/3	0
Theophylline	35	30/100	1
Trimellitic acid anhydride	1250	>1000	1
Tryptophan	53	>3	1
4-Tert-Butylphenol	53	2/5	0
Quinic acid	26	100/300	1

Classifier 1: MIE > 10 mJ, Classifier 2: MIE < 10 mJ